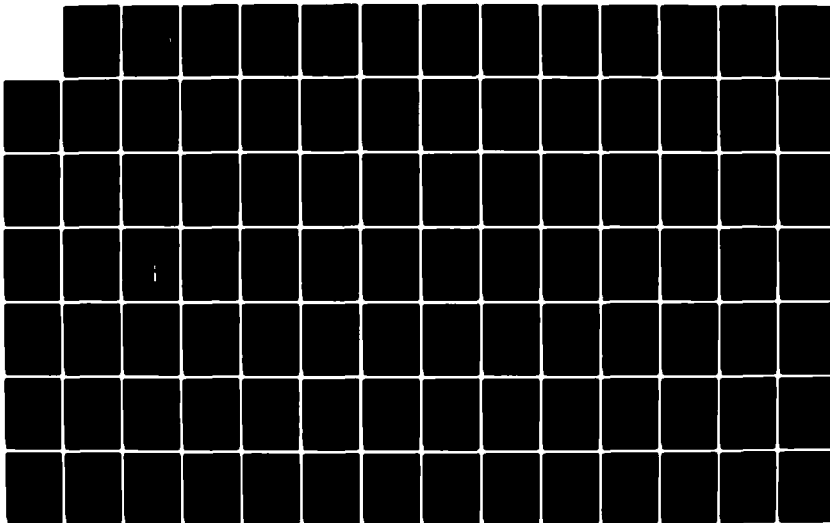AD-A145 425   EFFECTS OF ATMOSPHERIC WATER VAPOR AND CLOUDS ON NOAA   1/⬦
                (NATIONAL OCEANIC A..(U) AIR FORCE INST OF TECH
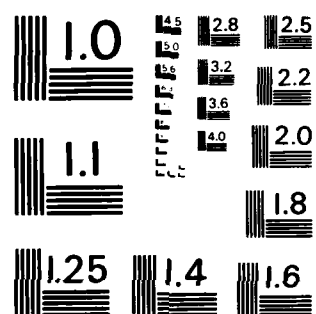   WRIGHT-PATTERSON AFB OH   D J KNIPP JUL 84
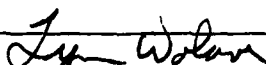UNCLASSIFIED   AFIT/CI/NR-84-55T   F/G 17/5   NL

MICROCOPY RESOLUTION TEST CHART

NATIONAL BUREAU OF STANDARDS-1963-A

AD-A145 425

DTIC FILE COPY

REPORT DOCUMENTATION PAGE		READ INSTRUCTIONS BEFORE COMPLETING FORM
1. REPORT NUMBER AFIT/CI/NR 84-55T	2. GOVT ACCESSION NO.	3. RECIPIENT'S CATALOG NUMBER
4. TITLE (and Subtitle) Effects Of Atmospheric Water Vapor And Clouds On NOAA AVHRR Satellite Data		5. TYPE OF REPORT & PERIOD COVERED THESIS/DISSERTATION
		6. PERFORMING ORG. REPORT NUMBER
7. AUTHOR(s) Delores J. Knipp		8. CONTRACT OR GRANT NUMBER(s)
9. PERFORMING ORGANIZATION NAME AND ADDRESS AFIT STUDENT AT: University of Missouri-Columbia		10. PROGRAM ELEMENT, PROJECT, TASK AREA & WORK UNIT NUMBERS
11. CONTROLLING OFFICE NAME AND ADDRESS AFIT/NR WPAFB OH 45433		12. REPORT DATE 1984
		13. NUMBER OF PAGES 148
14. MONITORING AGENCY NAME & ADDRESS(If different from Controlling Office)		15. SECURITY CLASS. (of this report) UNCLASS
		15a. DECLASSIFICATION/DOWNGRADING SCHEDULE

16. DISTRIBUTION STATEMENT (of this Report)

APPROVED FOR PUBLIC RELEASE; DISTRIBUTION UNLIMITED

DTIC
ELECTE
SEP 13 1984
S D
B

17. DISTRIBUTION STATEMENT (of the abstract entered in Block 20, If different from Report)

18. SUPPLEMENTARY NOTES

APPROVED FOR PUBLIC RELEASE: IAW AFR 190-1

LYNN E. WOLAVER
Dean for Research and
5 Sep 84   Professional Development
AFIT, Wright-Patterson AFB OH

19. KEY WORDS (Continue on reverse side if necessary and identify by block number)

20. ABSTRACT (Continue on reverse side if necessary and identify by block number)

ATTACHED

DD FORM 1473   EDITION OF 1 NOV 65 IS OBSOLETE
1 JAN 73

84 09 13 024

ABSTRACT

The last ten years have seen a revolution in large area surveys
of the earth's biomass. Satellite spectral data have made a signi-
ficant contribution to these surveys by virtue of the fact that var-
ious combinations of the data have been found to be sensitive indi-
cators of the presence of green vegetation. Data from two solar
reflective channels of the NOAA-7 meteorlogical weather satellite
are being combined to provide a measure of the the greeness in the
satellite's instantaneous field of view. In numerous instances
the information content of this data can be limited by the varying
amounts of atmospheric constituents, by clouds, by view angle and
by solar angle. This paper reports on a study which was undertaken
to describe the effect of varying amounts of water vapor on
the infrared portions of the solar refolcted radiances and on the
earth emitted, far infrared radiances. By virtue of several data
screening processes, it was possible to determine that the change in
atmospheric water content over a several day period was responsible
for variations in the satellite derived infrared radiance values.
Similar variations were found in the far infrared radiance data.
The variation in the near infrared channel was and is a factor
in the variability of the vegetative index. A seperate but related
conclusion of this study is that view angle effects on the solar
reflected near infrared channel introduces a larger variabilty into
the data than was previously thought. This effect needs more study.

AFIT RESEARCH ASSESSMENT

The purpose of this questionnaire is to ascertain the value and/or contribution of research accomplished by students or faculty of the Air Force Institute of Technology (AU). It would be greatly appreciated if you would complete the following questionnaire and return it to:

AFIT/NR
Wright-Patterson AFB OH 45433

RESEARCH TITLE: Effects Of Atmospheric Water Vapor And Clouds On NOAA AVHRR Satellite Data

AUTHOR: Delores J. Knipp

RESEARCH ASSESSMENT QUESTIONS:

1. Did this research contribute to a current Air Force project?

( ) a. YES   ( ) b. NO

2. Do you believe this research topic is significant enough that it would have been researched (or contracted) by your organization or another agency if AFIT had not?

( ) a. YES   ( ) b. NO

3. The benefits of AFIT research can often be expressed by the equivalent value that your agency achieved/received by virtue of AFIT performing the research. Can you estimate what this research would have cost if it had been accomplished under contract or if it had been done in-house in terms of manpower and/or dollars?

( ) a. MAN-YEARS _____   ( ) b. $_____

4. Often it is not possible to attach equivalent dollar values to research, although the results of the research may, in fact, be important. Whether or not you were able to establish an equivalent value for this research (3. above), what is your estimate of its significance?

( ) a. HIGHLY   ( ) b. SIGNIFICANT   ( ) c. SLIGHTLY   ( ) d. OF NO
     SIGNIFICANT   SIGNIFICANT   SIGNIFICANCE

5. AFIT welcomes any further comments you may have on the above questions, or any additional details concerning the current application, future potential, or other value of this research. Please use the bottom part of this questionnaire for your statement(s).

NAME   GRADE   POSITION

ORGANIZATION   LOCATION

STATEMENT(s):

EFFECTS OF ATMOSPHERIC WATER VAPOR AND CLOUDS

ON

NOAA AVHRR SATELLITE DATA

A Thesis
Presented to
The Faculty of the Graduate School
University of Missouri-Columbia

In Partial Fulfillment
of the Requirements for the Degree
Master of Science

---

by

Delores Jane Knipp

G. L. Darkow   Thesis Supervisor

July 1984

84 09 13 024

TABLE OF CONTENTS

LIST OF FIGURES

ACKNOWLEDGEMENTS

CHAPTER I

INTRODUCTION

GENERAL BACKGROUND

World political and economic stability is closely tied
to the availability and price of food. Accordingly, assess-
ment of global food supplies has become a primary concern
for government planners. Supply information is important
not only to the government sector, but to the private
sector, as well. Even small farmers feel the effect of
inadequate information about world food supplies. The
impact of the Soviet grain buys of 1972 are a case in point.

The last ten years have seen a revolution in large area
surveys of the earth's biomass. Satellite spectral data
have made a significant contribution to these surveys by
virtue of the fact that the various combinations of the data
have been found to to be sensitive indicators of the pres-
ence of green vegetation. Earth Resources Technology Satel-
lites, now known as the Landsat satellites, provided much of
the original crop yield data in this technological revo-
lution. A specific application of this technology was, and
is, crop yield forecasting, based on satellite assessment of

planted acreage and crop health.

Thompson and Wehmanen (1979) used Landsat data to develop a method for monitoring drought conditions for various crops in the major United States crop regions. They reported successful monitoring of the 1977 drought in the USSR and Australian wheat regions. Gray and McCrary (1981a) showed that data extracted originally from the Landsat Multispectral Scanning (MSS) system and, more recently, from the polar orbiting weather satellites, TIROS-N, NOAA-6, NOAA-7 and NOAA-8, were useful in studying and monitoring terrestrial vegetation on a global basis.

The National Oceanic and Atmospheric Administration (NOAA) satellites are platforms for several sensors. One of these sensors, the Advanced Very High Resolution Radiometer (AVHRR), is a multi-channel scanner designed to simultaneously measure radiant energy in each of four or five selected spectral bands. Combinations of the measured energy values from Channels 1 and 2 of the AVHRR provide a measure of "greeness," as defined by Kauth and Thomas (1976), of the viewed target area. Barnett and Thompson (1982), among others, found the greeness value, also called a vegetative index (VI), to be highly correlated with the health and vigor of vegetation and crops. A vegetative index is an algebraic relation of satellite radiance measurements from two or more different spectral bands.

Vegetative indices vary, not only as a function of vegetative health and vigor, but also with sun angle, sensor

view angle and with atmospheric effects such as path radi-
ance, scattering by dust and aerosols, sub-pixel size clouds
and absorption by water vapor. One objective of this study
has been to find a direct relationship between satellite
radiance data and the amount of water in the atmosphere.
Determining if the amount of water is directly related to
variations in a particular vegetative index was a second
objective.

This study investigated, on a case study basis, effects
of atmospheric water on one of the vegetative indices, the
VIN, which is computed using the formula:

$$VIN = AVHRR\ Channel\ 2 - AVHRR\ Channel\ 1$$

where Channel 2 is the measured radiance value of AVHRR
Channel 2 and Channel 1 is the measured radiance value of
AVHRR Channel 1. Additionally, effects of atmospheric water
on the data from two "emissive channels" were investigated.
The water effects and associated cloud effects can explain a
part of the day to day variability of the VIN as it is used
in crop yield prediction.

SATELLITE BACKGOUND

During the last 25 years many research disciplines have
attempted to gather information from earth orbiting, remote
sensing platforms. Notable among these are surveyers of

natural resources, land use planners, oceanographers and atmospheric scientists. Satellite technology as it has developed from the 50's and 60's has played an especially important role in providing global assessment capability of many earth resources. This technology has become so important that each of these groups has developed satellites with instrumentation designed to sense data that can be interpreted in meaningful relationships and quantified for the particular groups of users. Lillisand and Kiefer (1979) state: "This remotely collected data can be of many forms including variations in force distributions, acoustic wave distributions or electromagnetic energy wave distributions."

Although pictures of cloud formations from rocket platforms were made public in 1949, atmospheric scientists' first attempt at satellite remote sensing of the atmosphere came in February 1959 with the launch of Vanguard II. A photo cell on the satellite built up a picture one line at a time. Kellogg (1982) describes this method of "picture" development as very similar to methods used on satellites now in operation.

Allison and Schnapf (1983) recount the development of the United States meteorological satellite program. The following is a summary of that recount. From Vanguard the meteorlogical satellite development matured to a polar orbiting series of weather satellites. First came TIROS-I (Televison and Infrared Observational Satellite) in the early 1960's. The TIROS Operational Satellite (TOS) or ESSA

(Environmental Science Services Administration) satellites followed in the late 60's. Later in the 1960's TIROS-M or the ITOS satellite (Improved TIROS Operational System) was launched. Finally, the current TIROS-N or the NOAA-X satellites become operational in the mid 1970's. Figure 1.1 depicts the evolution of the TIROS series.

A series of satellites designated as NIMBUS satellites served as a research and development test bed for many of the instruments flown on the TIROS series satellites. Also, in the mid 60's and early 70's, there was a simultaneous development of the geostationary satellites. The Advanced Technology Satellite (ATS) demonstrated the technologies which were to become operational on the SMS/GOES (Geosynchronous Orbiting Earth Satellite) System.

The late 1960's and the early 1970's also saw a parallel development effort in polar orbiting, earth sensing satellites which became known as Landsat. Their primary purpose was, and is, acquisition of information about earth resources. These satellites, in general have a much smaller field of view than the meteorological polar orbiters. As a result, Landsat returns to view the same area of the earth much less frequently than the weather satellites.

POLAR ORBITER BACKGROUD

TIROS-N, (see Figure 1.2) launched in October 1978, became the first satellite of the third generation opera-
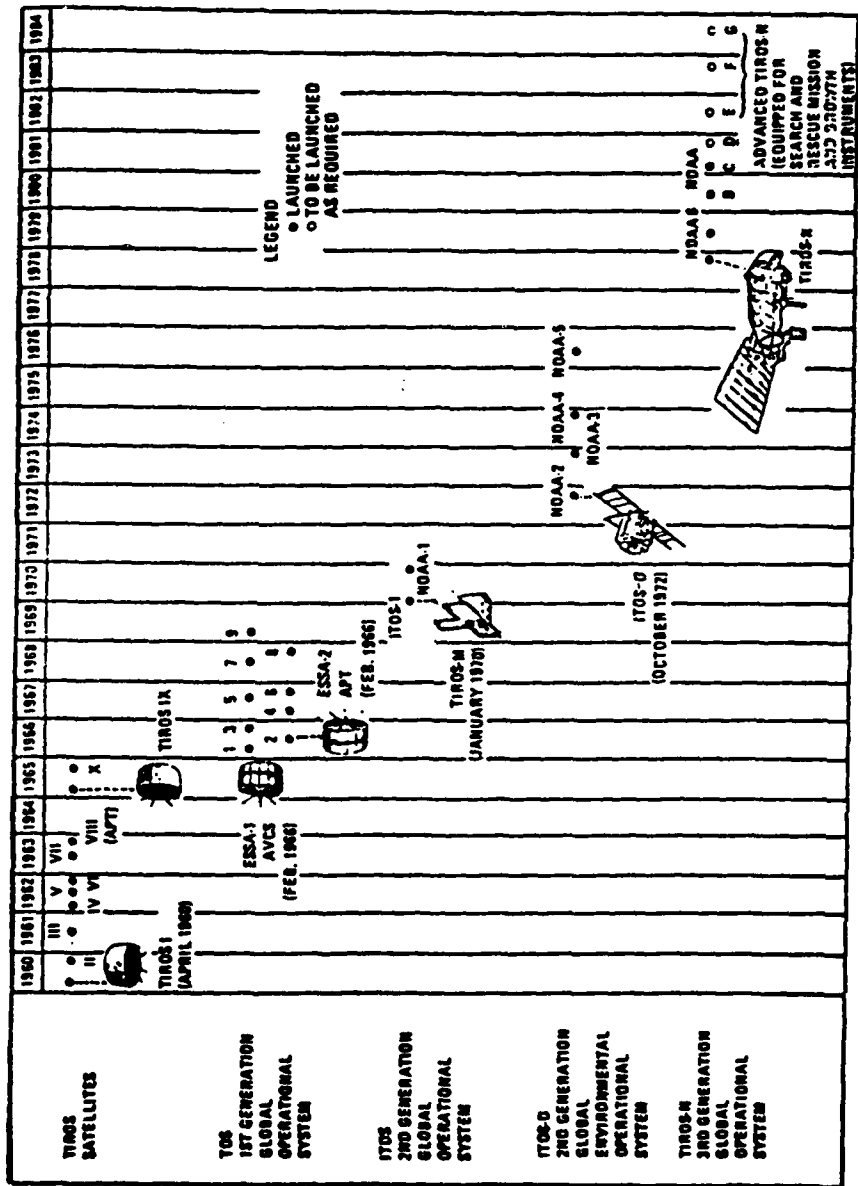
Figure 1.1 Evolution of TIROS/ESSA/ITOS/NOAA Meteorological Satellites
From Allison (1980, Figure 2)
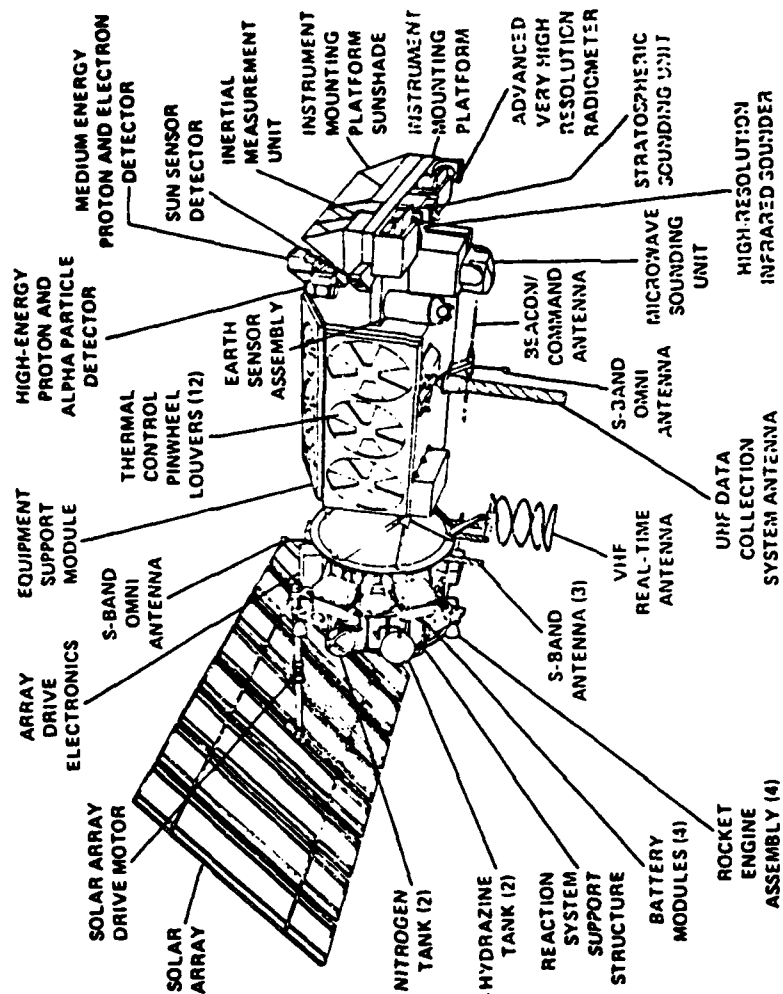
Figure 1.2 TIROS-N Spacecraft
From Allison (1980, Figure 6)

tional polar orbiting environmental satellite system.
TIROS-N, which was the research and development vehicle was
followed by the operational satellites: NOAA-6, NOAA-7, and
NOAA-8. Gray et al. (1981) and Barnes and Smallwood (1982)
summarize the characteristics of these satellites. The
satellites are near polar, sun synchronous, with an inclina-
tion of about 99°, a nominal height of 833 km (521 miles)
and an orbital period of 102 minutes.

The orbit period of the satellite determines the longi-
tudinal distance between successive equatorial crossings.
For the NOAA series satellites the longitudinal difference
is 25°. The satellites execute 14.2 orbits per day. See
figure 1.3. Because the number of orbits per day is not an
integer, the satellite subtrack precesses approximately 3°
longitude per day at the equator. Local equatorial crossing
time for NOAA-7, which provided the data for this study, is
1430 Local Time (2030Z).

NOAA-7 has several sensor systems on board: the
Advanced Very High Resolution Radiaometer (AVHRR), the TIROS
Operational Vertical Sounder (TOVS), the Data Collection
System and the Space Environmental Monitor (SEM). Allison
and Schnapf (1983) discuss these systems. Details of the
AVHRR are reviewed below.

AVHRR BACKGROUND

The AVHRR is a multispectral scanning system acquiring
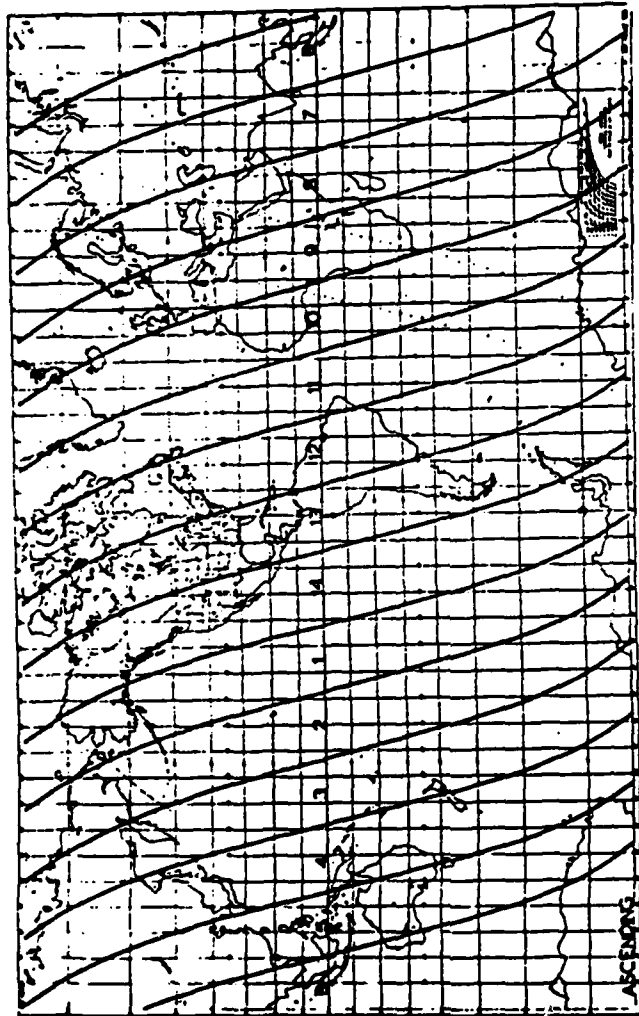
Figure 1.3 NOAA-7 Orbital Track
From Dismachek, et al (1980, Figure 9)

radiance data in two reflective spectral bands and three emittive bands. See Figure 1.4. Each channel or band has an instantaneous field of view of 1.4 milliradians. Nadir resolution is one kilometer. The channel characteristics are shown in Table 1.

The AVHRR scan is perpendicular to the orbital plane with a scan rate of six scans per second. NOAA-7 sees the earth in an angle of +56° from nadir. The scan line covers a swath approximately 2700 km long and consists of 2048 samples or targets. See Figures 1.5, 1.6 and 1.7. Each sample is termed a local area coverage (LAC) spot or pixel. Energy received at the sensor for each channel is sensed and digitized into 1024 levels (10 bit) for all bands. This combination of sensing and sampling results in a very large number of data values. Gruber et al. (1983) calculate that one second of data, equivalent to approximately seven kilometers movement of satellite nadir point, consisting of five channels times 2048 locations per scan times six lines equals 61440 data values.

Data taken during six minutes of orbit fill a 1600 bits per inch tape with more than 21.6 million radiance data values. The resulting "scene" is an earth swath of 2200 km X 2700 km. See Figure 1.7. Data from the AVHRR can be provided in four modes. Gray and et al. (1981) explain these modes. They note that two of the modes, Automatic Picture Transmission mode and the High Resolution Picture Transmission mode, send data earthward instantaneously for
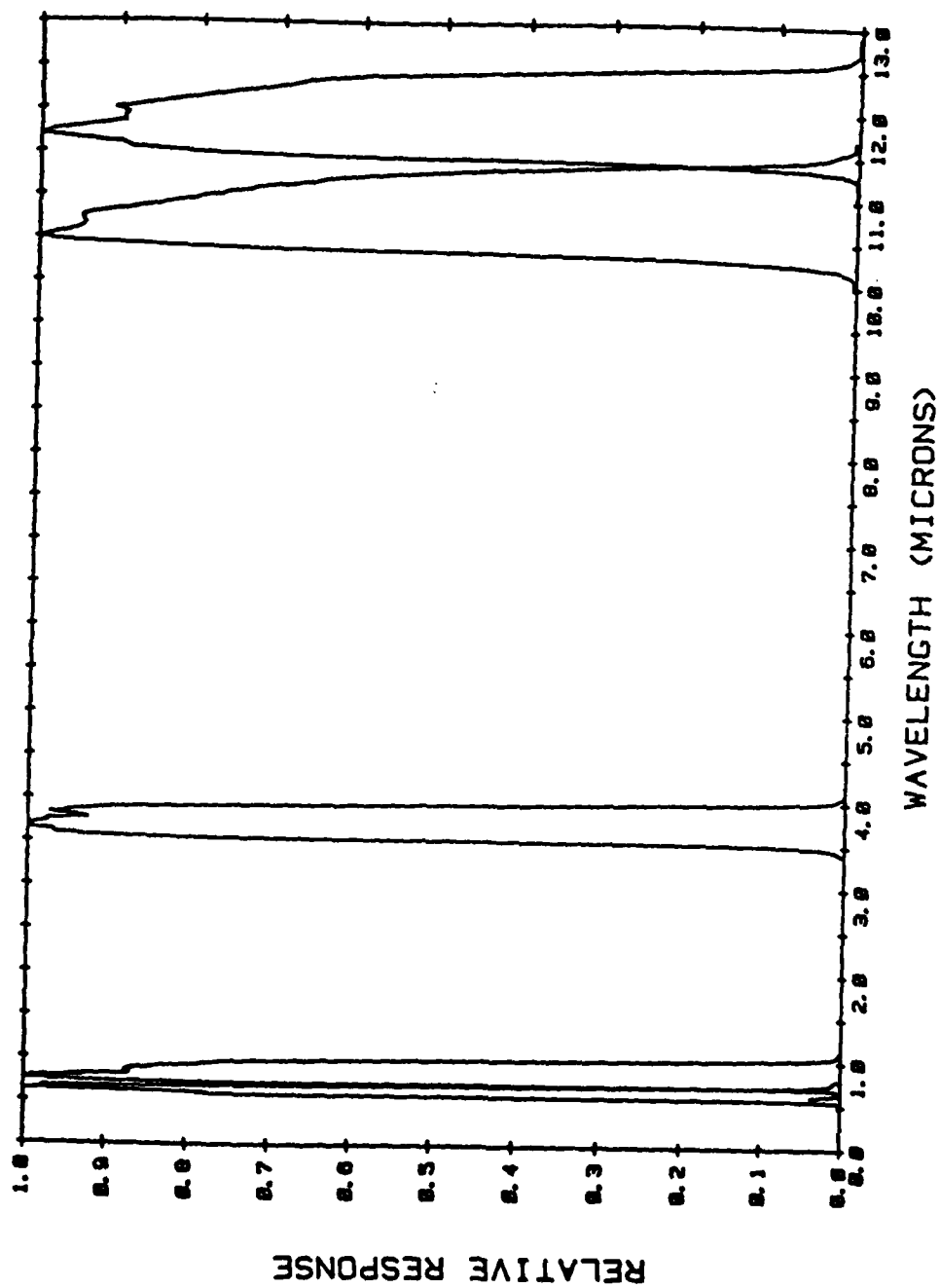
Figure 1.4 Spectral response of the five channels of the NOAA-7 AVHRR
From Gruber, Ruff and Earnest (1983, Figure 1)

NOAA-7 AVHRR Channel Characteristics

Channel*	Resolution at Subpoint	Wavelength (µm)	Primary Use
1	1 km	0.55 – 0.68	Daytime Cloud and Surface Mapping
2	1 km	0.725 – 1.10	Surface Water Delineation
3	1 km	3.55 – 3.93	SST, Nighttime Cloud Mapping
4	1 km	10.5 – 11.5	SST, Day/Night Cloud Mapping
5	1 km	11.5 – 12.5	SST

Table 1
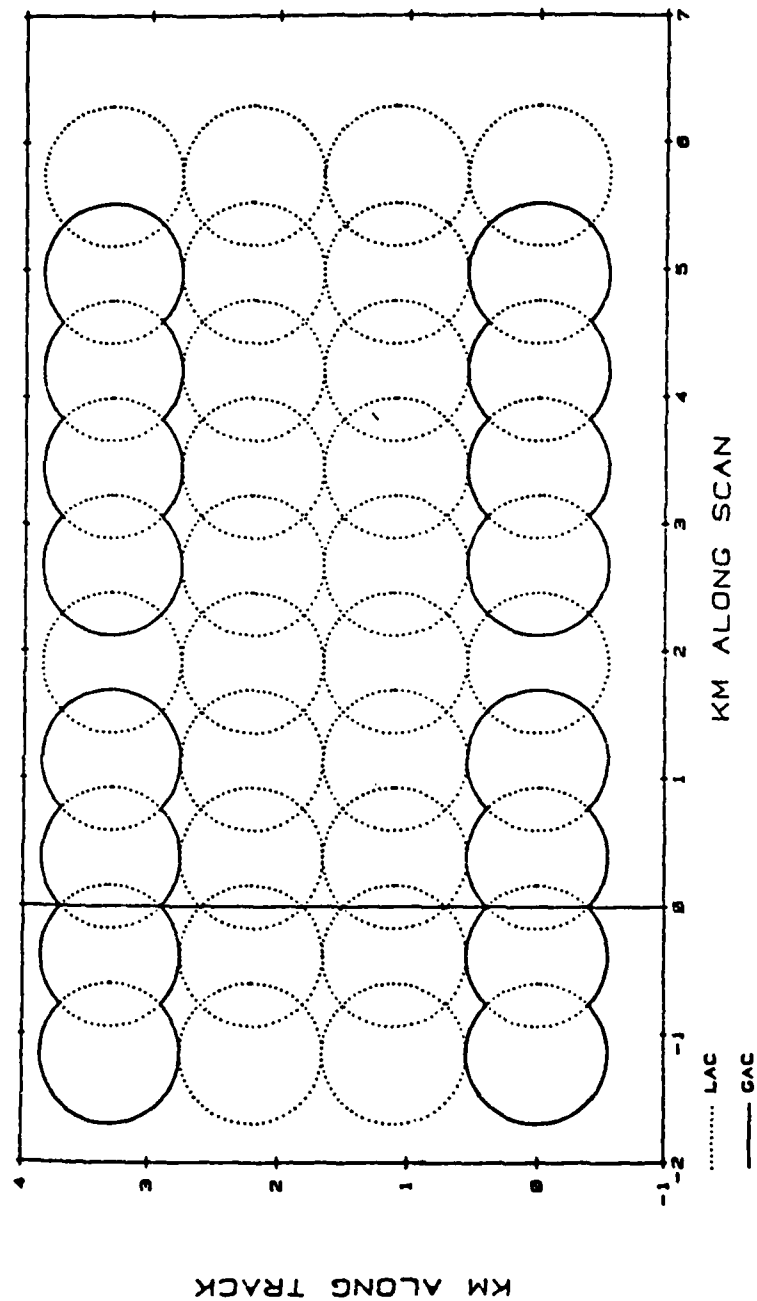
Figure 1.5 Local Area Coverage and Global Area Coverage Spots
From Gruber, Ruff and Earnest (1983, Figure 3)

KM ALONG SCAN

KM ALONG TRACK

.... LAC

——— GAC
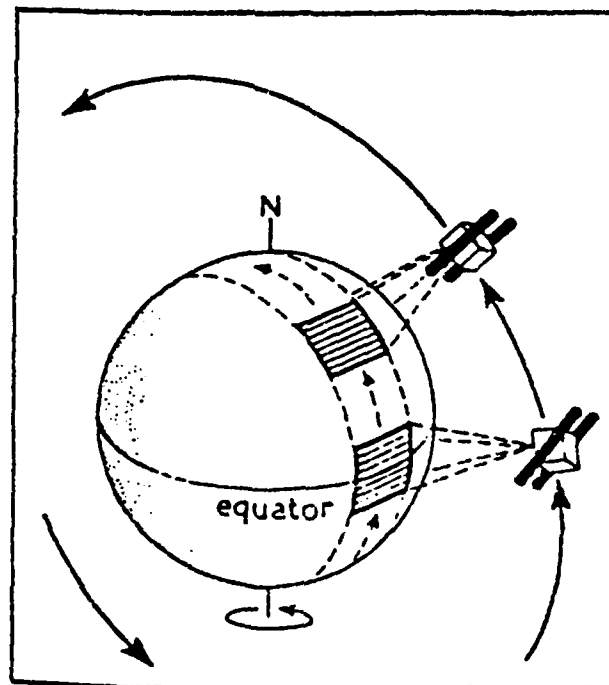
Figure 1.6 Orbital Characteristics of NOAA Weather
Satellites
After Barrett (1974, Figure 2.1)
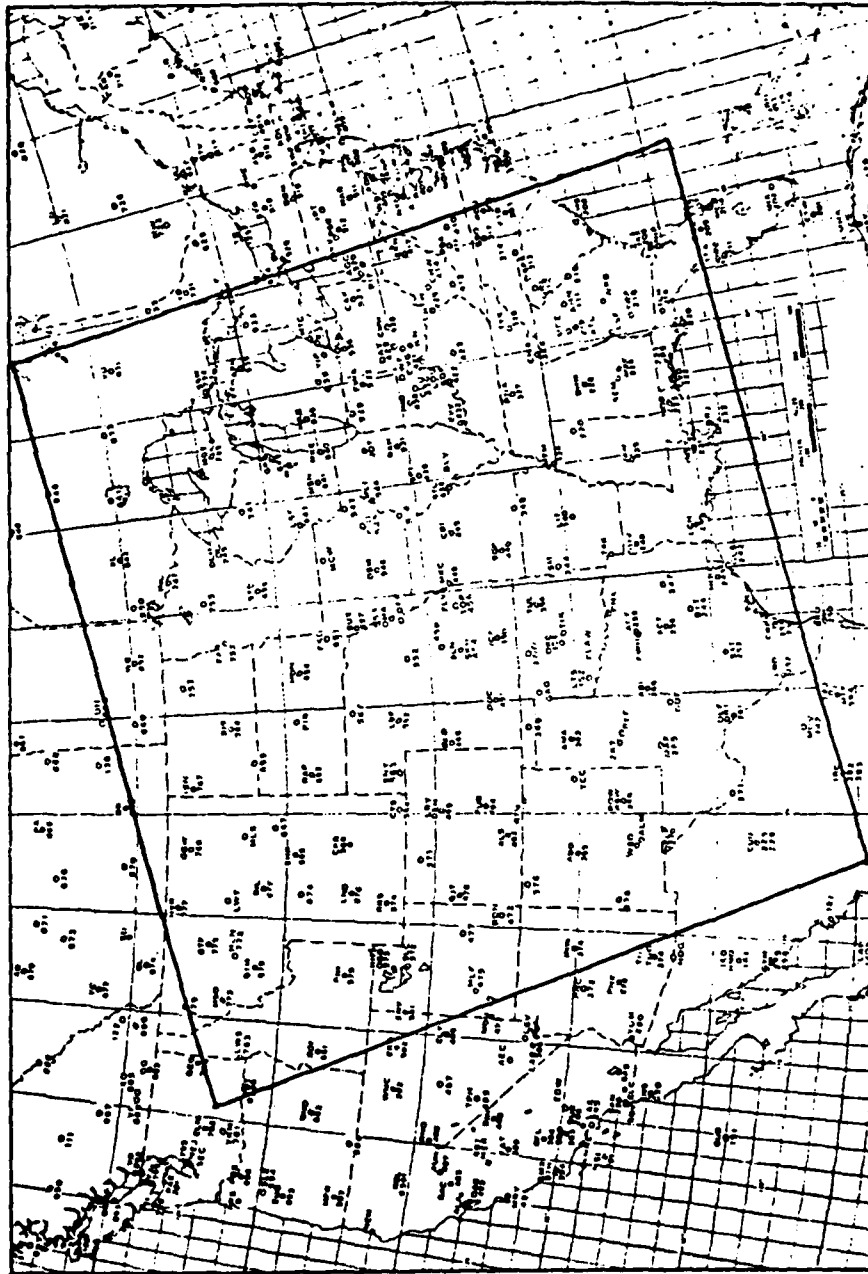
Figure 1.7 Typical LAC Scene

operational use. The other two modes store data on board for later playback. LAC data is one kilometer resolution data which is first stored on board the satellite, then played back to designated receiving stations where it is stored on tape. Global Area Coverage (GAC) data are an averaged and sampled subset of LAC data which is first stored on board the satellite, then played back to ground receiving stations. See Figure 1.5.

GAC data, in general, is the source of most vegetative index products. The large number of data values producd by LAC coverage makes data management unfeasible for routine use. This fine resolution data is most useful however, for case studies and research and development of new methodologies.

REMOTE SENSORS AS VEGETATIVE ASSESSMENT TOOLS

The Landsat satellites with their Multispectral Scanner (MSS) system expanded the ability to generate, process and apply data remotely sensed from space. Data from the MSS afforded the capability to provide timely information of global extent, about the condition of various crops needed for food throughout the world. Lillisand and Kiefer (1979) explain that Large Area Crop Inventory Experiment (LACIE), conducted by NASA, NOAA and the United States Department of Agriculture (USDA), combined Landsat data with climatic data to predict the yield of the world's major wheat crops.

Also, according to Lillesand and Kiefer, the inventory
experiment was designed to achieve monthly at-harvest
production estimates that would converge to within ten
percent of the true estimate at the national level with a
confidence of ninety percent. Myers (1983) states that the
success of LACIE led to further research and development in
the assessment of crop conditions. A brief theoretical
background of the assessment method is given in Chapter II
of this paper.

Agriculture and Resources Inventory Surveys Through
Aerospace Remote Sensing (AgRISTARS), a joint program
between USDA, NASA, NOAA, the Agency for International
Development and the United States Department of the
Interior, supported research which applied Landsat data to
assessment of the world's agriculture. An AgRISTARS group,
Early Warning/Crop Condition Assessment (EW/CCA) evaluated
kinds of crops, health of of crops, stages of growth and
crop yield/productivity. Data used in the assessment came
from Landsat spectral channels sensing in the visible and
near infrared (channels 4 through 7). Unfortunately, acqui-
sition times for complete data sets were (and are) so infre-
quent that important information about time varying-physical
events and earth surface features often could not be
captured. The shortest time between Landsat acquisitions
for the same area is 18 days.

In addition to the low frequency of Landsat coverage
clouds often obscured the surface resulting in unacceptable

temporal gaps in assessment data sets.   A combination of
temporal gaps and Landsat breakdowns forced researchers to
seek other data sources.   Gray and McCrary (1981a) showed
that the NOAA-6 AVHRR vegetative index correlated well with
the vegetative index calculated from MSS data.   They found
the AVHRR response provided useful information about vegeta-
tive responses to moisture availability.   This fact combined
with NOAA-X satellites' nearly daily data acquisition led
Gray and McCrary (1981a and 1982) and Horvath et al. (1982)
to conclude that the TIROS-N/NOAA-X satellites met many of
the needs of the crop assessment community.

CHAPTER II

VEGETATIVE INDICES

BACKGROUND

Allison and Schnapf (1983) note that the TIROS satel-
lites have been the principal global operational meteorolog-
ical satellites for the United States for the last 22 years.
As mentioned in Chapter 1, researchers during the last five
years have expanded the use of TIROS-N/NOAA-X data to other
than meteorological applications. Vegetation assessment is
one of these applications.

Research using visible and near infrared spectral bands
for monitoring vegetation have been reviewed by Tucker et
al. (1981), Holben et al. (1983) and numerous others. Tuck-
er et al. (1981) reported that red and photographic infrared
specral data were highly related to vigor and condition of
the plant canopy and were quantitatively correlated with
total dry-matter accumulation in winter wheat. Tucker et
al. further proposed a satellite system to provide large
area assessment of total dry matter accumulation or net
primary production from terrestrial vegetation.

Schneider et al. (1981) investigated the use of the

AVHRR for land remote sensing. They determined that: (1) vegetation response is greater in the near infrared than in the visible and (2) the spectral responses or albedo difference of plants is related to chlorophyll content or green leaf biomass. Schneider went on to recommend that albedo difference pictures, i.e., AVHRR Channel 2 minus Channel 1 pictures, be generated on computer interactive systems and color coded for use in general terrain classification. (Work in this area continues at the University of Missouri Geographic Resources Center). Additionally, Gray and McCrary (1981a) found that plant stress detection could be accomplished by relating the albedo differences to browning and/or drying of vegetation.

Applications of these findings expanded immediately and related research reports continue to fill the remote sensing journals. Barnett and Thompson (1982) reported success in using large area spectral data in wheat yield estimation. Most recently Tucker et al. (1984) determined that AVHRR data were useful for monitoring large areas of vegetation in the Nile River Valley. Tucker et al. emphasized that atmospheric effects must be quantified for specific inventory purposes. They also noted that the addition of thermal emissive channel data was valuable for detecting clouds. Norwine and Greegor (1983) developed a technique for vegetation classification and formulated a vegetation gradient based on climatic and meteorological satellite data.

THEORY

Solar radiation impinging upon the earth's surface is either reflected, absorbed or transmitted. Total radiation received at the earth's surface can be expressed as:

$$E(INC) = E(REF) + E(ABS) + E(TRN) \qquad (2.1)$$

E(INC) denotes incident energy
E(REF) denotes reflected energy
E(ABS) denotes absorbed energy
E(TRN) denotes transmitted energy

The terms in equation 2.1 can be divided by the incident energy resulting in

$$REF + ABS + TRN = 1 \qquad (2.2)$$

REF is reflectivity

ABS is absorptivity

TRN is transmissivity

Since most land features are optically dense, transmitted energy for these features is approximately equal to zero. Thus, equation (2.1) reduces to

$$E(INC) = E(REF) + E(ABS) \qquad (2.3)$$

or

$$REF + ABS = 1 \qquad (2.4)$$

Curves of reflectivity versus wavelength or of absorptivity versus wavelength for various surface features can be constructed from laboratory or field measurement. For plant-soil surfaces there are very discrete physical phenomena which cause the characteristic shapes of reflectivity curves.

Numerous studies about the interaction between plants and electromagnetic energy have been made. See, for example, Knipling (1970), Hoffer and Johannsen (1969), Tucker et al. (1981) and Horler et al. (1983). Smith (1983) summarizes the work published before 1982.

Figure 2.1 shows the reflectivity of a green leaf. Figure 2.2 shows reflectivity curves for typical green vegetation and soil. Myers (1983) and Horler et al. (1983) describe green leaf reflectivity properties. They note that the chlorophyll of green leaves usually absorbs seventy to ninety per cent of the light in the blue part of the spectrum, resulting in low reflectivity in that region. Another chlorophyll absorption peak occurs at .68 μm. Chlorophyll is a less effective absorber near .55 μm, hence, there is an absorption minima or a reflectivity peak in the curve.

According to the authors of _Biology Today_, seventy to ninety percent of the impinging radiation is absorbed by plant chlorophyll and used to convert two extremely stable,
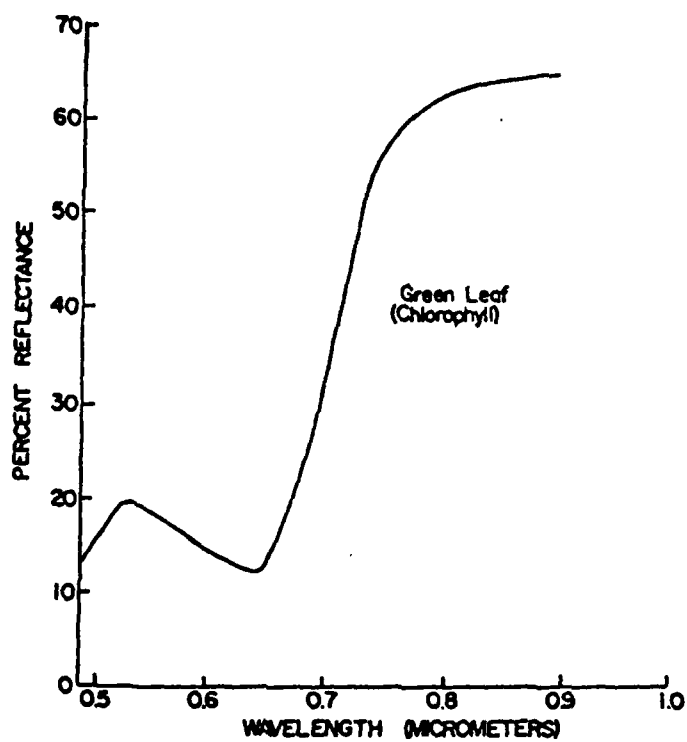
Figure 2.1 Spectral Response Curve for a Green Leaf
After Hoffer and Johannsen (1969)
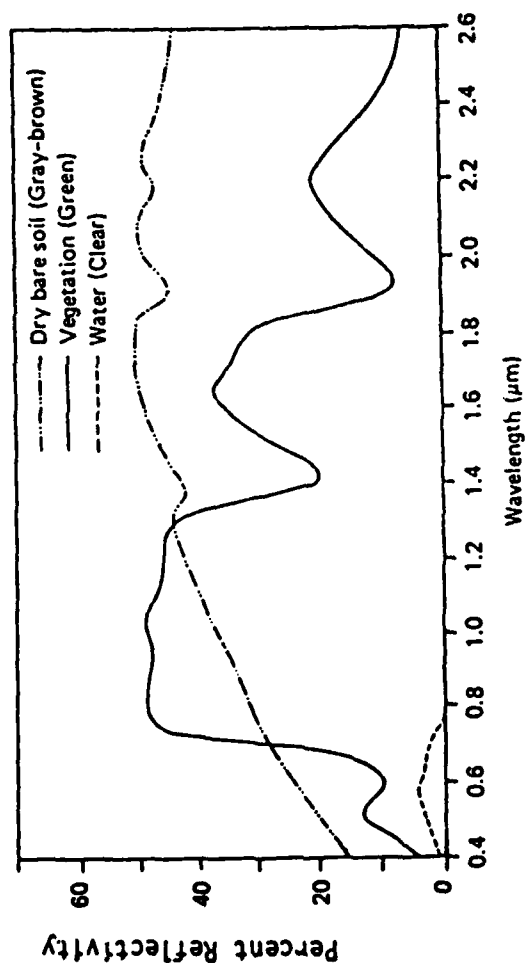
Figure 2.2 Typical Spectral Reflectance Curves for
Vegetation, Soil and Water

After Lillesand and Kiefer (1979, Figure 1.10)

low energy molecules (carbon dioxide and water) into an unstable energy-rich system consisting of organic matter and free oxygen. Most of the organic molecules created are sugars which can be further processed into starch and cellulose. Knipling (1970) reported that any physiological disturbance to a leaf usually results in an increase in visible light reflectivity. Chlorophyll degradation is a primary factor in this response. Myers (1983) suggests that a plant undergoing senescence shows an increase in light reflectivity in the .55 - .68 μm spectral band (AVHRR Channel 1) with respect to reflectivity in the near infrared band (AVHRR Channel 2).

Horler et al. (1983) describe the near infrared properties of leaves. They report that from .70 -1.10 μm chlorophyll is a poor absorber and that high, internal leaf scattering causes large, near infrared reflectivity. Hence, leaf reflectivity in the near infrared shows a dramatic increase over visible reflectivity. Reflectivity changes in the .70 - 1.10 μm band are associated with changes in the size and shape of cells and intercellular spaces. Myers (1983) reports that healthy leaves have high infrared reflectivity, usually in the range of sixty to seventy percent in the .70 to 1.30 μm range, as compared with low infrared reflectivity for unhealthy leaves. The difference in infrared reflectivity of well watered wheat and stressed wheat is shown in Figure 2.3.

These differences in reflected solar radiation are the
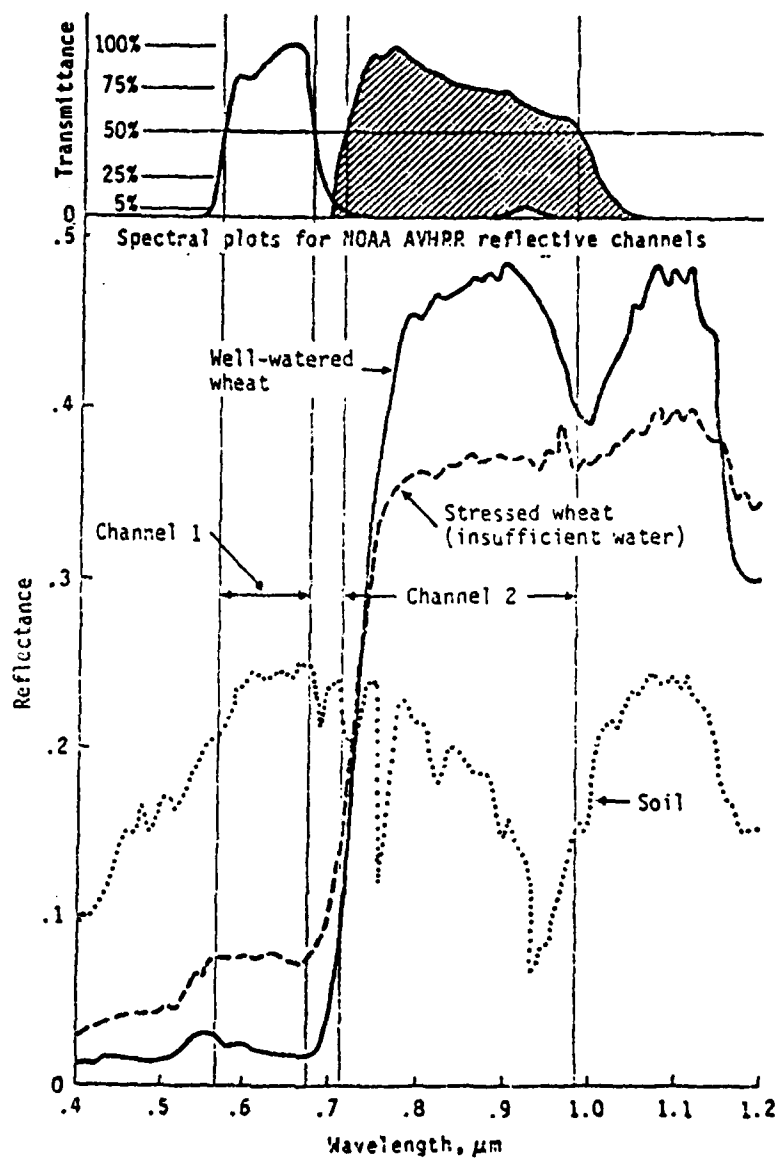
Figure 2.3   Response of NOAA AVHRR reflective channels
(wheat)
From Gray and McCrary (1981b, Figure 1)

basis for vegetative indices. The AVHRR senses reflected
solar energy in Channels one and two. A simple vegetative
index (VIN) can be computed by subtracting the value of
energy sensed by Channel 1 from the value of energy sensed
by Channel 2, as described in Chapter 1. To repeat:

$$VIN = CH2 - CH1 \tag{2.5}$$

As plants become less healthy or as senescence sets in, the
Channel 2 value drops while the Channel 1 value increases.
Thus, large values of VIN (holding viewing angle and sun
angle constant) indicate healthy green plants in the target
area while lower values indicate stress, end of growing
season, or a sparsity of green plants since Healthy plant
"scenes" have high Channel 2 values and low Channel 1
values. See figure 2.3.

   Yates et al. (1984)) states that a normalized vegeta-
tive index (NVI) can also be computed using:

$$NVI = \frac{CH2-CH1}{CH2+CH1} \tag{2.6}$$

He goes on to say that the normalized vegetative index is
preferred for global vegetation monitoring because it
partially compensates for changing illumination conditions,
surface slope and viewing aspect.

   Response curves for objects or surfaces other than
plants and soil are shown in Figure 2.4. Additionally,
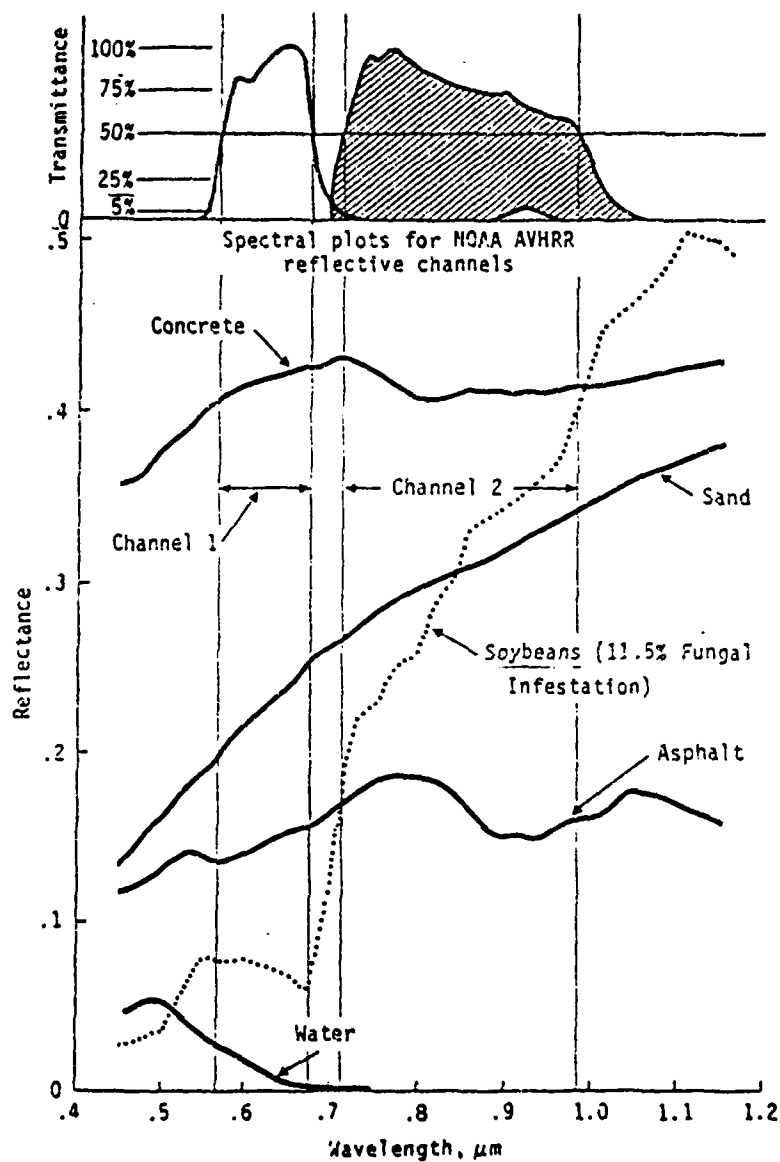
Figure 2.4 Response of NOAA AVHRR reflective channels
(concrete, asphalt, water, sand and beans)
From Gray and McCrary (1981b, Figure 2)

clouds, water and snow have the same or higher reflectivi-
ties in Channel 1 than in Channel 2, so these features have
a VIN equal to zero or a negative VIN. Rock and bare soil
have similar reflectivity in the two channels, which results
in a vegetative index near zero. Pixels containing large
amounts of clouds can usually be identified by their high
Channel 1 values, thus permitting the development of a
simple cloud screening scheme. Liquid water, on the other
hand, is a good absorber of energy sensed by Channel 2. As
a result, low Channel 2 values are recorded for water-filled
pixels. Thus, water-filled pixels can also be identified.
Tappan et al. (1983) used this fact for land/water discrimi-
nation.

Rarely does the AVHRR view a pixel that is pure vege-
tation. Even a pixel as small as one square kilometer will
contain bare soil, roads, water and possibly clouds. These
features do not exhibit the sharp differences in reflectivi-
ty curves that occur with plants. The VIN for a pixel which
includes these features will be reduced by comparison to
vegetation-filled pixels. Figure 2.5 show the result of
mixed pixel returns to the AVHRR.

According to the NOAA Satellite Data Services Division
Vegetation Index User's Guide, atmospheric effects such as
Rayleigh scattering, scattering by dust and aerosols and sub
pixel-sized clouds all tend to increase Channel 1 with
respect to Channel 2 and reduce the computed VIN. Further,
the Guide states that this reduction tends to be greater at

Pure pixel VIN value
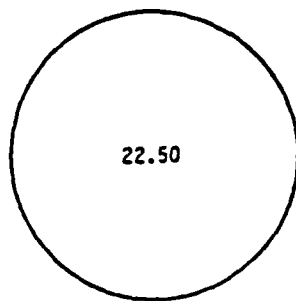
Mixed pixel VIN value

22.50

14.04
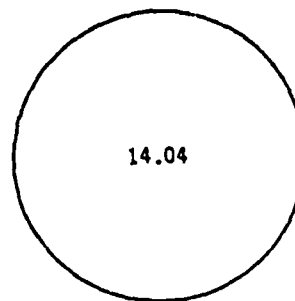
Surface	VIN Value	Surface	VIN Value
100% well-watered wheat	24.50 (channel 2)	60% well-watered wheat	13.50
	2.00 (channel 1)	20% soil	.80
		15% clouds	- .23
	22.50 VIN	5% water	- .03
			14.04 VIN

Figure 2.5   Comparison of synthetic VIN values for pure and
mixed pixels.   After Horvath et al (1982, Figure 3.2)

higher scan angles.

Recent studies by Holben and Fraser (1984), Barnett (1984) and the results of this study dispute these statements. Holben and Fraser found that Mie Scattering, which increases Channel 2 with respect to Channel 1, causes an increase in the VIN, especially at higher scan angles. See Chapter III for a more in-depth discussion of scattering.

CHAPTER III

ELECTROMAGNETIC RADIATIVE TRANSFER

GENERAL

This chapter is a general summary of the properties of electromagnetic (EM) radiation, the interaction of this radiation with matter and the application of the properties of EM radiation to remote sensing. In this chapter the development of EM theory and the description of the way it interacts with matter is derived from similar developments by Wallace and Hobbs (1977) and Fleagle and Businger (1980).

Radiative energy transfer is responsible for nearly all energy exchange between the earth and the rest of the universe. Battan (1984) states that the earth intercepts approximately 1.8×10^{17} watts of solar energy. This is five orders of magnitude larger than any other extraterrestrial source. Hence, the sun, for meteorological purposes, can be considered the sole source of extraterrestrial energy.

Electromagnetic radiative transfer is one of several exchange mechanisms for transferring energy between the atmosphere and the underlying surface and between layers in

the atmosphere.   Fleagle and Businger (1980) assert that for

the atmosphere alone, EM radiation transfer is the most

important energy transfer process.

PROPERTIES OF ELECTROMAGNETIC ENERGY

An EM wave is energy in transit or radiant energy Q.   Q

is expressed in units of joules.   Suits (1983) writes that:

"The energy carried by an electomagnetic wave is a measure

of the capacity of the radiation to do physical work by

moving something by a force, to heat an object or to cause a

change of state of matter."   All EM energy is inherently

similar and propagates in a vacuum at 2.9979×10^{10} cm per

sec and through air at nearly the same speed.   This speed is

also known as the velocity of light, C.   From basic physics,

waves obey the formula C equals frequency times wavelength

or, symbolically,

$$C = f \times \lambda \qquad\qquad (3.1)$$

Another important property of radiation is its wave-

length.   All wavelengths greater than zero are possible.

The collection of all possible EM wavelengths is called the

electromagnetic spectrum.   The EM spectrum and its important

categories are shown in Figure 3.1.   Electromagnetic energy

in the visible part of the spectrum is commonly referred to

as light.
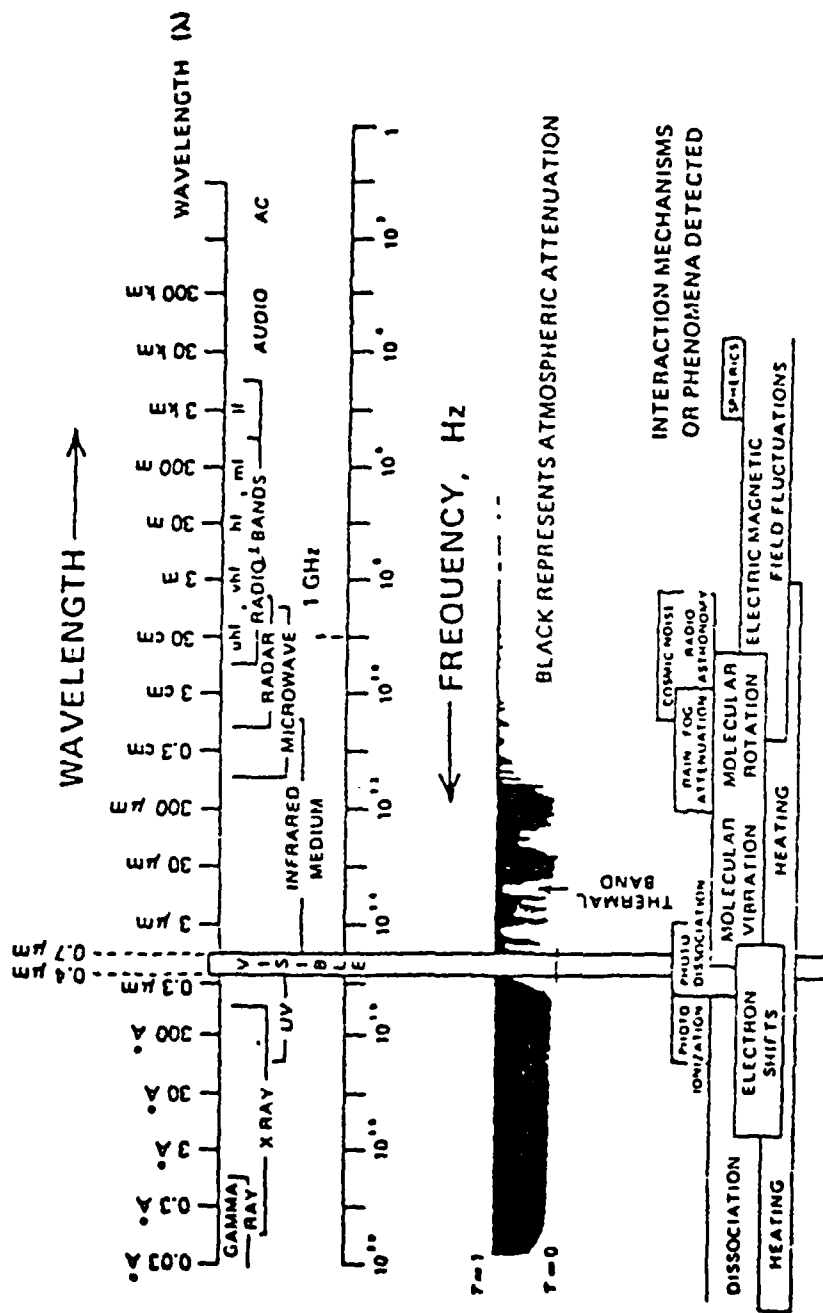
Figure 3.1 The Electromagnetic Spectrum From Suits (1983, Figure 2.3)

The amount of radiant energy passing an area per unit time is the radiant flux, Φ. The units of radiant flux are joules per second or Watts. Radiant flux per unit area is flux density, or irradiance. Irradiance can be expressed as

$$E = \frac{d^2 Q}{dAdt} \qquad (3.2)$$

where Q is radiant energy and E is expressed in units of watts per square meter. Irradiance may consist of contributions of radiant energy from an infinity of different directions.

Several basic interactions between matter and energy can be described using irradiance and the basic law of conservation of energy. First, materials have certain intrinsic properties: monochromatic absorptivity, monochromatic reflectivity, monochromatic transmissivity and monochromatic emissivity. The first three properties are a measure of absorbed, reflected, and transmitted irradiance, respectively, compared to incident irradiance, i.e.,

$$a_\lambda = E_\lambda (ABS)/E_\lambda (INC) \qquad (3.3)$$

$$r_\lambda = E_\lambda (REF)/E_\lambda (INC) \qquad (3.4)$$

$$\tau_\lambda = E_\lambda (TRN)/E_\lambda (INC) \qquad (3.5)$$

E_λ (ABS) is the absorbed irradiance

E_λ (REF) is the reflected irradiance

E_λ (TRN) is the transmitted irradiance

E_λ (INC) is the incident irradiance

The subscript λ indicates that the quantity is for one wave-length. As previously noted, conservation of energy implies:

$$a_\lambda + r_\lambda + \tau_\lambda = 1 \qquad (3.6)$$

Monochromatic emissivity, as a function of wavelength and temperature, will be discussed after a review of emitted energy.

Radiance, L, is defined as the radiant energy per unit time (or irradiance) coming from a specific direction within some specified infinitesimal arc of solid angle $d\omega$, and passing through a unit area perpendicular to that direction. Thus, radiance may be expressed as:

$$L = \frac{dE}{\cos \theta \, d\omega} \qquad (3.7)$$

θ is the zenith angle which is the angle between the direction of the radiation and the normal to the surface receiving the radiation

dω is the solid angle through which energy is
received

Radiance is expressed in units of watts per square meter per

steradian.   Equation 3.7 can be rearranged to express the

radiance normal to the surface receiving the radiation:

$$L \cos \theta = \frac{dE}{d\omega} \qquad (3.8)$$

If the radiance does not vary with direction (isotropic

radiation) then the irradiance is the sum of the normal

component of radiation coming from the entire hemisphere:

$$E = \int_0^{2\pi} L \cos \theta \, d\omega \qquad (3.9)$$

Radiation originating at a distant point source can be

considered to propagate in a single direction toward the

receiving surface.   Hence, dω vanishes and L is undefined.

This special case is referred to as parallel beam propa-

gation.   Coulson (1975) notes that solar energy reaches the

earth as an approximately parallel beam.

Any substance whose temperature is greater than abso-

lute zero radiates energy.   The maximum radiation that can

be emitted by any body at a given temperature is called

blackbody radiation.   The distribution of emitted radiation

for a blackbody with temperature T is called the Planck

Function. It can be expressed by Planck's Law of Blackbody
Radiance:

$$L_{bb} = c_1/\lambda^5 [\exp(c_2/(\lambda T)-1] \tag{3.10}$$

$$c_1 = 3.74 \times 10^{-16} Wm^2$$
$$c_2 = 1.44 \times 10^{-2} m^\circ K$$
$$\lambda = wavelength$$
$$T = temperature\ in\ degrees\ Kelvin$$
$$L_{bb} = blackbody\ radiance$$

The higher the temperature the greater the emitted energy.

The quantity of energy emitted at all wavelengths by a
unit area of a body having a Kelvin temperature of T, is
proportional to the fourth power of T, or:

$$L_{bb} = bT^4 \tag{3.11}$$

where b is a combination of all the constants involved in
the integration of the Planck Function. Since blackbody
radiation is isotropic:

$$E_{bb} = \pi bT^4 = \sigma T^4 \tag{3.12}$$

This equation is the Stefan-Boltzman Law where σ, the
Stefan-Boltzman constant, is equal to 5.67×10^{-8} W m^{-2} $\circ$ E
is the irradiance of a blackbody. Figure 3.2 is a graph of
the blackbody spectra of the sun, a typical incandescent
lamp and the earth.

Of course, real materials rarely behave as blackbodies.

In general, real materials emit an irradiance that is some
fraction of what would be emitted if the material were a
blackbody at the same temperature. This fractional flux is
called the emissivity and may be expressed as

$$e_\lambda = E_\lambda (EMT)/E_{bb} \qquad (3.13)$$

   $E_\lambda(EMT)$ is the irradiance emitted by a real material
           or the emittance

Emissivity is an intrinsic property of each substance in the
universe.

   The Stefan Boltzman Law, equation 3.12, can be modified
to describe the reduced irradiance, or graybody irradiance,
by including the emissivity factor. Thus, for a graybody

$$E = e\sigma T^4 \qquad (3.14)$$

where e is the graybody emissivity. The emissivity is less
than one but constant for all wavelengths. If the emissivi-
ty of any object varies with wavelenghth the object is
called a selective emitter. Most materials are selective
emitters

   Kirchoff's Law, which can be expressed as

$$a_\lambda = e_\lambda \qquad (3.15)$$
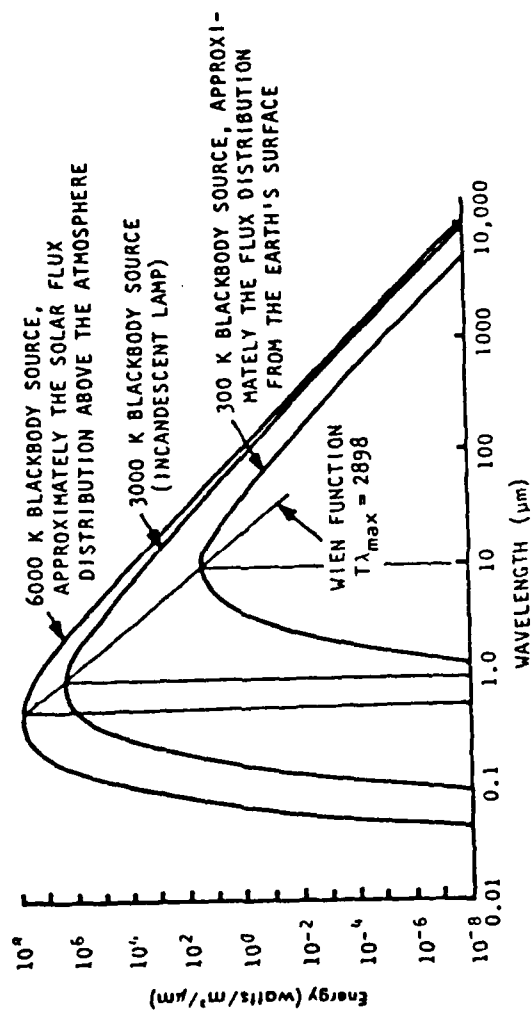
Figure 3.2 Blackbody spectra for the sun, an incandescent lamp and the earth's surface

states that a strong absorber will be a strong emitter.
This law applies at any given wavelength. Caution must be
exercised in applying this law across the EM spectrum since
it is only at radiative equilibrium that total emission over
all wavelengths equals total absorption over all
wavelengths.

Differentiating the Planck function with respect to
wavelength and setting the result equal to zero will give
the wavelength of maximum energy emission, $\lambda(MAX)$. The
resulting equation is Wein's Displacement Law.

$$\lambda(MAX) = \frac{2897 \mu m^\circ K}{T} \tag{3.16}$$

Figure 3.2 illustrates that lower temperatures result in
lower emitted energies (area under the Planck curve equals
emitted energy) and that the wavelength of maximum energy
emission shifts to longer wavelengths as the temperature of
a body decreases.

Fleagle and Businger (1980) state that, for all practi-
cal purposes, the entire solar spectrum is at wavelengths
less than 4 μm and the whole terrestrial spectrum is at
wavelengths greater than 4 μm. The two spectra are effec-
tively divided by the 4 μm line. The sun emits the maximum
energy in the visible portion of the EM spectrum near .5 μm,
while maximum earth emission is near 10 μm.

The latter emission correlates with terrestrial heat

and is often called "thermal," "thermal infrared," or "emit-
ted infrared," energy. According to Lillisand and Kiefer
(1979) this energy is best sensed with radiometers. Sensors
operating in the 8-14 μm region detect the thermal infrared
energy emmitted by the earth and the atmosphere. Sensors
operating in the spectral bands from .3 μm to approximately
1.3 μm detect reflected solar energy. Energy in this region
is either reflected visible or reflected infrared.
Reflected infrared may also be called "near infrared."

ENERGY INTERACTIONS WITH THE ATMOSPHERE

Radiation travelling from the sun through essentially
free space arrives at the outer reaches of the earth's
atmosphere almost completely unattenuated. However, inter-
action with atmosphere reduces the intensity of solar radi-
ation reaching the earth's surface and alters its spectral
composition. Figure 3.3 shows, among other features, the
relative amount of energy from the direct solar beam reach-
ing the earth's surface after attenuation through "one
optical air mass" or "one path length."

Otterman and Robinove (1981) note that the task of
detecting changes on the earth's surface based on measure-
ments of changes of spectral reflectivity,

> "...is complex because the surface is not directly
> measured by a satellite borne radiometer; it is
> the radiance above the atmosphere, which is
> affected by the atmospheric conditions as well as

Figure 3.3 Calculated and Observed Spectra of Radiant Energy from the Sun and the Earth. The blackbody radiation, at 6000°K, is reduced by the square of the ratio of the sun's radius to the average distance between the sun and the earth in order to give the energy flux that would be incident on the top of the earth's atmosphere. After W.D. Sellers, (1965)
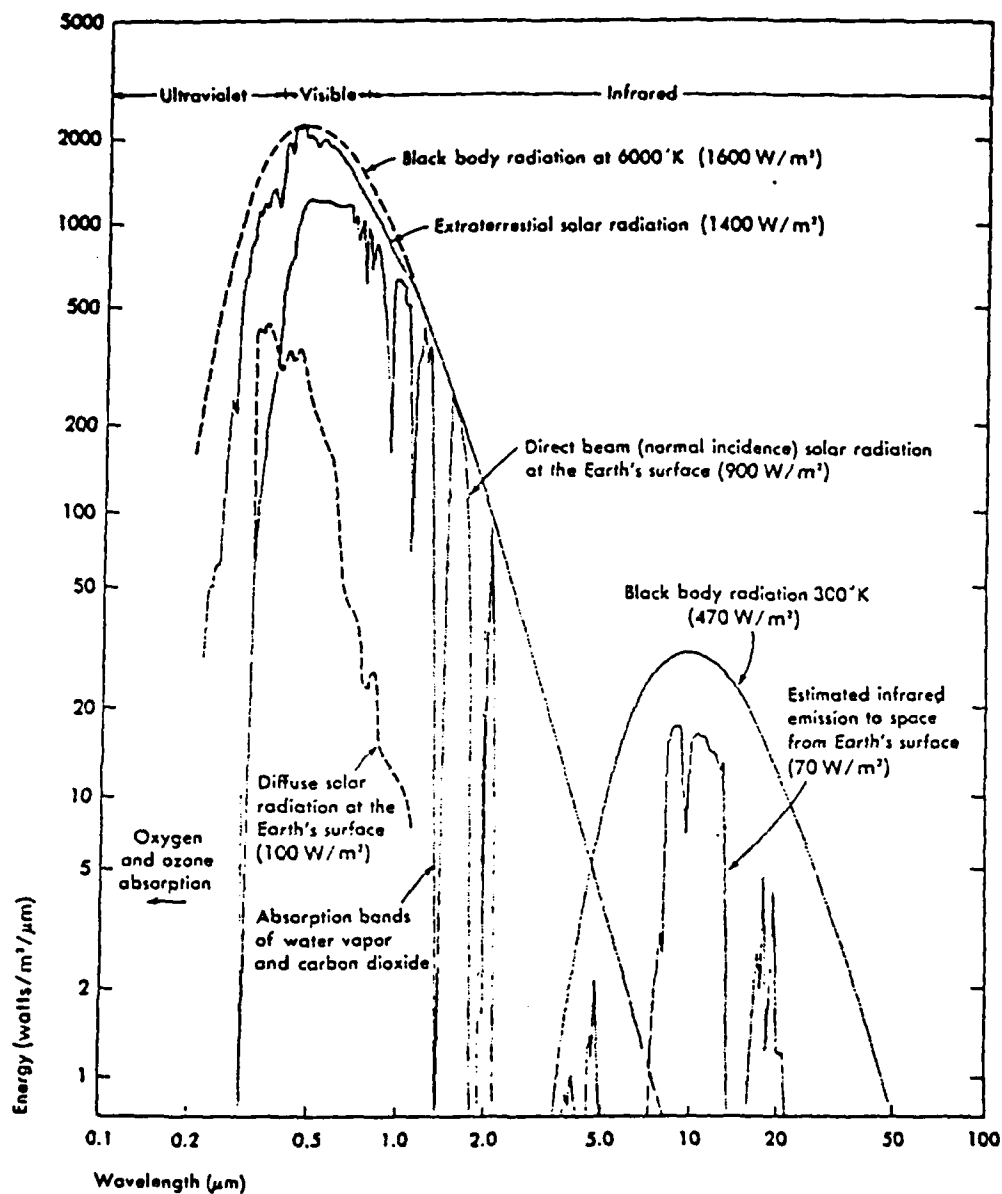
by surface characteristics which is measured
instead."

The net effect of the atmosphere varies with differ-
ences in path length, magnitude of the energy being sensed,
the atmospheric conditions present and the wavelength
involved. It is generally accepted that attenuation effects
are principally the result of scattering and absorption.

ATMOSPHERIC SCATTERING

Lillisand and Kiefer (1979) write that atmospheric
scattering is the unpredictable redirection of radiation by
particles in the atmosphere. Scattering in the atmosphere
is almost always a multiple process. Slater (1980)
describes this scatte. ig process as dependent on the size
distribution of the scattering elements, their composition
and concentration and the wavelength or wavelength distrib-
ution of the radiant flux incident on them. According to
Sabins (1978) atmospheric scattering effects are generally
limited to the solar portion of the EM spectrum.

Slater (1983) presents a very useful diagram in
explaining scattering. A modified version of the diagram is
shown Figure 3.4. When particles are much smaller than the
wavelength, the scattered power is inversely proportional to
the fourth power of the wavelength. This scattering is
termed Rayleigh scattering. Rayleigh scattering is most
pronounced in the shorter solar wavelengths from the ultra-
violet wavelengths to approximately .7 μm. See figure 3.4.
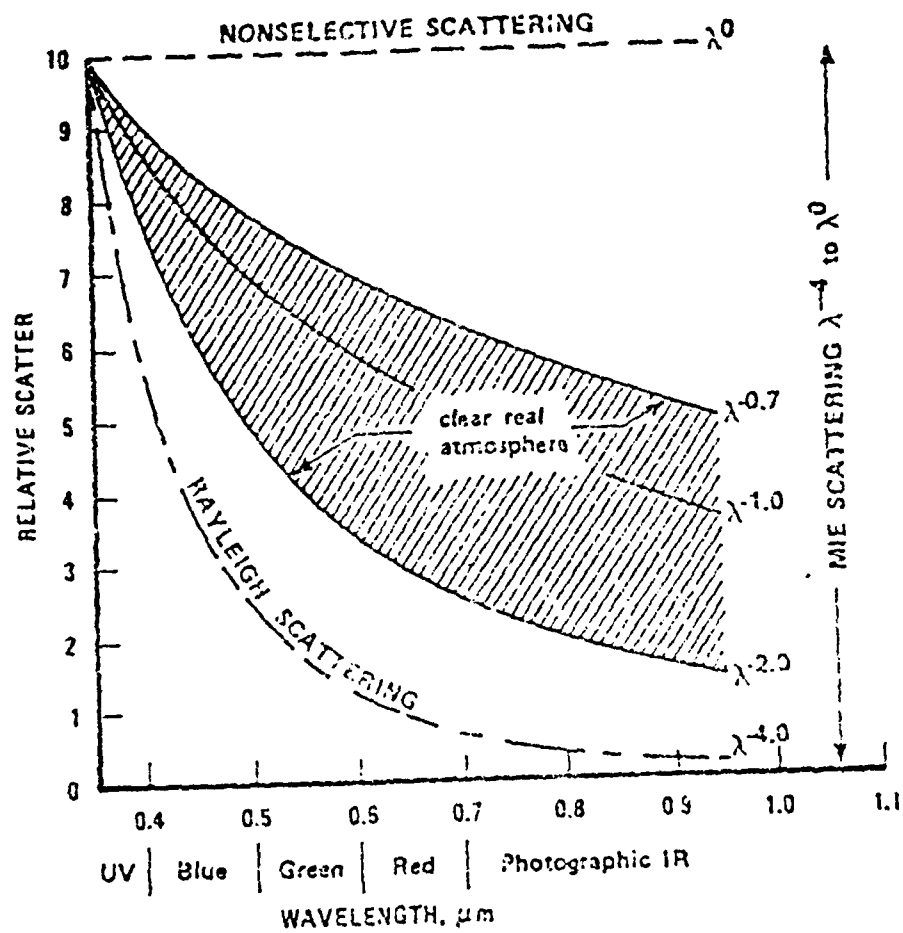
Figure 3.4 Selective Scattering (Rayleigh and Mie) and
Nonselective Scattering as a Function of Wavelength. The
shaded region indicates the range of scattering caused by
typical atmospheres. From Slater (1983, Figure 6-15).

According to Lillisand and Keifer (1979) this type of scat-
tering is the primary cause of "haze" or loss of contrast in
visible imagery. Wallace and Hobbs (1977) state that, in
general, with Rayleigh scattering as much radiation is back-
scattered as is forward scattered. Figure 3.5 illustates
this phenomenon.

Besides Rayleigh scattering, radiation entering or
leaving the atmosphere may be affected by Mie scattering.
Generally, Mie scattering is inversely proportional to the
first power of wavelength. Mie scattering occurs when atmo-
spheric particle diameters are essentially equal the energy
wavelengths being sensed. Lillisand and Kiefer (1979) note
that, as a result, this type of scattering tends to influ-
ence longer wavelengths compared to Rayleigh scattering.
With Mie scattering, forward scattering predominates over
backscattering. See Figure 3.5. The scattering of sunlight
by haze, smoke, smog, dust and water aerosols usually falls
within the Mie Regime. The combination of Rayleigh and Mie
scattering causes the selective scattering of light shown in
Figure 3.5. These phenomena produce significant effects on
the VIN as will be discussed in Chapters IV and V.

Sabins (1978) lists a third scattering phenomenon,
nonselective scatter. The scattering particles are much
larger than the wavelengths being scattered. Effects on
visible and reflected infrared wavelengths are nearly equal.
Thus, the scattering is nonselective. Fog and clouds appear
white in the visible spectrum because blue, green and red
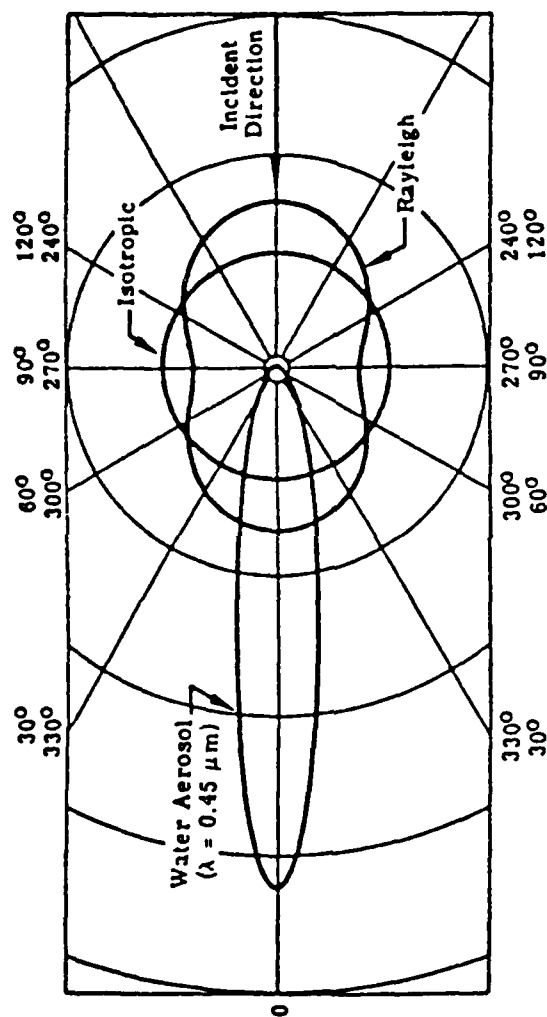
Figure 3.5 Angular Dependence of Single-Scattering Phase Functions in any Azimuthal Plane. The isotropic and Rayleigh functions have been multiplied by 10. After LaRocca and Turner, (1975)

light are equally scattered.

According to Chahine (1983) radiance above the atmosphere or spectral radiant emittance E, can be expressed as the sum of two terms:

$$E = E_1 + E_2 \qquad\qquad (3.18)$$

where E_1 is the solar energy that is scattered by the atmosphere and never reaches the earth's surface. E_2 is the component of solar irradiance that reaches the earth's surface, is reflected, and emerges from the top of the atmosphere. Figure 3.6 illustrates the relationship. Information about the surface is contained in the E_2 component. Chahine states that the E_1 component limits the amount of information that can be extracted from the measured radiation.

The downwelling radiation at the ground can be broken into two components as follows:

$$E_T(\mu) = E_D(\mu) + E_S(\mu) \qquad\qquad (3.17)$$

$E_T(\mu)$ is the total spectral irradiance or global flux

$E_D(\mu)$ is the direct sunlight irradiance

$E_S(\mu)$ is the skylight irradiance which is light that has been scattered at least once

μ is the optical pathlength or optical depth

A plot of the ratio of direct solar irradiance to the global
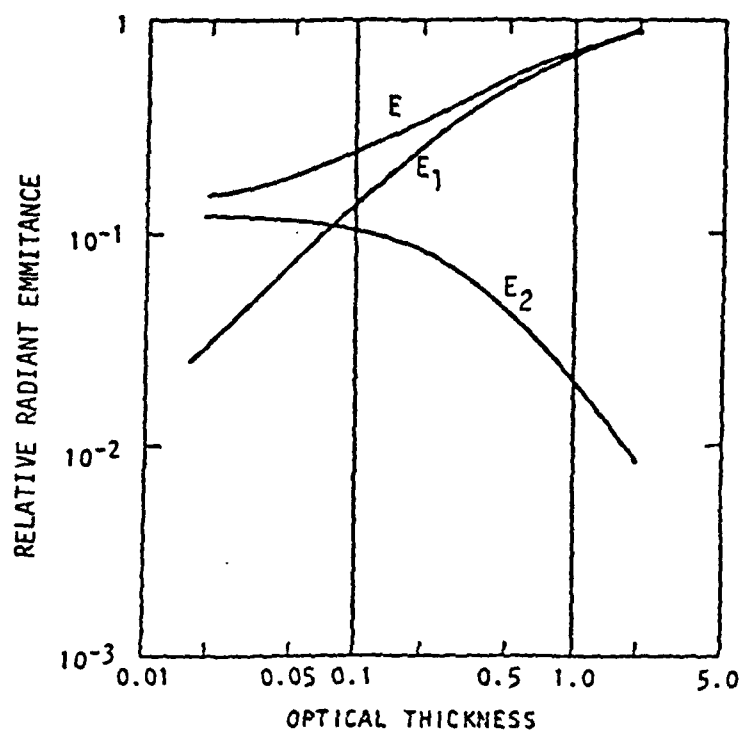
E = Total Radiant Emittance

E_1 = Atmospherically Scattered Upwelling Light

E_2 = Surface Interacting Upwelling Light

Figure 3.6 Computed Radiant Emittance at the Top of a Rayleigh Atmosphere (no absorpiton or large particles) as a Function of Optical Thickness. The reflectance of the ground is 1; the solar zenith angle = 66.4°. From Chahine 1983 (Figure 5.16)

irradiance versus optical depth is shown in Figure 3.7. The E_s component also serves to limit the amount of information which can be extracted from satellite measured radiances.

In general, scattering reduces the amount of solar energy available for measurement by a remote sensor like the AVHRR. There is one exception to this generalization: backscattering. Backscatter may result from any of the scattering mechanisms. Its effect is to add a radiance which is backscattered from the sky into the sensor.

ATMOSPHERIC ABSORPTION

Miller et al. (1983) define absorption as the retention of incident radiation by a substance resulting in a transfer of radiant energy to internal energy. If substances are thought of as consisting of infinitesimally thin layers, then the incident radiation, as it passes through each layer, is depleted as a result of the energy transfer. As previously mentioned, the ratio of the irradiance absorbed by a particular substance to that which is incident upon it is called absorptivity. Absorption is wavelength dependent, so different amounts of energy are absorbed by the same substances at different wavelengths. The dimensionless quantity κ measures the depletion of the monochromatic irradiance of the incident beam.

Absorbing gases are, of course, made up of individual atoms or molecules. Atoms and molecules can exist only in
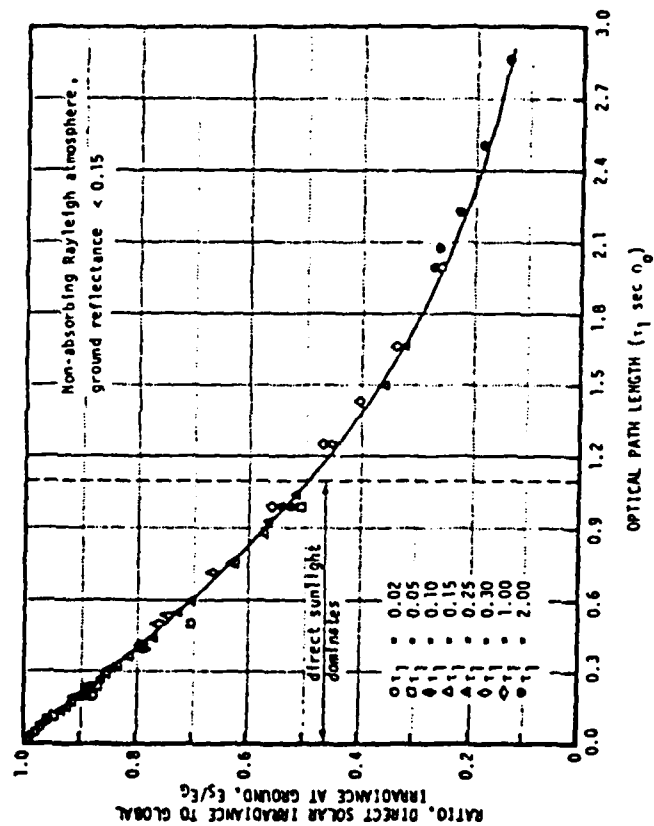
Figure 3.7 Ratio at the Direct Solar Irradiance to the Global Irradiance. From Chahine (1983, Figure 5.12)

certain states of rotational, vibrational and electronic configurations with characteristic energies. Iribane and Cho (1980) note that these atoms or molecules can change energy states by absorbing or emitting finite amounts of energy which are equal to (1) the energy required for electrons of the atom or molecule to transfer from one orbital level to another or (2) the energy needed for changing the vibrational or rotational state of the atom or molecule. Figure 3.8 illustrates the relationship between wavelength and the types of energy transitions. Each possible combination of electron orbit, vibration and rotation may be identified with a discrete energy level which represents the sum of the three energy types.

Because the atoms and molecules comprising the atmosphere have discrete and characteristic energy levels, the wavelengths of radiation with which the molecules and atoms interact is also characteristic and discrete. These discrete wavelengths of energy may be thought of as absorption or emission lines in the EM spectrum. The lines of absorption or emission are, theoretically, separated by gaps where absorption and emission are not possible. In practice, however, these lines are broadened by random molecular motions and collisions with other atoms or molecules. Molecular collisions increase as pressure increases and an increase in pressure results in pressure broadening of the spectral lines into peaked curves with wings. Thus the lines have a characteristic shape suggestive of a
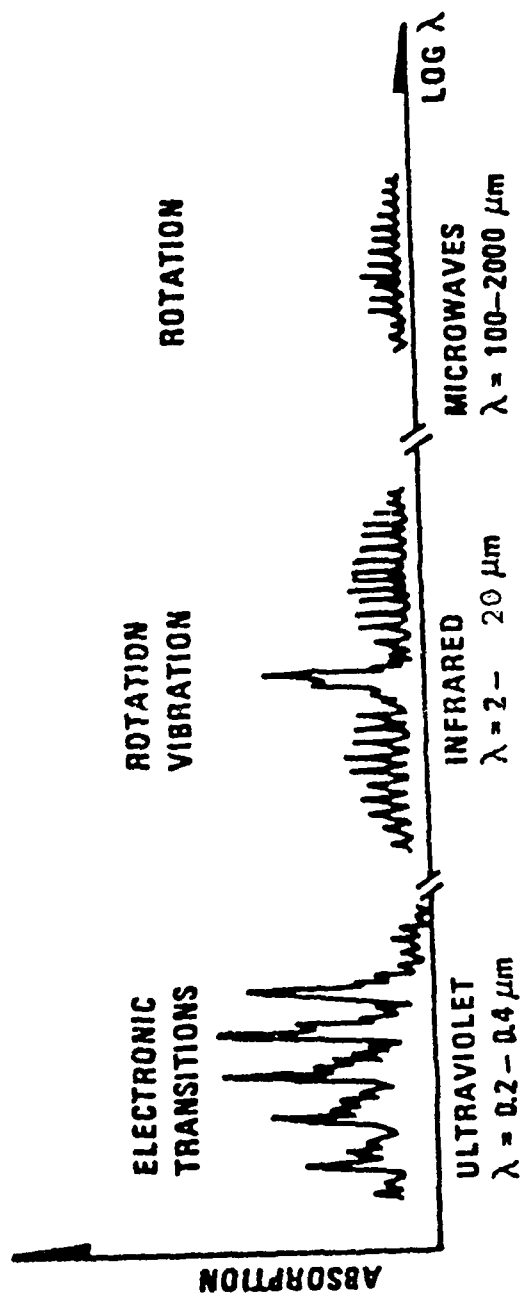
Figure 3.8 Typical Form of Molecular Absorption Spectra.
Note that the vibrational transitions are split up by the
rotational transitions. After Gjessing (1978)

Maxwellian distribution function, or a peaked curve with wings. The spectral distance covered by a wing also expands as pressure increases, as molecular speed increases and as the mass of the absorbing material, or optical mass, increases. The superposition of a wing from one spectral line with a wing from another results in increasing amounts of absorption over additional wavelengths. See Figure 3.9.

The actual absorption spectrum of the atmosphere contains innumerable lines, some of which are organized into absorption bands of limited spectral interval. A collection of these lines, associated with a given type of atom or molecule, is called a line spectrum.

Radiation passing through an infinitesimally thin layer of the atmosphere will be absorbed in an amount indicated by the absorptivity of the spectral line or the absoption coefficient of the spectral band. The remaining radiation is transmitted to the next atmospheric layer where absorption equal to the absorption coefficient of that layer again attenuates the radiation. After passing through several layers all of the energy in a particular spectral band near the central absorption peak may be attenuated, and thus, no further absorption takes place. However, absorption in the line wing may continue, as noted in Figure 3.9.

Because the sun is so distant, solar irradiance can be thought of as a parallel beam of radiation. For parallel beam radiation the solid angle dω vanishes, thus radiance is undefined. Hence, one deals only with irradiance in calcu-

WAVELENGTH
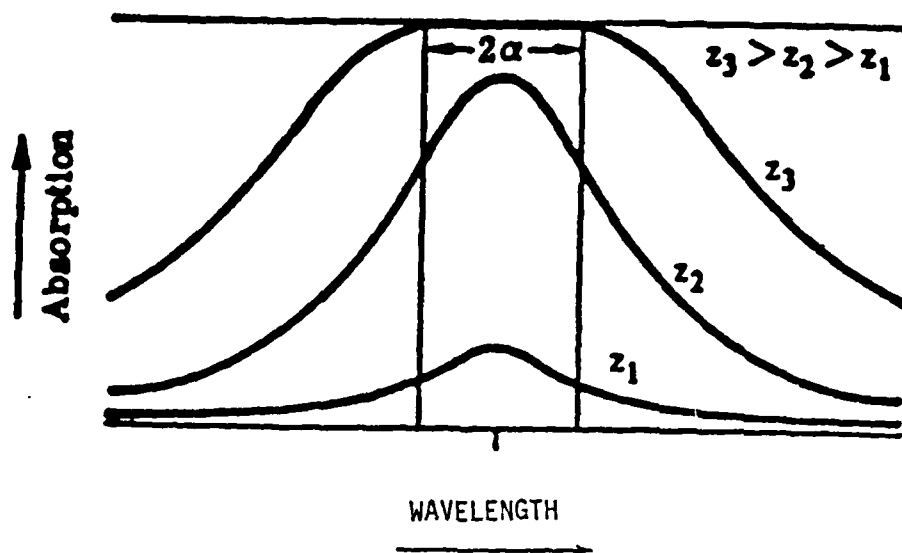
For an optical path length of z_1 the absorption is small
even at the center of the line. For a path length of z_3,
the center of the line is completely absorbed and further
increase in the path length would only change the absorption
in the wings of the line.

Figure 3.9 Absorption versus frequency for a single line and
for different absorber amounts. From Wolfe and Zissis
(1978, Figure 5-4)

lations of attenuation of the incoming solar beam. As this
beam of energy passes through the atmosphere some of the
energy is depleted from the beam. The depletion of the beam
due to absorption as it passes downward through a horizontal
layer of gas of infinitesimal thickness dz is proportional
to the number of molecules per unit area that are absorbing
radiation along the path. Depletion can be expressed as:

$$-dE_\lambda = E_\lambda \kappa_\lambda \rho \sec \theta \, dz \quad (3.19)$$

ρ is the density of the gas
θ is the zenith angle
κ is a measure of the fraction of gas molecules per unit
λ wavelength that are absorbing radiation at the
         wavlength in question
dz is the pathlength through which the radiation propagates
dE is the incremental depletion of irradiation

This equation can be intergrated from any level of the
atmosphere z, to the top of the atmosphere resulting in:

$$\ln E_\lambda - \ln E_{\lambda_z} = \int_{\lambda_z}^{\infty} \sec \theta \, \kappa_\lambda \, \rho \, dz \quad (3.20)$$

Going one step further,

$$E_{\lambda_0} = E_\lambda -\exp\left(\int_z^{\infty} \kappa_\lambda \sec \theta \, \rho \, dz \right)$$

$$= E_\lambda \exp\left(-\kappa_\lambda \int_z^{\infty} \sec \theta \, du \right) \quad (3.21)$$

where du, which is the increment in absorbing mass, is

$$\rho \sec \theta \, dz \qquad\qquad (3.22)$$

and

$$u = \int_z^\infty du \qquad\qquad (3.23)$$

Equation 3.21, which is known as Beer's Law, is the mathematical description of the way absorptivity and the mass of absorbing material interact. With this equation one can calculate the depletion of the irradiance of the solar beam after it has passed through an absorbing medium. Individual lines in the absorption spectrum broaden in a nonlinear fashion as the path length increases resulting in a monotonic decrease of solar irradiance with increasing path length. After the beam has passed through a layer of optical depth equal to one, the irradiance of the beam is diminished by a factor e. Taken to the ultimate, as u approaches infinity the absorption bands merge so that absorptivity approaches one at all wavelengths and the gas absorbs and emits as a blackbody. It is important to note that κ is (1) very small for visible wavelengths and (2) that κ increases for the solar reflected infrared wavelengths.

Recognizing that the radiation emitted from the earth-atmosphere system is diffuse, an analogous treatment of this radiation can be developed. To do this one must recognize that the radiation is no longer parallel beam radiation. Thus, one must substitute the radiance L, for

irradiance E.   Thus, equation 3.19 becomes

$$-dL_\lambda = L_\lambda \kappa_\lambda \rho \sec \theta \, dz \qquad (3.24)$$

or

$$-dL_\lambda = L_\lambda \kappa_\lambda \, du \qquad (3.25)$$

For an atmospheric layer the absorptivity must equal
the emissivity. Thus, the layer not only absorbs energy,
but emits it as well. There is a contribution to the
upwelling radiance by the layer. Because absorptivity
equals the emissivity which equals the absorption coeffi-
cient, this contribution can be expressed as:

$$(dL)_{\lambda(EMT)} = L_{bb\lambda} \kappa_\lambda \, du \qquad (3.26)$$

where L_{bb} is the blackbody spectral radiance. The total
change in radiance which is known as Schwarschild's equation
is

$$dL_\lambda = (L_{\lambda_0} - L_{bb\lambda}) \kappa_\lambda \, du \qquad (3.27)$$

This law allows one to describe the depletion of
earth-emitted radiation as it passes upward to the top of
the atmosphere.

An absorption spectra for atmospheric gases in standard concentrations are shown in figure 3.10. Goody and Robinson (1951) proposed the original version of this graph. They assumed the atmosphere contained 2 gm cm^{-2} of water vapor above ground level and 10 gm cm^{-2} above 11 km and that carbon dioxide and nitrous oxide were mixed in equal portions within the atmosphere at all heights. McClatchey, et al. (1973), Kyle and Goldman (1975), and Dave and Braslau (1975) have refined this work. Dave and Braslau have varied the concentrations of atmospheric constituents in their models.

Oxygen and nitrogen are the primary absorbers of energy with wavelengths shorter than .3 μm. According to Fleagle and Businger (1980) approximately 99 percent of this energy is absorbed from the solar beam before it reaches the earth's surface. Energy in the visible wavelengths passes through the earth's atmosphere virtually unabsorbed. Slater (1980) states that solar infrared energy, on the other hand, suffers significant absorption. Jackson et al. (1983) note that near infrared radiance may suffer up to a 20 percent reduction due to water vapor absorption.

Infrared solar radiation received at the earth's surface is significantly less than visible radiation for two reasons: (1) Solar emission, as described by the Planckian energy distribution, decreases rapidly at wavelengths greater than .8 μm and (2) atmospheric absorption, in some bands significantly depletes the near infrared portion of the

Wavelength (μm)

1.98   1.99   2.00

Absorption coefficient (rel. units)

Detail
of H_2O
spectrum

CH$_4$

N$_2$O

O$_2$ and O$_3$

CO$_2$

H$_2$O

Atmosphere

Absorptance

0.1   0.2   0.3   0.4   0.6   0.9 1   1.5   2   3   4   6   8   10   20   30

Wavelength (μm)
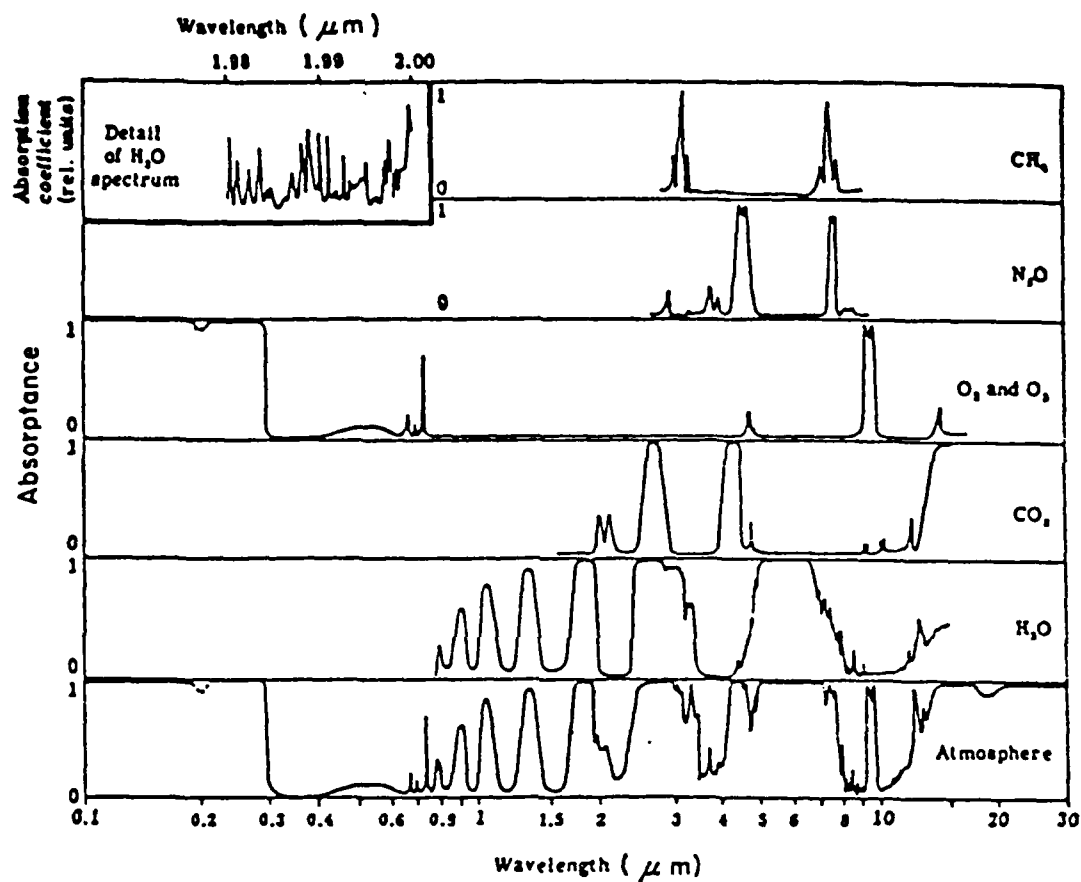
Figure 3.10 Absorption Spectra for the Atmosphere as a Whole
and for Individual Atmospheric Components.   After Goody and
Robinson (1951) and U.S. Air Force (1961)

solar beam before it reaches the earth's surface. Signif-
icant water absorption bands occur at 2.66 μm, 2.74 μm and
6.25 μm. Carbon dioxide and water vapor are the primary
absorbers.

Water vapor is a highly variable substance in the
atmosphere. Valley (1965) reported variations of sea level
water vapor densities from 10^{-3} g m^{-3} in very cold, dry
climates to 30 g m^{-3} in hot humid regions. According to
Chahine (1983) the average total mass in the atmospheric
column is 2.5 g m^{-2}. Because atmospheric water vapor is a
highly variable quantity, the amount of infrared radiation
reaching the earth's surface is also variable. This vari-
ability manifests itself in lower radiance returns to chan-
nels of the AVHRR that are affected by water vapor, i.e.,
Channel 2 and as will be discussed, Channel 5. As previous-
ly mentioned, absorption is not a linear function of absor-
ber concentration and absorber concentration varies both in
time and in space so calculation of water vapor absorption
can present many difficulties. Fortuntely, as Fraser and
Curran (1976) note that "the absorption does not have to be
computed with great accuracy for many applications because
relative differences in radiance for the same scene are more
commonly used than absolute values."

Carbon dioxide is another strong absorber of radiation
propagating through the atmosphere. However, Chahine (1983)
notes that the homogeneous nature of the gas makes the
determination of its attenuating effects easier to

calculate. The atmosphere is virtually opaque at 4.3 μm and at 15 μm and beyond due to carbon dioxide absorption.

Water vapor and carbon dioxide are both strong absorbors of earth emitted-infrared energy. The two constituents effectively block the outgoing infrared energy between 4 and 8 μm and the energy beyond 12 μm. There is, however, a "window" between 8 and 12 μm where neither gas absorbs strongly. While ozone has two narrow absorption bands centered at 9.6 μm, the 8 to 12 μm band is usually considered an effective energy transmission window. In general, the 8-12 μm band is described as unaffected by water vapor or carbon dioxide. See, for example, Fleagle and Businger (1980) and Coulson (1975). However, the far edge of the window near 12 μm does show some signs of increasing absorption. Referring to Figure 3.10 one can see the role water vapor has in absoption in the interval. As water vapor concentrations increase beyond standard atmospheric concentrations, recorded radiances should, theoretically, show an exponential decrease. Callison and Cracknell (1984) report that absorption due to water vapor in a moist atmosphere can attenuate the upwelling radiation in the 8 to 12 μm window by as much as ten percent. Although carbon dioxide has some effect in the far edge of the 8 to 12 μm window, Chahine (1983) states that the effect is small.

CLOUDS AS REFLECTORS AND EMITTERS

The fraction of irradiance that is reflected is called reflectivity. According to Hecht and Zajac (1979), reflection is a special case of scattering in which the irradiance is diverted back rather than transmitted forward. Reflected energy travels in a more predictable direction than scattered energy. The term reflection is almost always associated with clouds when one discusses EM interaction with tropospheric constituents.

The radiative properties of clouds, like many other objects, changes as a function of wavelength. Most clouds are very good reflectors and, therefore, poor absorbers of solar radiant energy. Miller et al, (1983) suggest that the reflective properties of clouds depend primarily on their thickness, but also to some extent on the nature of the cloud (i.e. whether the cloud is made ice or water), and the size of the cloud particles. Figure 3.11 shows the relationship between cloud thickness and reflectivity. In the visible and near infrared regions the sizes of the cloud particles are equal to or just larger than the wavelength of the incident radiant energy. Fraser and Curran (1976) note that the energy/matter interaction is at a maximum under these circumstances. In general, reflectivity varies from 50 to 90 percent. Figure 3.12 shows variation of cloud reflectivities with wavelength. Clouds are slightly less reflective in the near infrared than in the visible.

Obviously, clouds can have severe impacts on interpre-tation of remotely sensed data. Impacts include: (1) total
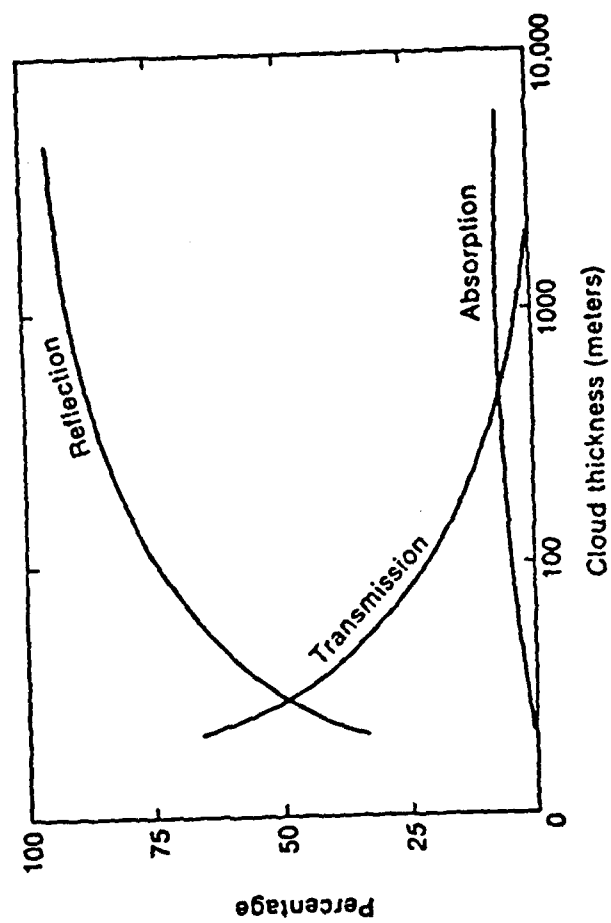
Figure 3.11 Percentage Reflection, Absorption, and Transmission of Solar Radiation by Clouds. After Miller et al. (1983, Figure 4.8)
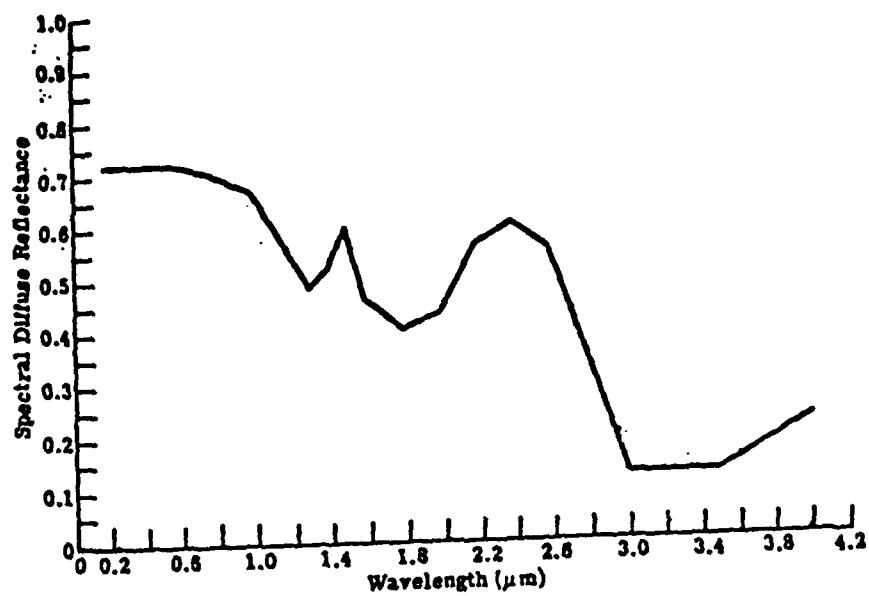
Figure 3.12 Spectral Diffuse Reflectance of a Middle Layer
Cloud. From Wolfe and Zissis (1978, Figure 3.19)

obscuration of the scene, (2) cloud shadow on the surface and (3) introduction of inordinately high reflected energy values to the sensor. The effect of sub-pixel sized clouds falls in the later category. All of these factors affect computation of the VIN.

Large scale cloud contamination of pixels, while difficult to correct for, can at least be monitored and affected pixels removed from a scene before data interpretation is attempted. Sub-pixel sized clouds, on the other hand, present a detection problem. Recall that Figure 2.6 showed how the VIN of a "scene" might be altered when clouds are added to the scene. Duggin et al. (1982b) determined that, at nadir, clouds with dimensions just less than one square kilometer could exist and not be resolved by the AVHRR. Further, they found up to a five-fold decrease in the VIN would result from as little as 20 per cent cloud coverage in a scene made up of varying amounts of soil and wheat. Figure 3.13 illustrates their results. While the effects of sub-pixel sized clouds have been demonstrated, studies to develop methods of detection are still underway.

Various techniques have been developed for computer cloud screening. See, for example, Horvath et al. (1982), Gray and McCrary (1981a) and Nixon et al. (1983). Nixon et al. (1983) present a series of methods for computer screening of cloud contaminated pixels from data of various satellite systems. Their methods include use of scatterplots of both solar reflected energy and earth-emitted and cloud

Figure 3.13 Simulated Vegetative Index for View Angle = 0 (Nadir) for Pure Wheat and for a 70% Wheat, 30% Soil Target for Various Percentages of Pixel Filled by Cloud. From Duggin et al. (1982b)
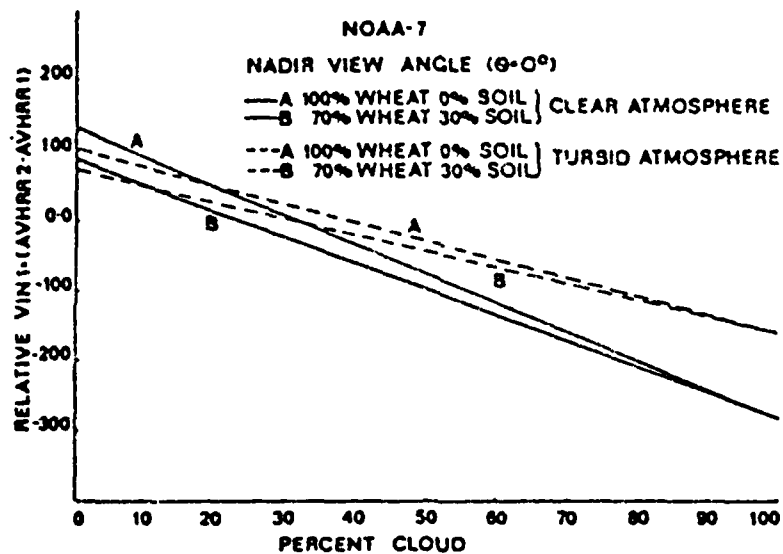
emitted-thermal energy.

Liquid water clouds more than a few meters thick behave as black-body radiators. Cloud tops radiate energy in an amount proportional to T^4, where T is the cloud top temperature. Using Wein's Displacement Law and a cloud top temperature of -20 °C, one could determine that a cloud top emits a maximum of energy near 11.4 μm. Figure 3.14 shows that at least some part of the emitted energy is within the bands of energy sensed by AVHRR channels 4 and 5.

Clouds, because they are typically cooler than the earth's surface would tend to reduce the amount of earth-emitted energy sensed from a pixel or collection of pixels. This fact leads to an emissive cloud screening technique. The technique involves scatterplotting the Channel 4 pixel value against the Channel 1 pixel for each pixel in a scene. Those pixels showing high Channel 1 values and low Channel 4 values relative to other pixels may be assumed to be cloud-filled and/or cloud-contaminated. Nixon et al. (1983) used cluster analysis of these types of plots to determine which pixels (and how many) of a scene were contaminated. Most analysis schemes will allow an analyst to remove cloud contamination with various degrees of confidence by simply varying the threshold for cloud identification. Of course, removing all clouds from a partly cloudy scene will necessarily result in a high loss of other useful information from the scene. On the other hand, a cloud screening technique which preserves most of the useful data
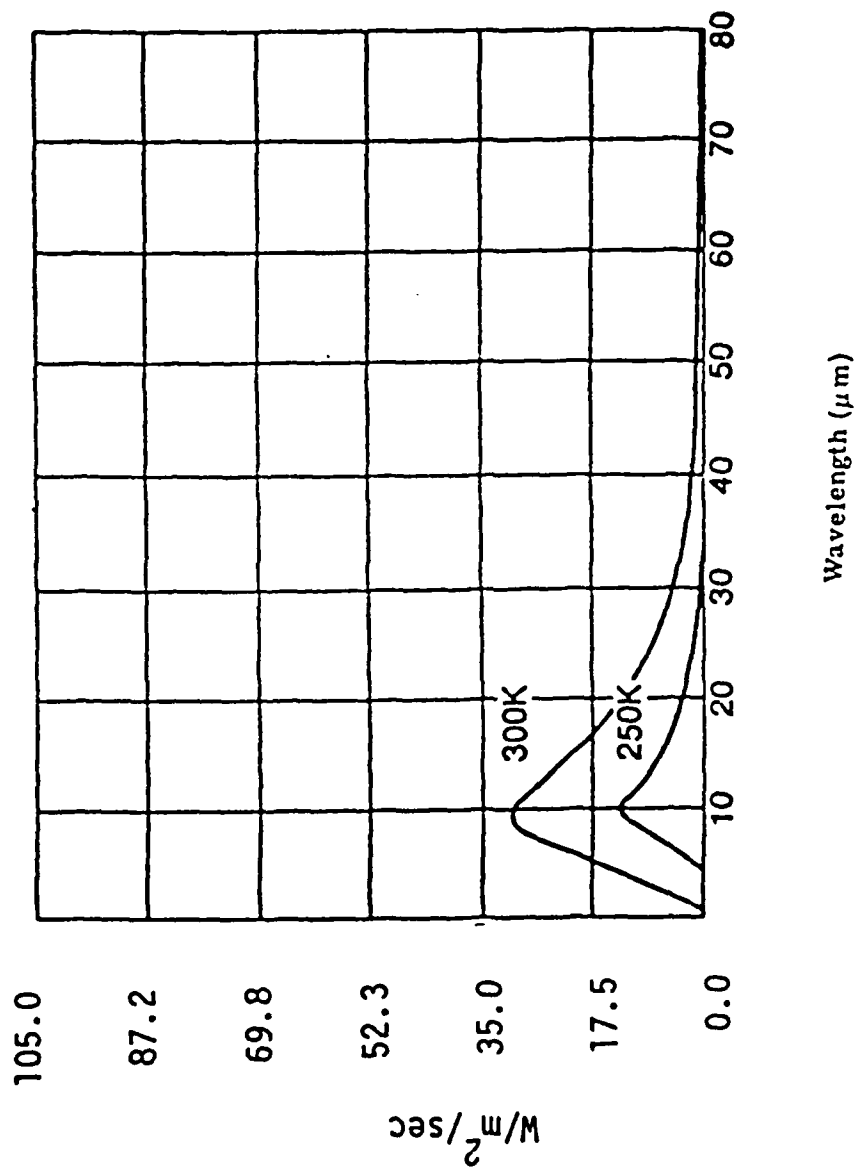
Figure 3.14 Blackbody Spectra for Typical Cloud Top and Earth Temperatures.

will not eliminate cloud contamination.

In many instances satellite data users must be content with interpreting data that is partially cloud-contaminated. However, the relative amounts of cloud contamination can be determined if a view of the scene on a cloud-free day is used as a baseline emissive scene. Figure 3.15 illustrates how one might determine, qualitatively, the amount of cloud contamination in a scene. It is a plot of AVHRR Channel 1 radiance values against Channel 4 radiance values. Figure 3.15a is a "clear day" plot and it would be considered a baseline plot. Figure 3.15b is a similar plot for a partly cloudy day. Note the higher Channel 1 (reflected radiance) values and the lower Channel 4 (emitted radiance) values in Figure 3.15b. The horizontal line is a threshold value used operationally for visible cloud screening by the Center for Assessment Services at Columbia, Mo. (LeDuc, 1984). Any pixels having Channel 1 values above this threshold are discarded before a VIN is calculated.

ENERGY INTERACTIONS WITH THE EARTH'S SURFACE

Energy at the earth's surface can be separated into two components for the purposes of remote sensing: solar reflected and earth-emitted. As previously mentioned, little attenuation occurs in the visible part of the EM spectrum. The atmosphere is also fairly transparent to radiaton in the 8 to 12 μm region. The effective radiating

LONGVIEW 189

a

LONGVIEW 192

b
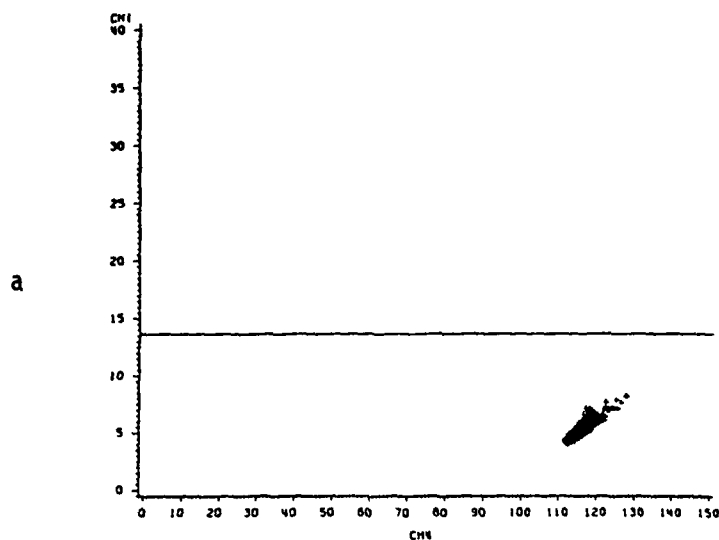
Figure 3.15 Cloud Screen Scatterplots. a) Channel 1 vs Channel 4 scatterplot for a cloud free day near Longview, Texas b) Channel 1 vs Channel 4 Scatterplotr for a cloud-contaminated day at the same location.

temperature of the earth is approximately 288 °K, which implies a maximum emitted energy near 9.7 μm. Thus, the emission maxima occurs in the 8 to 12 μm window.
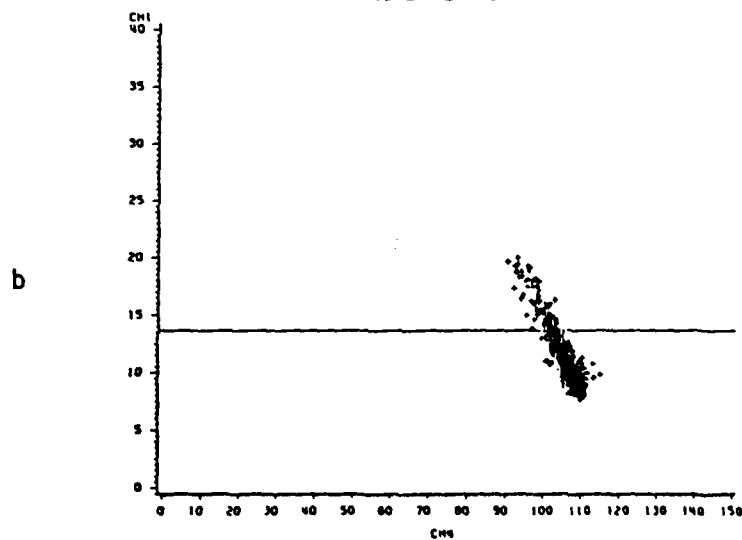
Electromagnetic energy interacting with the surface obeys the same basic laws as energy interacting with the atmosphere. The proportion of energy reflected, absorbed and transmitted will vary for different earth features, depending on their material type and condition and the wavelengths involved. Within a given feature type the proportion of reflected, absorbed and transmitted energy will vary at different wavelenghts. This allows analysts to distinguish different features on a remotely sensed image. In the visible portion of the EM spectrum these spectral variations result in objects having different colors.

The geometric manner in which an object reflects energy is also important. Surface roughness plays a large role here. Very smooth surfaces have a mirror-like reflection or specular reflection. For a specular reflection the angle of reflection equals the angle of incidence of the incident radiation. Rougher surfaces reflect uniformly in all directions. A truly uniform reflector is called a Lambertian reflector or a diffuse reflector. Most surfaces are somewhere between the two extremes. In general, reflectance modelers tend to use the concept of a Lambertian surface when constructing a model of surface reflectance. See, for instance, Slater (1980) and Duggin et al. (1982b).

Chapter 2 gave a brief review of energy interaction

with vegetation.   Remote sensing of vegetation is based
primarily on the sharp difference in the visible and infra-
red reflectance of plants.   Besides plant chlorophyll
content and atmospheric conditions, there are several other
factors which influence the radiometric measurements of a
plant scene: (1) leaf orientation, which may be affected by
the amount of wilt or the wind speed; (2) standing water on
plant leaves from rain or dew; (3) sun angle; (4) angle of
view of the radiometer and (5) amount of non-plant material
in the scene, i.e., soil, roads, clouds, etc.   All of these
items impact on the calculated VIN.

Other than water, most objects in a scene transmit very
little visible solar radiation.   The energy conservation
law for these objects becomes

$$E(INC) = E(REF) + E(ABS)$$

or, dividing by E:

$$REF + ABS = 1$$

Since by Kirchoff's Law emissivity equals absorptivity:

$$REF + EMT = 1 \qquad (3.30)$$

As previously stated, the varying relative proportion of
reflected and absorbed energy allows one to distinguish
between different types of objects.   Age, moisture and
surface roughness are factors in the relative amounts of

surface absorptivity/emissivity and reflectivity. For
instance, a field will have a different reflectivity depend-
ing upon whether or not it has been recently plowed and if
so, how recently. The wavelength dependence of reflectivity
and absorptivity permits analysts to use multispectral scan-
ners to discriminate between several different objects that
have similar visible characteristics, e.g., snow and clouds.

Visible reflection from water surfaces depends on the
amount of suspended particles in the water, the sun angle,
the view angle and the roughness. As previously mentioned,
liquid water is an effective absorber/emitter in the near
infrared, but a poor reflecter. According to Lillisand and
Kiefer (1979), locating and delineating water bodies with
remote sensing data is done most easily in reflected infra-
red wavelengths because of this absorption property.

Surface features not only reflect energy but emit ener-
gy as well. The emissivity of an object is important when
measuring the temperature of an object and subsequently
converting that temperature to kinetic temperature. The
emittance which is viewed by the radiometer through some
angle is measured as a radiance. This radiance can be
converted to an equivalent blackbody temperature which is
related to the actual kinetic temperature by

$$T_{RAD} = \sqrt[4]{e}\, T_{KIN} \tag{3.31}$$

This equation states that for any given object, with an
average emissivity less than one the radiant temperature
will be less than the kinetic temperature of the object.
Therefore, the emissivity of the object must be known before
an accurate estimation of the object's kinetic temperature
can be made using satellite radiances. Sutherland and
Bartholic (1977) report that although, the radiative proper-
ties of many objects deviate significantly from that of a
blackbody in the 8 to 14 μm region, vegetation generally has
an emissivity from .95 to 1.00.

CHAPTER IV

Electromagnetic Theory Applied to the Sensor and the
Atmosphere

GENERAL

This chapter summarizes some of the important elements
of an operational remote sensing system. Several of the
basic complicating factors in the sensor-atmosphere-surface
system are briefly discussed. Their impacts on the study
presented in Chapter V are discussed when appropriate.
Additionally, the concept of differential absorption is
highlighted.

REFLECTIVE DATA

The properties of radiation and the radiative inter-
action with matter result in a radiative output from the
earth-atmosphere system that can be sensed by the AVHRR.
The AVHRR, although usually referred to as one system, is
actually made up of several detectors. These detectors use
the same optical system to collect data in all spectral
bands simultaneously.

The different detectors independently process and record information about the scene. Energy from the target enters the AVHRR's optical system and encounters a grating which separates the incoming radiation into its reflected component and emitted component. The reflected wavelengths travel to a prism where they are split into visible and reflected infrared bands (Channel 1 and Channel 2, respectively). The grating further processes and separates the emitted component into three wavebands (Channels 3, 4 and 5).

Lillisand and Kiefer (1979) explain the operation of the detectors like those on board the AVHRR as follows: The detectors ..."operate on the principle of direct interaction between photons of radiation incident on them and the energy levels of electrical charge carriers within the detector material."

An array of detectors receives the five bands of energy. Each detector is filtered to accept and respond to only one band of energy. The impinging energy causes the detector to generate a signal proportional to the magnitude of the energy. This signal is amplified by the system electronics and recorded on board or broadcast to earth. For Channel 1 and Channel 2 the response to incident energy is a digital radiometer count, which relates to the combined effects of surface reflectivity and atmospheric interaction with the energy in the bandpass. The sensor, of course, detects energy from an interval of wavelength, or a channel,

so a summation or integration of the albedos at the differ-
ent wavelengths is necessary to describe the response.
Further complicating the response is an angle dependency of
the recorded radiance and a non-uniform response of the
sensor to various wavelengths of energy. To properly
account for these complicating factors Duggin et al.
(1982a) developed a normalized sensor response function
which is shown and explained in Figure 4.1. The last
equation in Figure 4.1 is the form used by Duggin et al.
for modelling AVHRR response.

    To get the albedo from the normalized sensor response,
one must recall that

$$\text{Albedo} = \frac{\text{Reflected Irradiance}}{\text{Incident Irradiance}} \qquad (4.1)$$

Recalling, also, that the normalized sensor response is a
function of the reflected irradiance, the albedo can be
written as

$$\text{Albedo} = f(\text{NSR}) \qquad (4.2)$$

Calibration of the AVHRR and the assumption that there is no
dependence of reflectivity on zenith angle results in a
simple equation for albedo that is a linear function of the
digital radiometer count, X. Lauritson et al. (1979) give
the equation:

$$NSR\ (\theta,\ z,\ \phi,\alpha) = \frac{\int_{\lambda_2}^{\lambda_1} I\ (\lambda) \cdot (E(\theta,\lambda) \cdot R\ (\theta,\phi,\alpha,z,\lambda) \cdot \tau(\alpha,\lambda)\ +\ L_{path}\ (\theta,\phi,\alpha,z,\ \lambda)) \cdot d\lambda}{\int_{\lambda_2}^{\lambda_1} I\ (\lambda)\ d\lambda}$$

θ is solar zenith angle ϕ is the solar azimuth angle

α is view zenith angle Z is the view azimuth angle

where $\int_{\lambda 1}^{\lambda 2}$ represents the summation over all wavelengths in the band pass or channel with λ_1, and λ_2 the upper and lower wavelength limits to sensor response at the zero-power level for the bandpass.
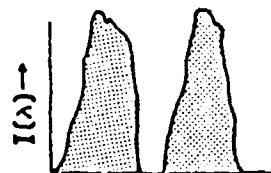
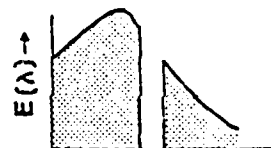**WAVELENGTH λ**

HYPOTHETICAL

CH 1   CH 2

$I\ (\lambda)$ is the instrument spectral response

$E\ (\theta,\lambda)$ is the spectral irradiance on the target which is also a function of the solar constant and the mean earth sun distance.

$R\ (\theta,\phi,\alpha,z,\lambda)$ is the radiant energy hemispherically reflected by the target into the solid angle viewed by the satellite (spectral hemispherical conical reflectivity).

$\tau(\alpha,\lambda)$ is the spectral transmission
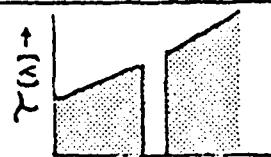
$L\ path\ (\theta,\phi,\alpha,z,\lambda)$ is the spectral atmospheric path radiance
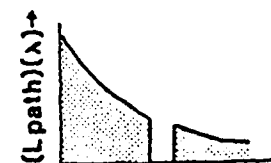
$$NSR = \frac{\int_{\lambda 2}^{\lambda 1} I\ (\lambda) \cdot (E\ (\lambda) \cdot R\ (\lambda) \cdot \tau(\lambda)\ +\ L_{path}\ (\lambda)\ ) \cdot d\lambda}{\int_{\lambda 1}^{\lambda 2} I\ (\lambda)\ d\lambda}$$

Figure 4.1   Development and explanation of the AVHRR nomalized sensor response.   After Duggin et al. (1982)

$$Albedo = GX + I \qquad\qquad (4.3)$$

The G and I are the slope and intercept values for a partic-
ular channel provided in the data stream of each LAC scan
line. These values consider the irradiance at the surface
and the sensor response function. Thus, by assuming reflec-
tive isotropy, calibrating the AVHRR detectors and assuming
independence of reflectivity and zenith angle, one can very
simply relate the radiance recorded in a particular bandpass
to albedo. This albedo can then be normalized to overhead
sun by multiplication by secant θ, where θ is the solar
zenith angle, which is also provided in the data stream of
each LAC scan line. Although the simplifications above are
necessary and beneficial, the user must be aware that the
recorded radiance values and, thus, the albedos contain the
effects of atmospheric attenuation, atmospheric pathlength
and cloud effect, in addition to the information on surface
reflectivity.

Several researchers, notably Duggin et al.(1982a),
Holben and Fraser (1984) and Justus (1984) have modeled the
AVHRR response to scattering and absorption. They investi-
gated the following "atmospheres": (1) atmospheres with
different aerosols and absorber contents and (2) atmospheres
with different optical depths, holding aerosols and absorber
content steady. Using NOAA-6 AVHRR data and a Lambertian
surface reflectance model, Duggin concluded that a turbid

atmosphere systematically increased sensor output in Channel 1 (thereby reducing contrast), while in Channel 2 turbidity reduced sensor output. As a result, even at nadir the VIN is reduced for a turbid atmosphere. They found that off nadir viewing caused further reductions. Figure 4.2 illustrates Duggin's findings. Duggin reports ten percent variations of radiance values when a scan angle of +14° is used. Justus (1984) used a nonisotropic refleecting surface in his model. He found an increase in the VIN with nadir angle out to 60°. He does note, however , (in agreement with Duggin) that the increase in VIN is less pronounced for a turbid atmosphere.

Holben and Fraser (1984) confirmed these results for NOAA-6 and extended them to NOAA-7 and NOAA-8. Holben and Fraser simulated the following situation: radiance for an "average" atmosphere alone, as described by Dave and Braslau (1975) at equinox at 30 north latitude. The "atmosphere alone" calculation was made by setting cloud and surface reflectance to zero. For NOAA-7 Holben and Fraser found that minimum radiances occurred near the nadir and increased with longer path length. This result is attributable to Mie scattering. See Figure 4.3a.

Holben and Fraser concluded that NOAA-7 channels 1 and 2 show only a weak horizon brightening from the atmosphere alone. See Figure 4.3b The addition of nonisotropic surface reflectance however, greatly alters the resulting VIN for off nadir viewing. Thus, the increase of VIN with view
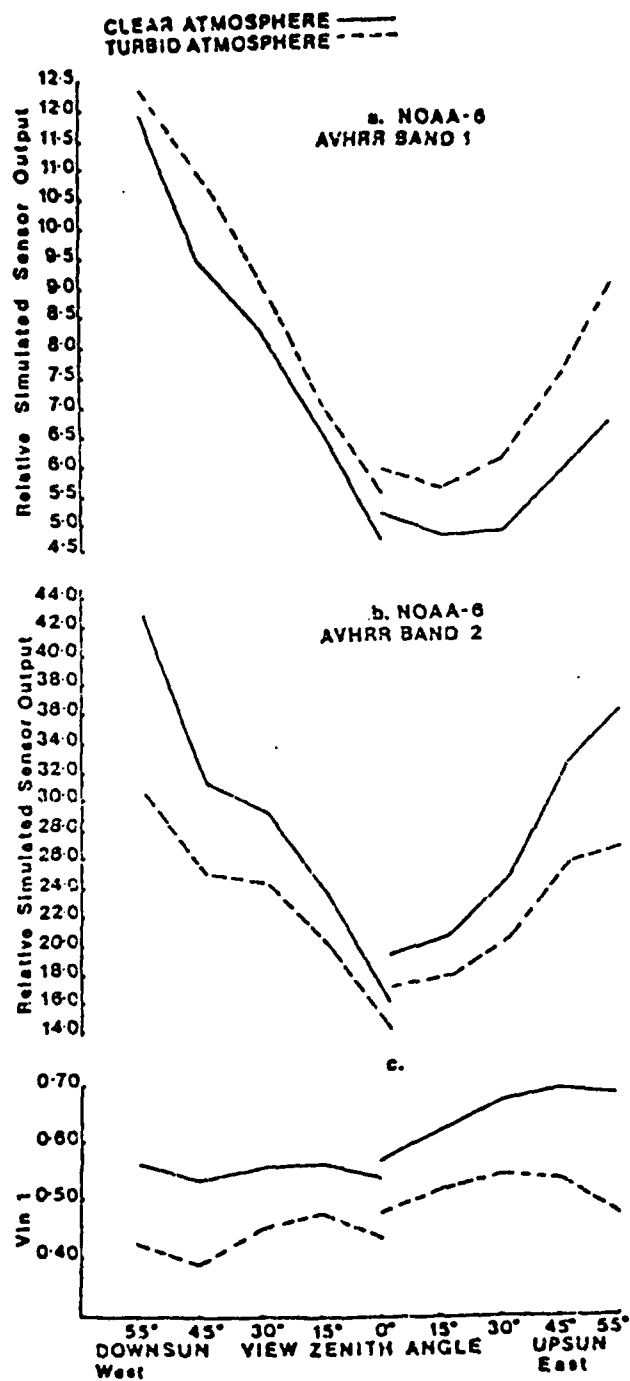
Figure 4.2 Simulated NOAA-6 AVHRR Sensor Output and Vegetative Index (normalized difference of sensor outputs) as a Function of View Zenith (scan) Angle. From Duggin (1982a. Figure 2)

Figure 4.3 (a) Radiances for the Visible and Near Infrared Channels as a Function of Scan Angle Increase with Increasing Amounts of Aerosols. From Holben and Fraser (1984, Figure 7) (b) Radiances for the VIS and NIR channels for NOAA-7. The radiances show only weak horizon brightening from the atmosphere alone. From Holben and Fraser (1984, Figure 5)

angle is the combined result of surface reflectance charac-

teristics and atmospheric Mie scattering.

Slater (1980) gives a good, general summary of scatter-

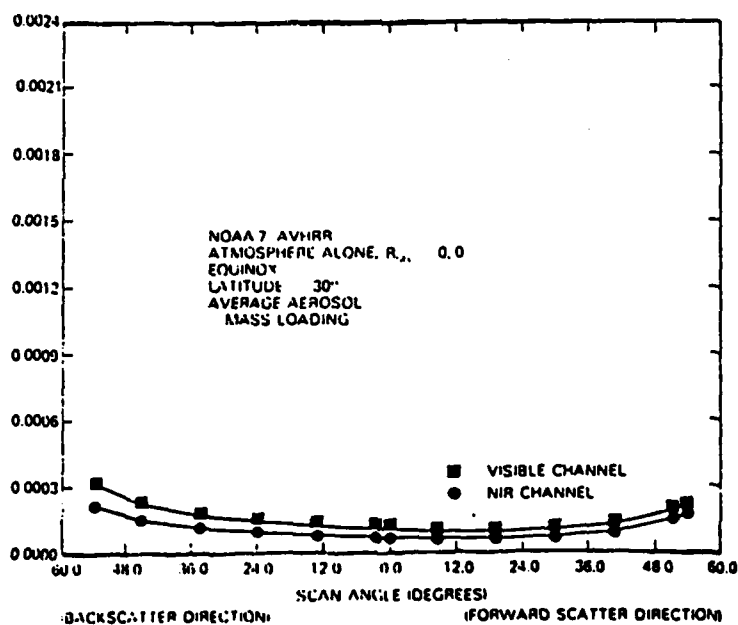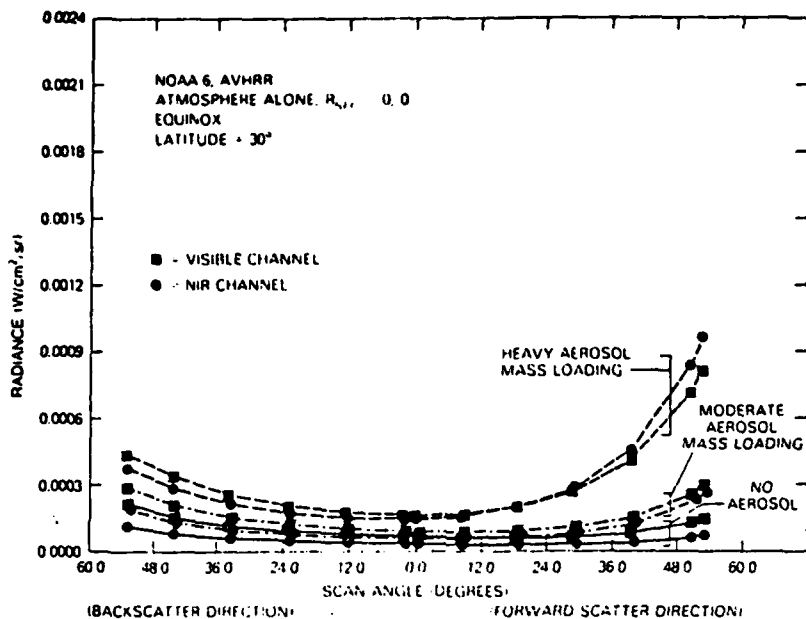ing effects related to remote sensing.   According to Slater:

> "Scattering causes the atmosphere to have a radi-
> ance of its own. Atmospheric scattering atten-
> uates the direct solar flux incident on the
> earth's surface and adds a hemispherical or
> diffuse component. The main effect of atmospheric
> scattering on remotely sensed data is the addition
> of upwelling atmospheric radiance or path radiance
> to the radiance of the ground scene. The amount
> of upwelling atmospheric radiance in remotely
> sensed data is a function of many variables
> including sensor altitude, atmospheric haze condi-
> tions, solar zenith angle, spectral sensativity,
> range of the sensor, angle of view from nadir,
> azimuth with respect to the sun and polarization"

EMITTIVE DATA

The emittive detectors operate somewhat differently

from the reflective detectors, in that, the detectors must

alternately view an internal blackbody temperature reference

and cold space before the surface radiative signal can be

processed and recorded. The signal from the detector is

processed electronically so that its amplitude is related to

the response difference between the blackbody reference and

cold space. Finally, the signal is recorded digitally.

The original purpose of the emittive channels of the

AVHRR was to measure earth radiance values for calculation

of sea surface temperatures. The radiance values are

inverted via the Planck function to provide the needed
brightness temperatures. In practice, before the brightness
temperatures are derived the the measured radiances must be
appropriately modified by the instrument's spectral response
and normalized. The values for the spectral response
modification are a result of temperature referencing
discussed above. These values are also included in the data
stream of each LAC scan line.

Once this modification is complete the brightness
temperature can be calculated using an inversion of the
Planck function:

$$T(L) = \frac{c_2 \lambda^{-1}}{\ln[1 + (c_1 \lambda^{-3})/L]} \qquad (4.4)$$

c_1 = 1.1910659 x 10^{-5} milliwatts/m^2 steradian cm^{-4}

c_2 = 1.438833 cm °k

L is the satellite radiance value

This radiant temperature can then be related to kinetic
temperature by equation 3.30. As with the reflective radi-
ances, the derived brightness temperatures also contain
information about the atmosphere between the sensor and the
target.

Proper interpretation of the radiance values from the
AVHRR requires a knowledge of the effects of the atmosphere
on the wavelengths of energy being sensed and application of

the appropriate radiative transfer equation. One method of
gaining this information involves calculation of the upwell-
ing radiance L at wavelength λ from atmospheric temperature
profiles and vertical profiles of concentrations of absorb-
ing gases. Wark and Fleming (1966) used the integral form
of the radiative transfer equation to calculate upwelling
radiance from the earth-atmosphere system:

$$L(\lambda) = [L_{bb}(T_s,\lambda) \cdot \tau(P_s,\lambda)0 \; d \; - \int_1^{\tau(P_s,\lambda)} [L_{bb}(T(P),\lambda) \; d\tau(P,\lambda)] \quad (4.5)$$

(T_s) is the surface temperature
(P_s) is the surface pressure
τ is the transmissivty
λ is the wavelength

The first term on the right hand side of the equation is the
"window radiation" from the earth's surface. The second
term is the radiative effect of the atmospheric layers after
attenuation. This equation is a fairly direct derivation
from Scharwchild's Equation. Equation 4.4 applies only to
monochromatic radiation of wavelength λ for a cloudless,
non-scattering, plane parallel atmosphere in local thermody-
namic equilibrium. Further modification of this equation is
usually necessary to accomodate the "real atmosphere." The
vertical profile of water vapor is of primary interest,
since the second term of Equation 4.4 is greatly affected by
by water vapor in the atmosphere. Thus, upper air soundings
can be used as a source of data for calculating upwelling
radiances.

When upper air soundings are not availble the satellite radiance data themselves can be used as a source of information about absorber profiles. (A substantial set of references on this subject, was compiled under the direction of Purdom, 1982.)

Otterman and Robinove (1981) researched the effects of water vapor and aerosols on the satellite-recorded radiances in the near infrared region. Using a simple model they broke the atmosphere up into two systems: a minimal atmosphere whose constituents are always present and a variable atmosphere which may change from one satellite passage to another. Further they outlined a general method for determining the atmospheric parameters of the model from imagery data. They conclude from their study of MSS data that:

> "...1) water vapor absorption can readily be
> distinguished from aerosol absorption because
> water vapor reduces the apparent reflectivity
> strongly in band MSS-7, weakly in band MSS-6 and
> not at all in bands MSS-4 and -5. 2) Reduction in
> the apparent reflectivity in all bands is sympto-
> matic of aerosol absorption."

Since AVHRR Channel 1 corresponds to a combination of MSS-4 and -5 and Channel 2 corresponds to MSS-6 and -7, one could assume that the reflectivity in Channel 1 would be unaffected by water vapor, while the reflectivity in Channel 2 will be reduced by water vapor vapor. Further, the reflectivity in both Channel and Channel 2 will be reduced by aerosol absorption.

Results of this study will show that water vapor absorption effects can be seen in a combination of AVHRR
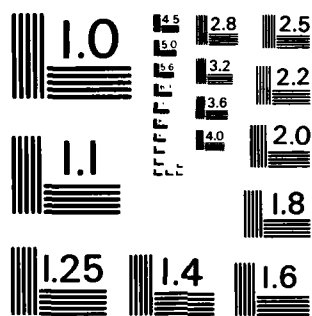
MICROCOPY RESOLUTION TEST CHART

NATIONAL BUREAU OF STANDARDS-1963-A

channels 4 and 5 radiance values. Close inspection of
Figure 3.10 indicates the atmospheric absorption in the 10.3
to 11.3 μm range (AVHRR channel 4) is small. Stated another
way, the radiation in the 10.3 to 11.3 μm is relatively
unaffected by water vapor. The radiation in the 11.5 to
12.5 μm band suffers more attenuation, most of which is due
to water vapor. Thus, as atmospheric water vapor concen-
trations increase (with earth surface temperatures constant)
the energy emitted by the earth and transmitted to space
remains nearly constant in the 10.3 to 11.3 μm range. For
the same conditions in the 11.5 to 12.5 μm range the
earth-emitted radiation transmitted to space suffers more
attenuation. A sensor "viewing" the radiation in the two
channels would receive relatively less energy in the 11.5 to
12.5 μm range on a moist day than on a dry day. A sensor
viewing the 10.3 to 11.3 μm channel under those circum-
stances should record similar radiance values on both days.

DIFFERENTIAL ABSORPTION

According to McClain (1979) the effect of the interven-
ing atmosphere on brightness temperature sensed by satellite
radiometers in the 10.5 - 12.5 μm band makes the brightness
temperature lower than surface temperature by a few tenths
of a degree Kelvin in very cold and dry atmospheres to near-
ly 10°K in very warm and moist atmospheres. Andig and Kauth
(1970) pioneered work in using two spectral bands to calu-

late the differential absorption in the atmsopheric window region to compensate for the effects of water vapor absorption and emission on sea surface temperature retrieval. Prabhakara et al. (1974) investigated this technique. They concluded that if two or more infrared detectors, each sensitive in a different and unequally transparent part of the atmospheric window region(s) view the same spot on the earth's surface simultaneously (i.e., through the same atmospheric column), then the differences in their measured radiances provide an atmospheric correction to either of the satellite derived brightness sea surface temperatures. McMillan (1975) reached the same conclusions. This early work was based on viewing in a cloud-free environment. McClain et al. (1983) applied this work to the TIROS-N AVHRR with promising results for improving the mapping of global sea surface temperatures as a result of the correction for atmospheric attenuation. Their work developed a method of accounting for cloud-contaminated data. Most recently Singh (1984) used NOAA-6 and NOAA-7 AVHRR data to develop an algorithm for atmospheric correction and derivation of sea surface temperature on a pixel by pixel basis. Singh states that there is a stronger attentuation in the 12 μm channel (Channel 5) than in the 11 μm channel (Channel 4). McMillan and Sanyal (1983) developed a method of using brightness temperature ratios of the differentially affected channels to retrieve atmospheric water vapor measurments.

VIEW ANGLE

The view angle problem continues to be controversial. Apparently some of the controversy comes from the terminology. Hoblen and Fraser (1984), in a very detailed report, show the normalized VIN to be significantly reduced by increasingly off nadir viewing. The backscatter direction is reduced slightly more than the forward scattering direction for NOAA-7. Further, relatively high biomass targets suffer a larger reduction than do lower biomass targets. Hoblen and Fraser report that these reductions are a result of Mie scattering. Channel 2 shows a significant increase in extreme forward scattering over the extreme backscatter direction because of preferential forward Mie scattering. While the impact of scattering tends to reduce the normalized vegetative index, its effect on the simple vegetative index is just the opposite. Since both indices are informally referred to as "the vegetative index," the terminology can be confusing. The research reported here dealt primarily with the simple index, so increases in the index were the norm for off nadir viewing.

Clouds also tended to mask the differential absorption effects in Channels 1 and 2. In accordance with the findings of Duggin et al. (1982b) increased cloudiness reduced the difference between Channels 2 and 1. An awareness of the degree of sub pixel cloudiness was especially important for this research, since even sub pixel clouds reduced the

Channel 2 minus Channel 1 difference (CH 2-CH 1) difference
on days that were thought to be dry in terms of precipitable
water. For these situations one expected a relatively larg-
er CH 2 - CH 1 difference but, in fact, there was a smaller
difference as a result of the sub pixel clouds. The view
angle and cloud effects, in various degrees and
combinations, were observed during this course of study.
They, along with the differential absorption effects, are
discussed in the results presented in Chapter V.

CHAPTER V

STUDY RESULTS

DATA ANALYSIS

During the 1983 growing season NOAA recorded and stored numerous AVHRR scenes. The LAC digital radiance values for the various channels provided the bulk of the data for this study. This study investigates the relationship between recorded radiance values for channels 1, 2, 4 and 5 and the amount of moisture in the atmosphere. Precipitable water is used as the atmospheric moisture measurement. The effects of water vapor, alone, and water vapor plus clouds are discussed. Several cases for different locations and varying amounts of atmospheric moisture will be discussed and illustrated after the data selection and analysis methods are presented.

DATA SELECTION AND PROCESSING

Three types of data were used for this study: 1) LAC digital video, or channel data with associated calibration coefficients, earth location points and solar zenith angles;

2) precipitable water amounts from upper air soundings and

3) the conventional hourly surface weather observations.

The LAC video data was supplied by NOAA's Assessment Infor-

mation Services Center. The precipitable water data came

from the National Weather Service Facsimile Network or was

derived from data supplied by the Techniques Development

Unit of the National Severe Storms Forecasting Center.

Surface observations were provided by the National Climate

and Data Center, the U. S. Air Force Third Weather Wing and

various local surface observing stations.

The selection of LAC scenes was based on two primary

factors: 1) availability of LAC data over the crop growing

region of the United States for three consecutive days and

2) the occurrence of successive, apparently cloud free, days

during which large moisture variations occurred. For

several cases the latter requirement was relaxed so that a

more comprehensive study of the channel responses could be

made. The latter factor tends to be very limiting for data

selection since the normal tendency of the atmosphere is to

produce more clouds as moisture increases.

As a "first guess" at scene selection daily maps from

the NOAA Weekly Weather Series were examined in conjunction

with National Weather Service (NWS) twelve hour precipitable

water analysis. The daily maps provided a starting point

for determining the degree of cloudiness for a given

location in a particular LAC scene. The preciptable water

analysis provided the initial information on atmospheric

moisture variation.

All digital data processing of the LAC scenes was done
on the University of Missouri AMDAHL computer. The LAC data
were first compressed from 1600 bit per inch data to 6250
bit per inch data and then converted from packed bit data to
FORTRAN readable data. A computer program which was devel-
oped by Lockheed and modified by programmers at the Univer-
sity of Texas-Austin was further modified to read the
processed LAC tapes. The program used the earth location
points from the beginning of each LAC scan line to retrieve
the channel radiance values for groups of selected pixels.
Kidwell (1983) provides the data format for the LAC tapes.

The pixel groups were associated with grid points from
an I-J grid developed by Charney and Phillips (1958). This
method of data selection and retrieval was used because of:
1) software availability, 2) storage and time constraints on
computer processing resources and 3) a desire to view
portions of the LAC scenes which were beneath one type of
air mass. The grid is shown in Figure 5.1. The groups of
pixels will be referred to as "sub-images". Depending on
the location of the grid point, the sub-images covered
between 1600 and 2500 square kilometers. Further, depending
on the locations of the ground site with respect to the
satellite nadir, the sub images or scenes contain from
approximately 700 to 2000 pixels.

Sub images were formed at forty different locations for
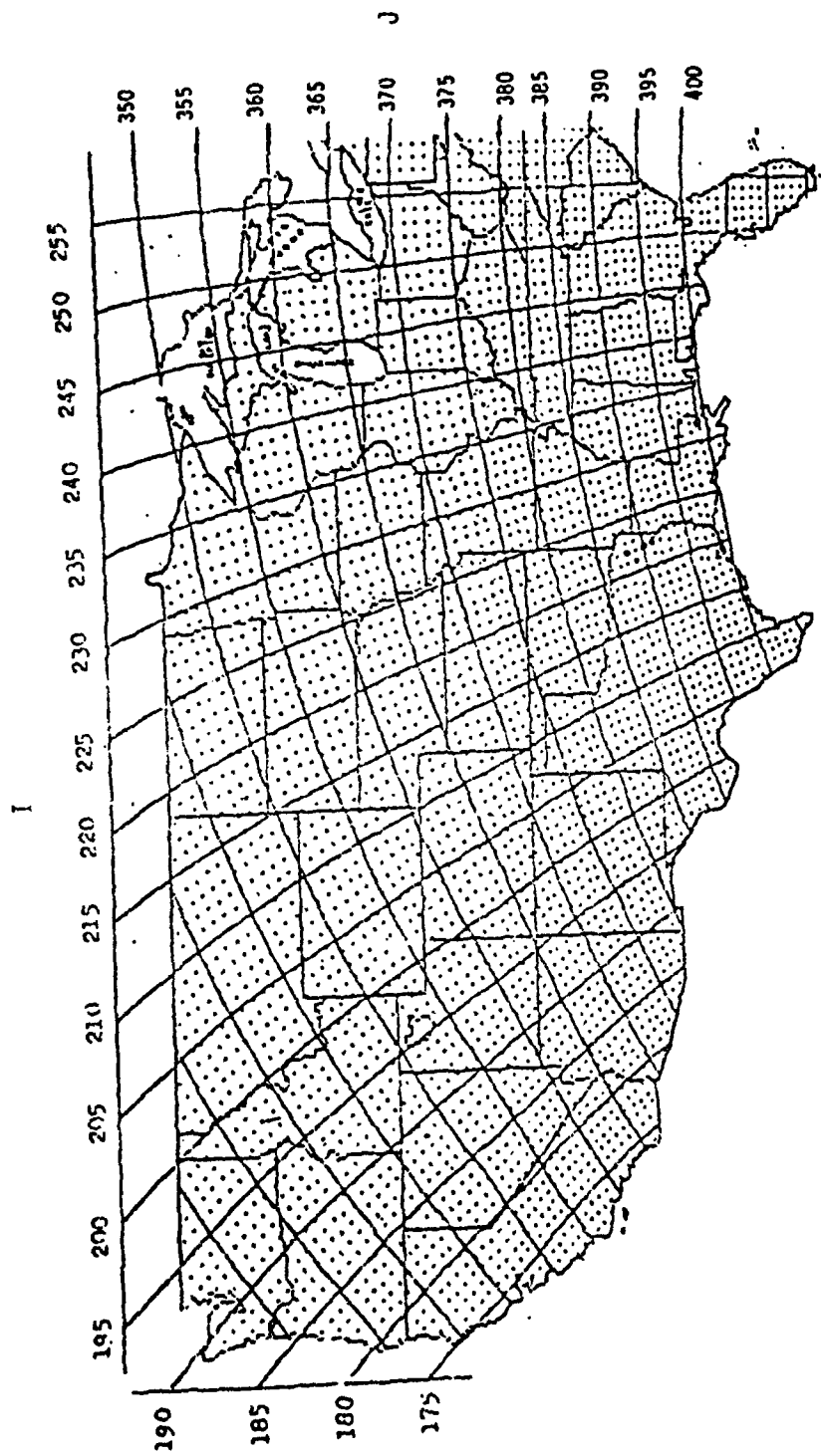various dates. A simple average of each channel value was

Figure 5.1   I-J Coordinate Grid   After Charney and Phillips (1958)

determined for each sub-image by averaging the values for
all individual pixels within each sub-image. Locations
whose Channel 1 and Channel 4 radiance values indicated
gross cloudiness were eliminated. In several instances a
location which promised to be interesting weather-wise was
eliminated from the study because the sub-image could not be
retrieved from the LAC scene. This happened for at least
two reasons, 1) precession of the satellite or 2) a malfunc-
tion in the LAC data gathering/handling system. Finally,
proximity to an upper air sounding station became a dominant
factor in selecting study areas from the remaining
locations. The elimination process discussed above limited
the case studies to the locations and dates shown in Figures
5.2 through 5.4.

The analysis for each sub-image consisted of the
following calculations and operations for cloud screened and
unscreened data: 1) computing averages and standard devi-
ations of the channel values for all pixels in each
sub-image; 2) computing uncorrected and sun angle corrected
Channel 2 Channel 1 differences 3) computing the ratios and
differences of Channels 1 and 2, and Channels 4 and 5; 4)
correcting the computed differences for sun and view angles;
5) contour plots of the values of Channels 1 and 2 and of
the Channel 2 Channel 1 difference. Additionally, upper
air soundings from the nearest upper air station were used
to calculate precipitable water for many dates and
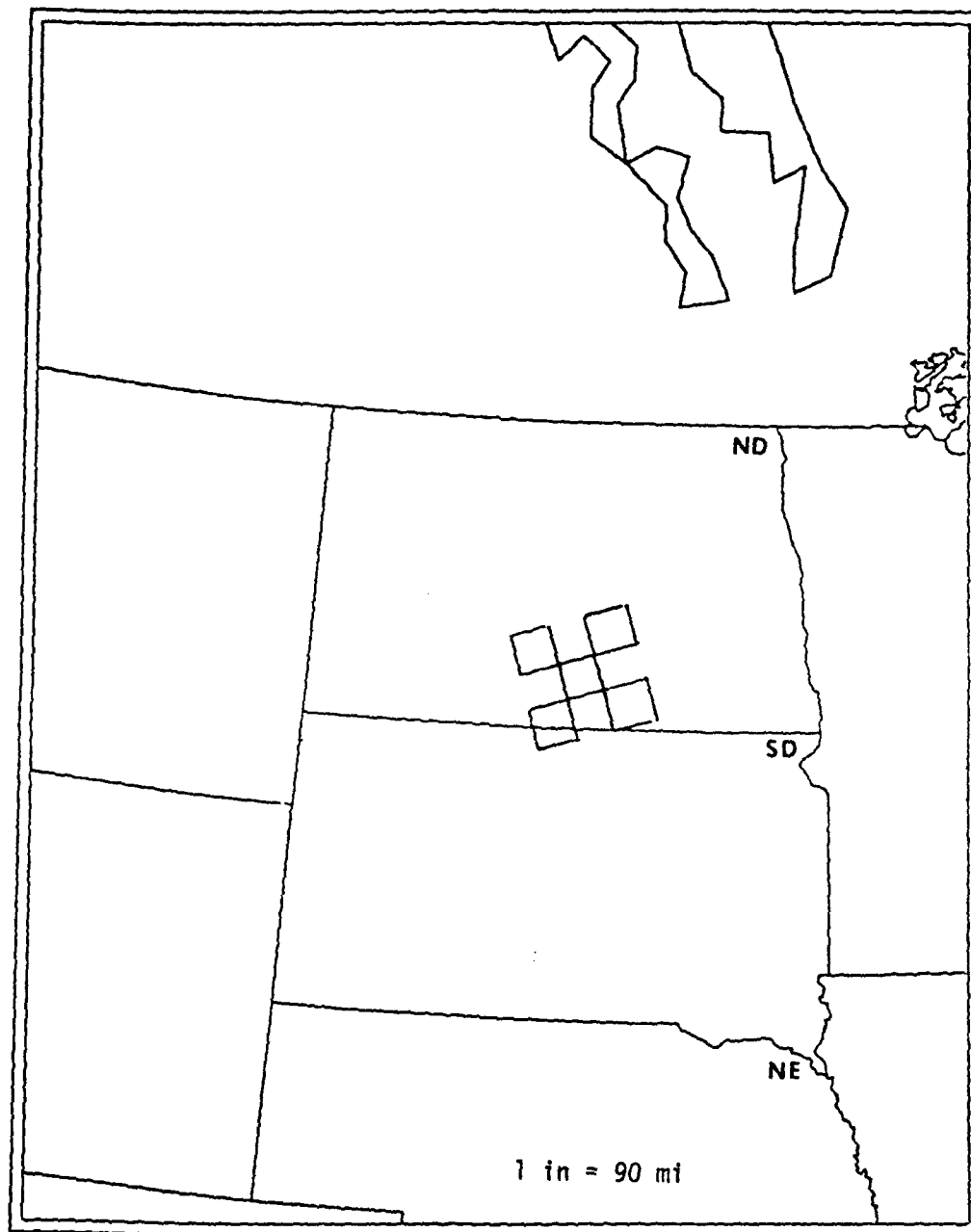locations. To provide a check on actual cloud conditions,
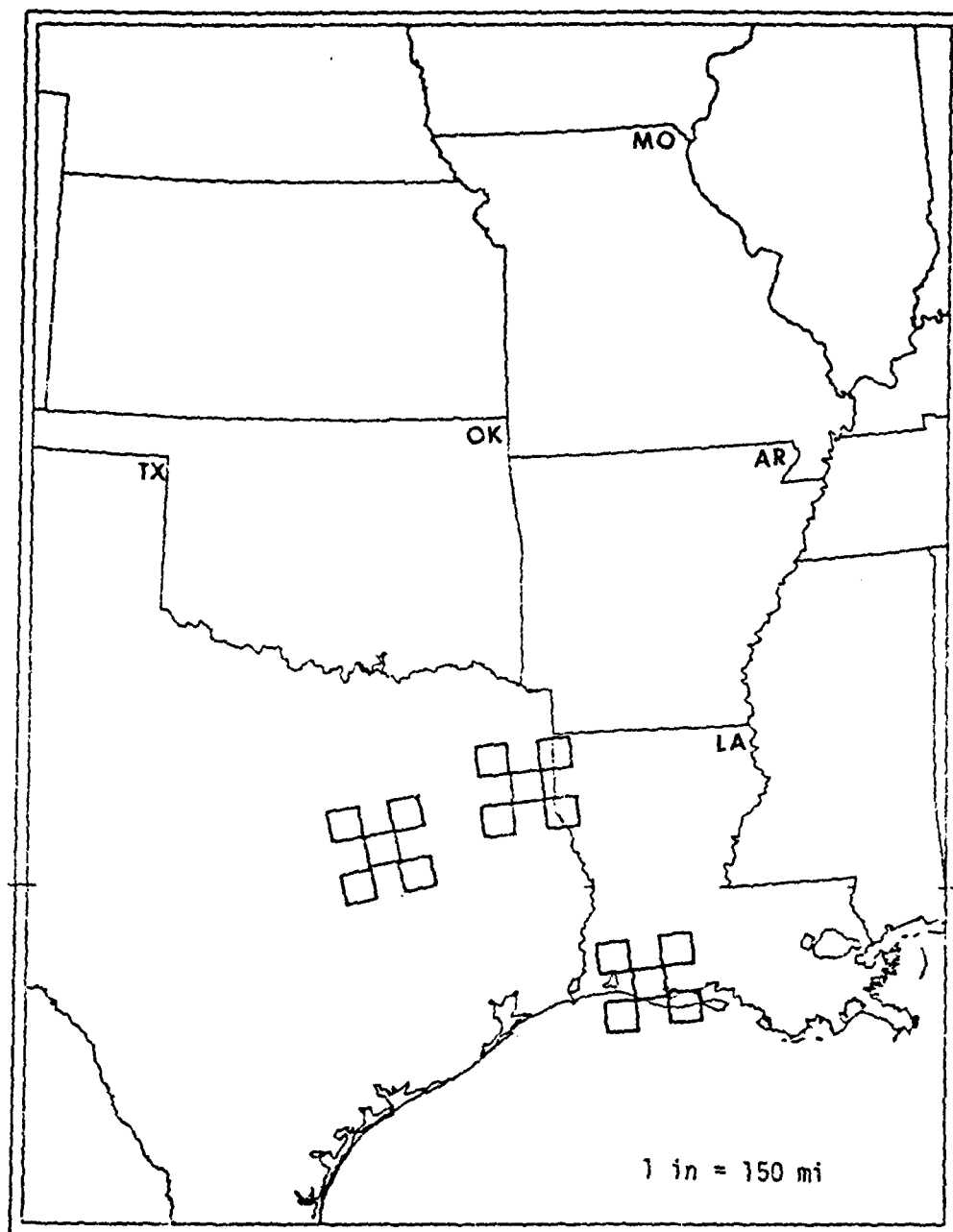
DAYS 106, 107 AND 108

APRIL 16, 17 AND 18 1983

Figure 5.2 Data Locations-Spring Cases
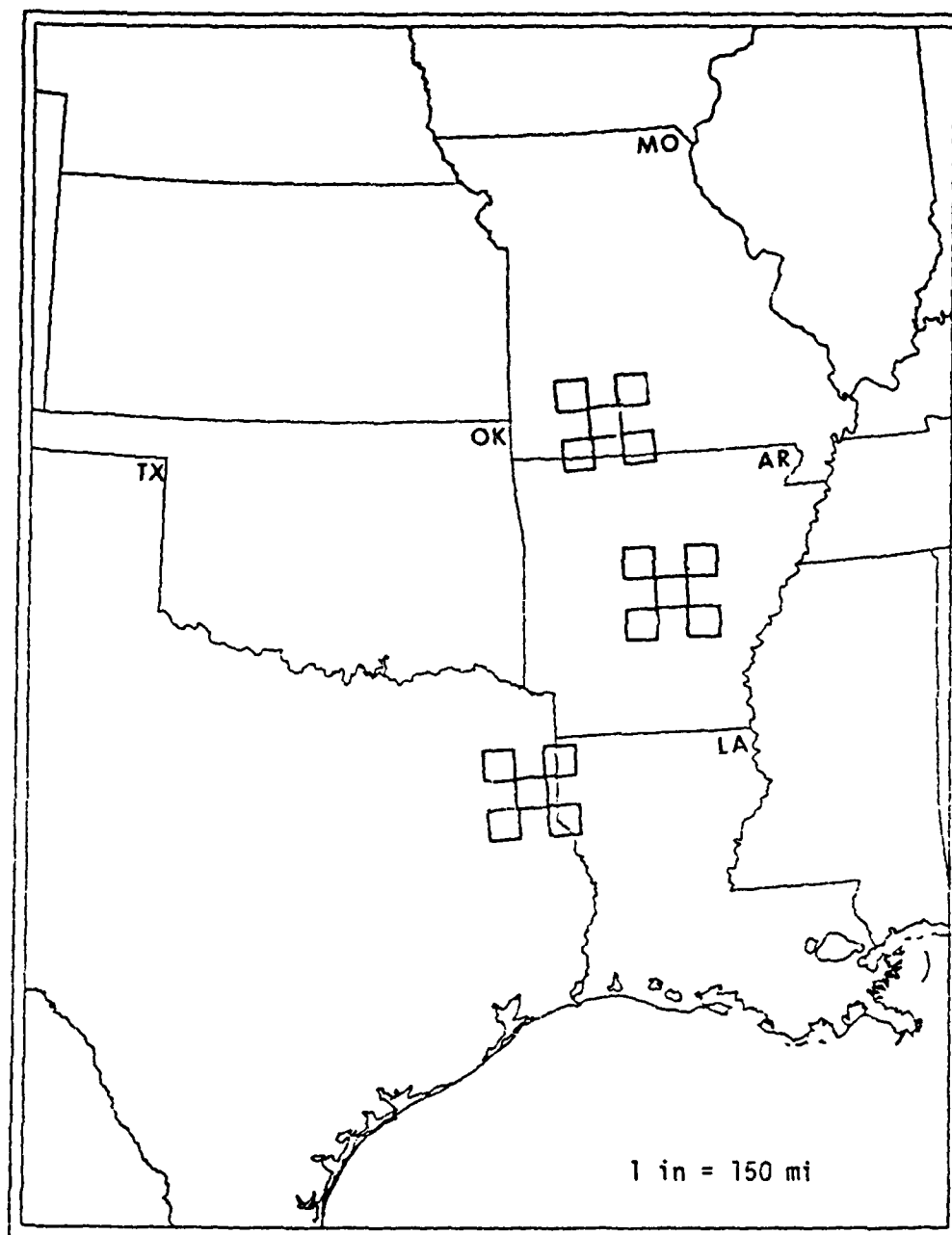
DAYS 188, 189, 191 AND 192
JULY 7, 8, 10 AND 11 1983

Figure 5.3   Data Locations-Mid Summer Cases

DAYS 222, 223, 224 AND 225

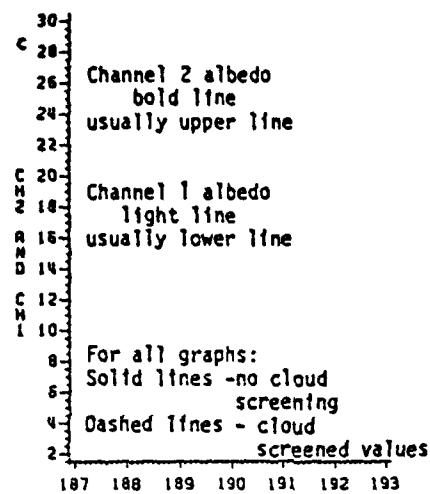AUG 10, 11, 12 AND 13 1983
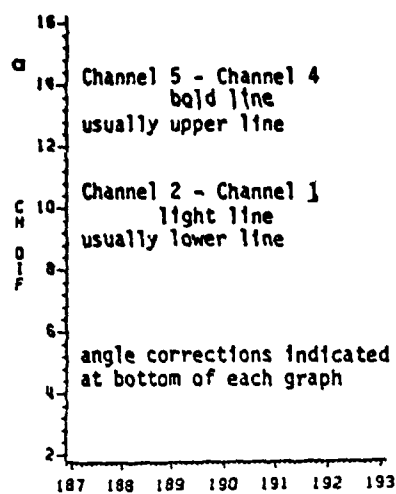
Figure 5.4   Data Locations-Late Summer Case

several sets of surface weather observations for the various locations were reviewed.

CASE STUDY DISCUSSION

To begin the discussion of the various case studies a few points should be made. Two important calculations for this study have been the Channel 5 minus Channel 4 radiance difference (CH 5-4) and the Channel 2 minus Channel 1 albedo difference (CH 2-1). These two differences are generally compared in this report and, thus, the graphs of the two differences are overlayed (see Figure 5.5) for comparison purposes. Because the energy sensed by Channels 2 and 5 is more susceptible to water vapor absorption than is the energy sensed by Channels 1 and 4, it was orginally thought that the trace curves would behave similary over time. This was not necessarily the case, as will be demostrated in some detail later.

A number of composite figures containing time graphs of the variations of the channel and channel difference data were prepared for each case study location. For illustrative purpose the composite figures of this chapter contain: 1) a channel difference graph (CH 5-4 and CH 2-1) without sun angle corrections; 2) a channel difference graph where the sun angle correction has been made to CH 2-1; 3) a graph of the Channel 2 and Channel 1 values; 4) a graph of the Channel 5 and Channel 4 values; 5) precipitable water time

a

16 —
15 —

Channel 5 - Channel 4
bold line
usually upper line

12 —

Channel 2 - Channel 1
light line
usually lower line

CH 01F
10 —
8 —
6 —

angle corrections indicated
at bottom of each graph

4 —
2 —

187 188 189 190 191 192 193
DAY
CH 5-4 BOLD   CH 2-1 LIGHT
ANGLE CORRECTION: NONE

Sky Conditions, visibility

and dewpoints hour before

and hour after satellite

overpass

LITTLE ROCK
LAT=.   LON=.

b

20 —
18 —
16 —

Latitude and Longitude
of center of pixel in
degrees and hundredths
of degrees

14 —

Channel data: same as
above except
Channel 2 - Channel 1
has been divided by cosine
of solar zenith angle

CH 01F
12 —
10 —
8 —
6 —

All dates are Julian

4 —

Circle Indicates Day of
Satellite Nadir

2 —

187 188 189 190 191 192 193
DAY
CH 5-4 BOLD   CH 2-1 LIGHT
ANGLE CORRECTION: 2-1 SUN

c

30 —
28 —
26 —

Channel 2 albedo
bold line
usually upper line

24 —
22 —

CH 2 AND CH 1
20 —
18 —
16 —
14 —
12 —
10 —

Channel 1 albedo
light line
usually lower line

8 —

For all graphs:
Solid lines -no cloud
              screening
Dashed lines - cloud
              screened values

6 —
4 —
2 —

187 188 189 190 191 192 193
DAY
CH 2 BOLD   CH 1 LIGHT
ANGLE CORRECTION: NONE

d

4.0 —
3.5 —

PCP WATER
3.0 —
2.5 —
2.0 —
1.5 —
1.0 —
0.5 —
0.0 —

Precipitable water
in atmospheric column
in centimeters
Vertical line is time
of satellite overpass
00Z sounding value
plotted at date value
12Z sounding value
plotted halfway
between date values

188 189 190 191 192 193
DAY

e

140 —
135 —
130 —
125 —
120 —

Channel 5 radiance
bold line
usually upper line

CH 5 AND CH 4
115 —
110 —
105 —
100 —
95 —
90 —
85 —
80 —
75 —
70 —

Channel 4 radiance
light line
usually lower line

For all channel graphs:
Observation time -
   approximately 2030 Z

187 188 189 190 191 192 193
DAY
CH 5 BOLD   CH 4 LIGHT
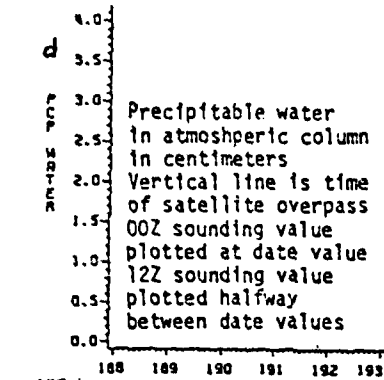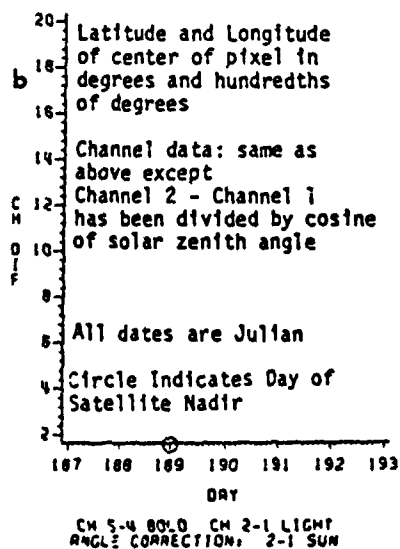ANGLE CORRECTION: NONE

Figure 5.5   Key to Composite Charts

series; and 6) appropriate weather observations. See Figure
5.5 for a key to the composite charts. As previously
mentioned a cloud screen was applied to all the sub-images
discussed in this report. The screen eliminates any pixel
whose albedo was greater than 13.65. This value is equiv-
alent to the value used operationally at the Assessment
Information Services Center. (LeDuc, 1984)

CASE STUDIES


WACO, TEXAS

Julian Dates 106, 107, and 108 (April 16, 17, and 18, 1983)

A study of sub-images around Waco, Texas was undertaken
because of the apparently cloud free conditions on days 106,
107, and 108. During this time rapid and significant atmo-
spheric moisture changes occurred. For the 72 hour period
of this case study the sky condition was continously clear.
The following discussion deals with only one sub image but
it is representative of the entire group of five Waco
sub-images.

Prior to day 106 a Continential High pushed southeast-
ward through the southern United States. On day 106 Waco
was under the influence of this High. The surface weather
was characterized by clear skies, twenty mile visibility,
light winds and very low dewpoints. Precipitable water

amounts (See Figure 5.6d) at Stephenville Texas, the closest upper air station, were less the half the normal seasonal average. (The NWS precipitable water charts provide a seasonal average for each location's precipitable water analysis). Because of the excellent atmospheric viewing conditions and because the Waco sub-images were near nadir, day 106 was considered a benchmark observation against which the day 107 and 108 sub-images were compared.

On day 107 southerly return flow around the high pressure system resulted in a marked increase in precipitable water, but the influence of an upper air ridge prevented the clouds usually associated with an increase in precipitable water. The surface map for day 108 showed a dry line just past the Stephensville, Texas upper air station. Judging from the Waco dew point decrease from 50°F at 15Z to 44 7°F at 19Z, the dry line "cleared" the Waco atmosphere of much of the previous day's water vapor loading prior to the 2030Z satellite overpass. This time change of the atmospheric water loading seems well recorded in the both CH 5-4 and CH 2-1 traces. As the precipitable water increases, the channel difference values go down. See Figure 5.6b.

Because the Waco sub-images were made within a three day period, large changes in the CH 2-1 differences were problably not the the result of increased greeness of the scene. View angle, absorption and clouds were considered as the most likely reasons for changes in the CH 2-1 difference. On day 106 Waco was at satellite nadir. On day
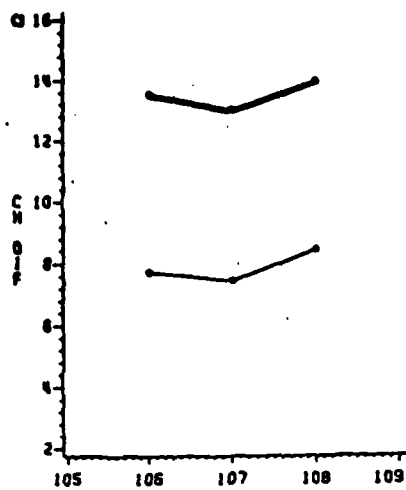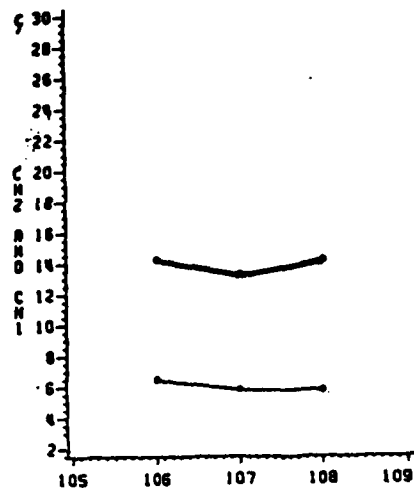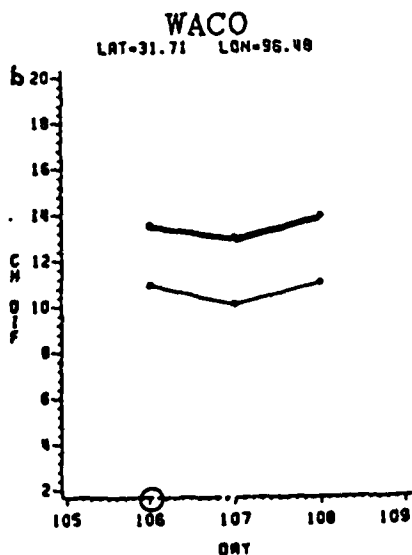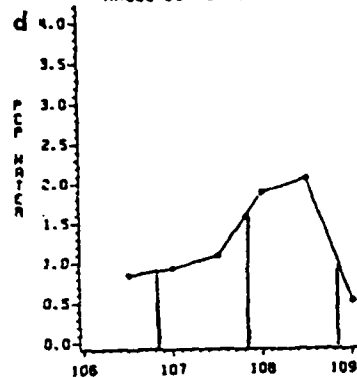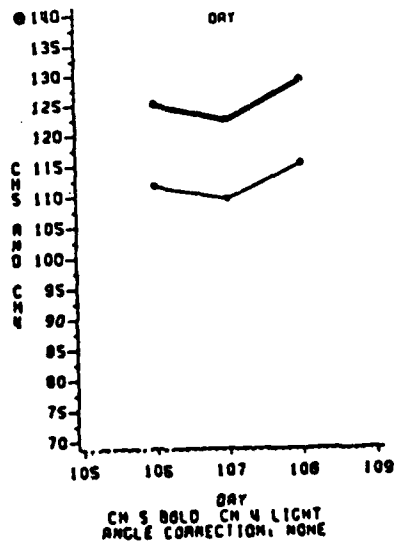
Figure 5.6 Waco, TX (Spring) Composite Chart

107 the satellite had precessed eastward. Day 108 had the largest view angle of the series. Based on the simulations by Holben and Fraser (1984) and Justus (1984), the view angle contribution to the scene radiance should have resulted in an increase in CH 2-1 on day 107. Thus, the decrease in the day 107 Ch 2-1 value has to be explained some other way. Increased clouds were considered as a source of the decrease, but the cloud screens indicated from very little to no increase in cloud cover in the day 107 sub-images. Therefore, the decrease in the trace is taken as an indication of the atmospheric water vapor loading.

LONGVIEW, TEXAS

Julian Dates 106, 107, AND 108 (APRIL 16, 17 and 18, 1983)

The Longview sub-images were also chosen for study because of their apparently cloud free nature. Significant moisture changes also occurred at Longview during the 72 hour period. The high pressure system which influenced Waco's weather also influenced Longview's weather during the period of days 106 to 108.

Day 106 was clear and very dry with dew points in the twenties. The 12Z sounding showed only .50 cm of precipta- ble water in the column. By 12Z on day 107 the preciptable water had doubled. During the hour of satellite overpass a scattered cirrus deck was observed at Longview. Dewpoints

were in the upper thirties. Day 108 was again clear and dewpoints dropped from a high of 50°F at 14Z to 33°F at time of satellite overpass. The precipitable water trace shows a similar change.

The composite figure (Figure 5.7) for Longview sub-image, location one, shows the behavior of the various channels and channel differences to be similar to the Waco sub-images. Both channel differences show a minimum in the trace on day 107. This minimum, most likely, is a combination of 1) the additional water loading of the atmosphere and 2) sub-pixel clouds or diffuse cirrus. The cloud screens are shown in Figure 5.8. Day 107 has several pixels whose lower Channel 4 and higher Channel 1 values relative to the day 106 and 108 values indicate clouds. These pixels most likely have very low CH 2-1 values, yet their Channel 1 values are not high enough to be screened out based on a visible channel test. (Only pixels with values above the horizontal lines on the cloud screen graphs are removed by the cloud screening process)

Referring to Figure 5.7c, while Channel 1 had only a small change from day 106 to 107, the Channel 2 value fell more sharply. It seems most likely that the slight change in cloud amount combined with the doubling of the precipitable water caused the CH 2-1 value to drop. The CH 5-4 difference for days 106 to 107 nearly parallels the CH 2-1 change. Between days 107 and 108 the CH 5-4 trace increased, as expected with decreasing precipitable water
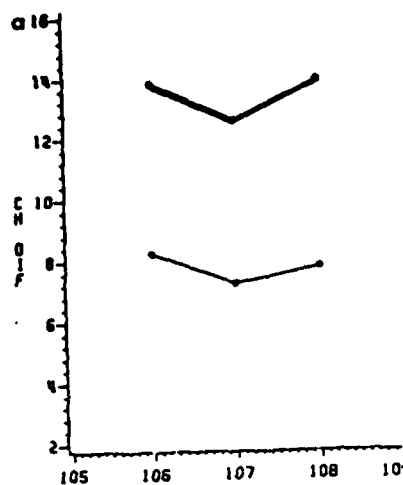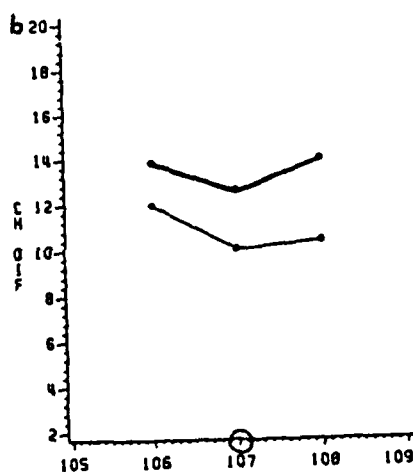
a

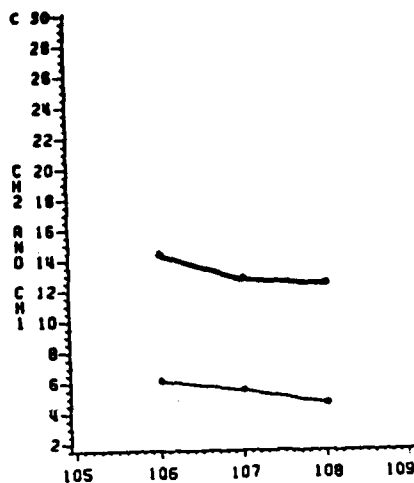CH S-4 BOLD   CH 2-1 LIGHT
ANGLE CORRECTION: NONE

c

CH 2 BOLD   CH 1 LIGHT
ANGLE CORRECTION: NONE

LONGVIEW SKY/SURFACE CONDITIONS

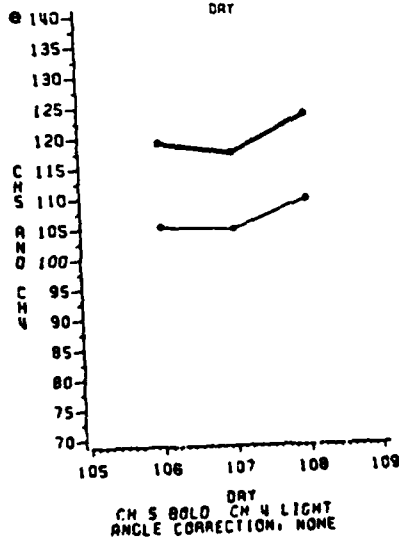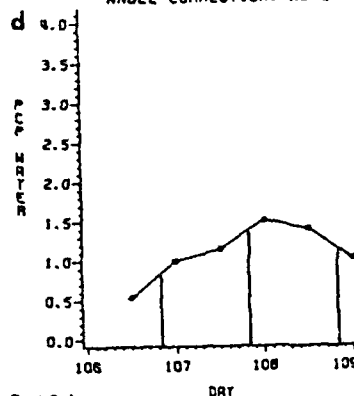| DAY	TIME	SKY	VSBY	DP
106	20Z	CLR	35	26
	21Z	CLR	35	27
107	20Z	250 SCT	35	39
	21Z	250 SCT	35	38
108	20Z	CLR	35	33
	21Z	CLR	35	34

LONGVIEW
LAT=31.75   LON=94.78

d

b

CH S-4 BOLD   CH 2-1 LIGHT
ANGLE CORRECTION: 2-1 SUN

e

CH 5 BOLD   CH 4 LIGHT
ANGLE CORRECTION: NONE

Figure 5.7   Longview, TX (Spring) Composite Chart, Location 1
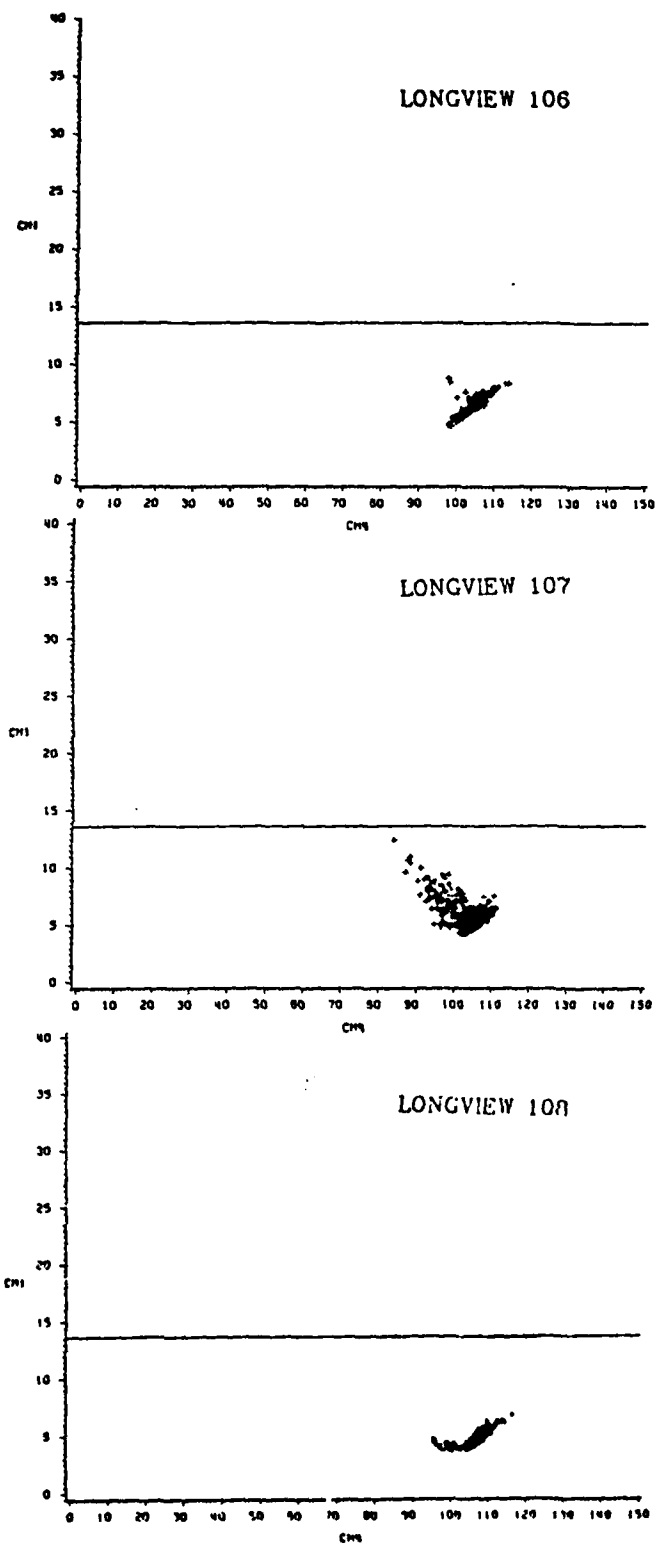
Figure 5.8   Longview, TX (Spring) Cloud Screens, Location 1

amounts. The CH 2-1 trace, while also increasing, rose less than the CH 5-4 trace. This seems to indicate that factors other than atmospheric water vapor were influencing the CH 2-1 behavior. View angle may have been the important factor in the CH 2-1 variation.

A second Longview sub-image,(see Figure 5.9) through the three day period displays nearly parallel CH 5-4 and CH 2-1 behavior. However, the sub-image was much more strongly influenced by clouds than the first sub-image. The cloud screens for the second sub-image are shown in Figure 5.10. Referring, again, to Figure 5.9, the Channel 1 and Channel 2 values indicate the cloud contamination. The dashed lines on the figure are cloud screened values. Figures 5.11c and 5.11d are contour "maps" of the day 107 Channel 1 scene, before and after cloud screening. The residual clouds and their distribution are evident from the darker "pixels" which stand out after rescaling of the of the contour limits. The "after cloud screening" map has an enhanced scaling to emphasize residual cloudiness. These maps can be compared to a similar maps for day 106 (see Figures 5.11a and 5.11b). Note that, despite rescaling in Figure 5.11b, the scene retains a nearly homogeneous appearance, thus indicating, no bright clouds. This sort of comparison was made for all scenes in each case study series to insure that the effects of clouds were accounted for in the analysis.

Despite the cloud screening, the day 107 scene remains quite cloud contaminated. The sharp changes in all the
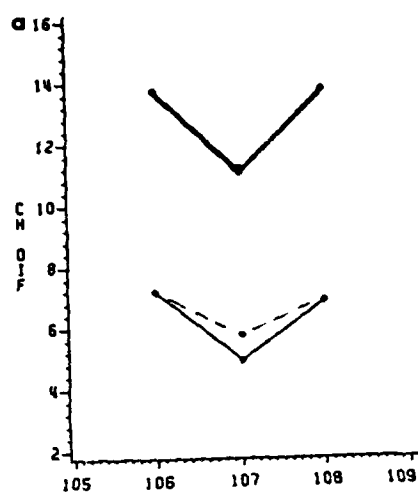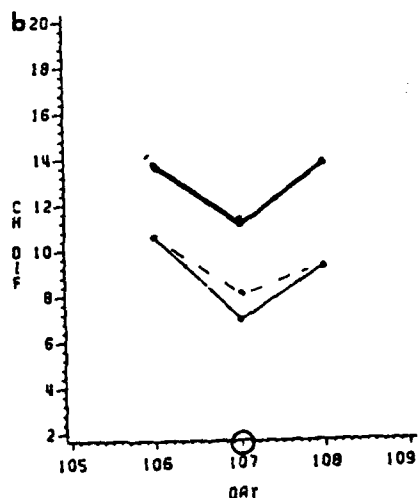
a

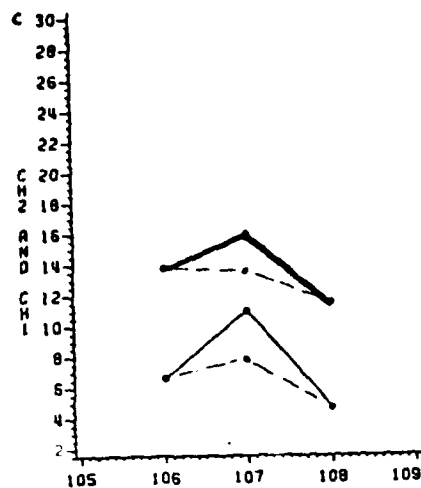CH 5-4 BOLD   CH 2-1 LIGHT
ANGLE CORRECTION: NONE.

LONGVIEW SKY/SURFACE CONDITIONS

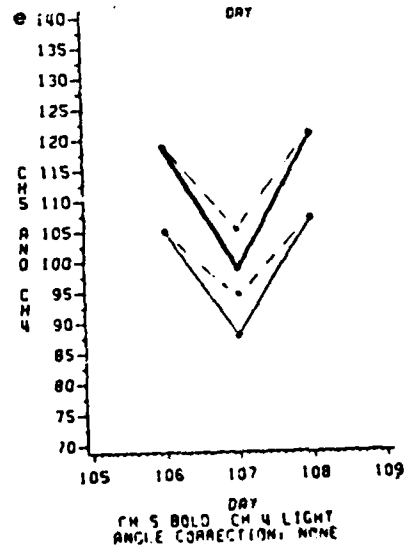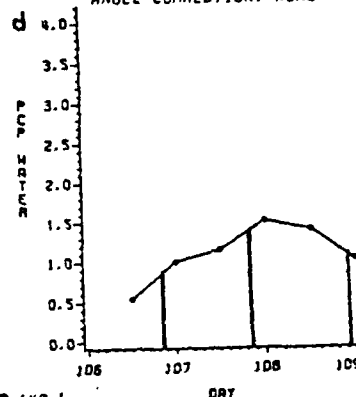| DAY	TIME	SKY	VSBY	DP
106	20Z	CLR	35	26
	21Z	CLR	35	27
107	20Z	250 SCT	35	39
	21Z	250 SCT	35	38
108	20Z	CLR	35	33
	21Z	CLR	35	34

LONGVIEW
LAT=32.61   LON=94.19

b

CH 5-4 BOLD   CH 2-1 LIGHT
ANGLE CORRECTION: 2-1 SUN

c

CH 2 BOLD   CH 1 LIGHT
ANGLE CORRECTION: NONE

d

e

CH 5 BOLD   CH 4 LIGHT
ANGLE CORRECTION: NONE

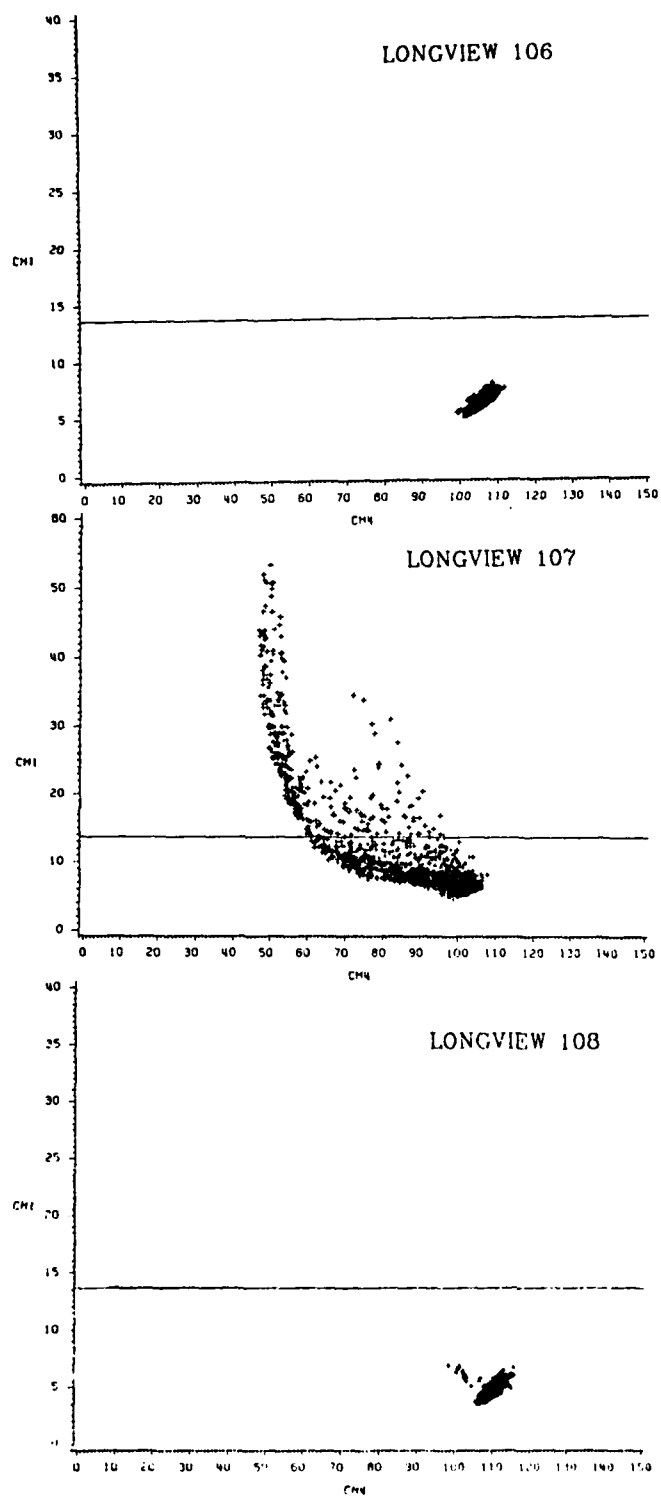Figure 5.9   Longview, TX (Spring) Composite Chart, Location 2

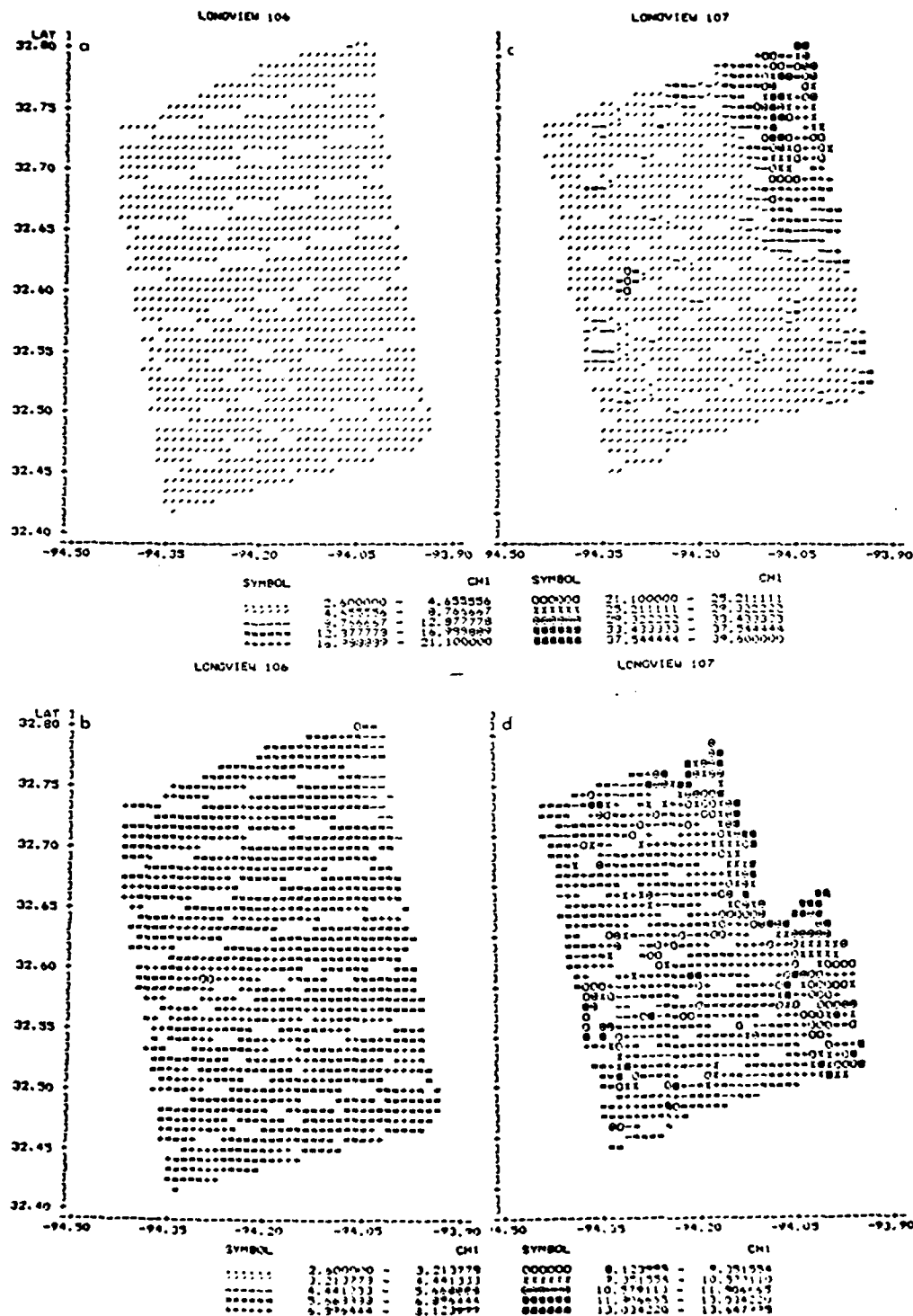Figure 5.10   Longview, TX (Spring) Cloud Screens, Location 2

Figure 5.11   Longview, TX (Spring) Channel 1 Contour Map,
Location 2
Days 106 and 107

channel and channel difference values for day 107 indicate the combined cloud/water vapor effect. It is quite evident from the screened trace value that much water vapor effect remains in the scene. Note that the CH 5-4 value does not change despite the screening.

LAKE CHARLES, LA

Julian Dates 106, 107, and 108 (April 16, 17 and 18, 1983)

The same high pressure system which cleared and dried the air over southeastern Texas on day 106 dropped the precipitable water to less than twenty percent of its seasonal normal for the day 106, 12Z, Lake Charles sounding. The dewpoint during satellite overpass was in the low thir-ties. The sky was clear on both days 106 and 107, but the day 107 dewpoints were in the mid forties. Very weak high pressure characterized the weather on day 108. The reported sky condition during satellite overpass on day 108 was scat-tered clouds at 2500 ft. The dewpoints were in the mid fifties and the precipitable water was between 1.5 and 2.8 cm.

The CH 2-1 trace decreases steadily through the period. See Figure 5.12b. The decrease can be attributed to increasing water absorption and changing view angle on day 107 and to increasing cloud cover on day 108. Some cloud screening was necessary for day 108. After the screen was
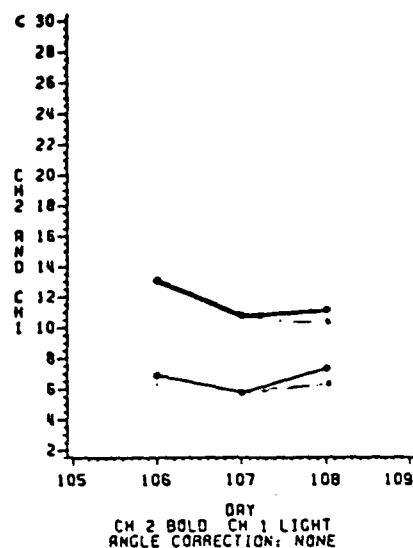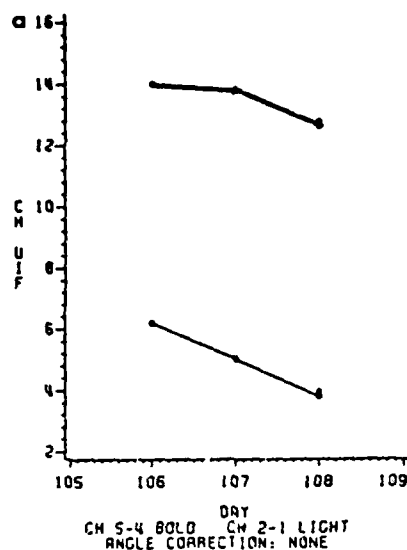
LAKE CHARLES SKY/SURFACE CONDITIONS

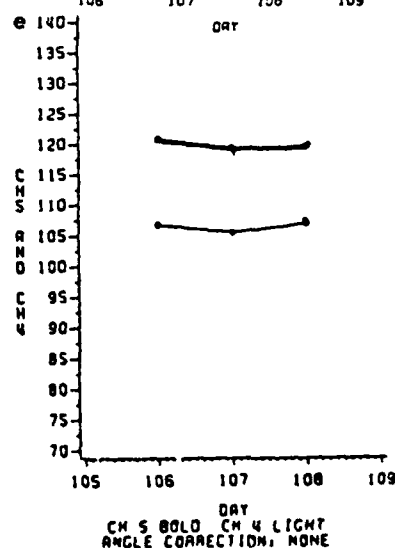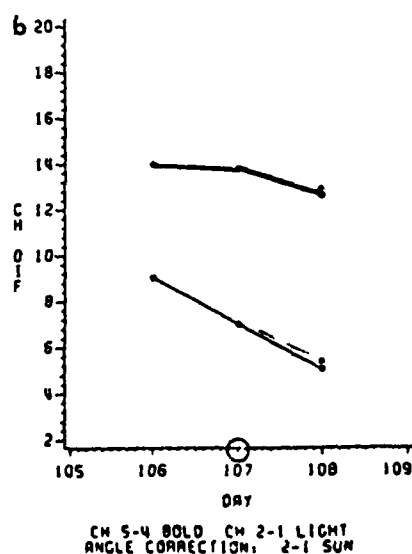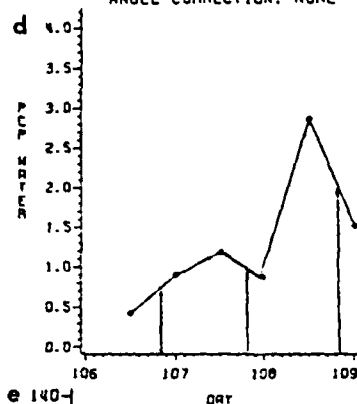| DAY	TIME	SKY	VSBY	DP
106	20Z	CLR	15	34
	21Z	CLR	15	33
107	20Z	CLR	15	44
	21Z	CLR	15	40
108	20Z	25 SCT	12	54
	21Z	25 SCT	15	52

LAKE CHARLES
LAT=30.23   LON=93.51

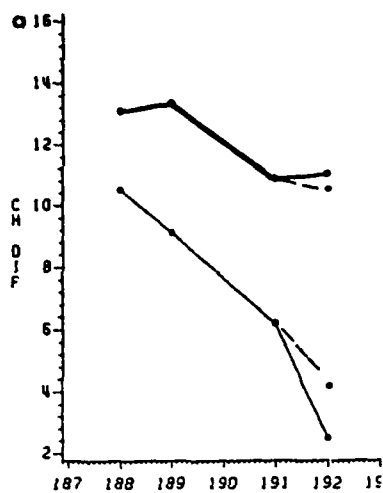Figure 5.12   Lake Charles, LA (Spring) Composite Chart

applied there was a small amount of residual cloudiness.
While CH 5-4 decreased, as expected, based on the increase
of precipitable water between days 107 and 108, it showed
only a shallow decline. The apparent increase in atmospher-
ic water vapor was large between the two days, leading one
to expect a sharper drop in CH 5-4. The rather shallow
decline may indicate the atmosphere at the time of satellite
overpass was actually drier than inferred by linear interpo-
lation of precipitable water amounts between upper air
sounding time. The fact that a 4° decrease in dewpoint
occurred between 19Z to 21Z lends some backing to this
explanation.

LONGVIEW, TEXAS

Julian dates 188, 189, 191 and 192 (July 7, 8, 10 and 11,
1983)

     Longview's weather on days 188 and 189 was influenced
by the remnants of a Continental High pressure system. High
pressure aloft had also set in and would remain an influenc-
ing factor for the entire case study period. Sounding data
indicated a moist atmosphere at 12Z on day 188. The expan-
sion of the upper air ridge during the following 36 hours
apparently caused the drying observed during that time. See
Figure 5.13d. The dry airmass provided excellent cloud free
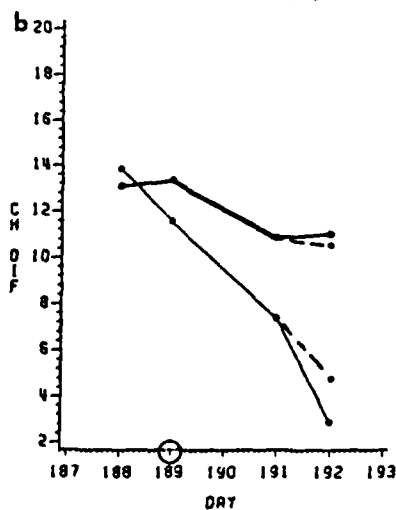viewing during satellite overpass. Sky conditions on day

a

16
14
12
C
H
10
D
I
F
8
6
4
2

187 188 189 190 191 192 19
DAY
CH 5-4 BOLD   CH 2-1 LIGHT
ANGLE CORRECTION: NONE

c

30
28
26
24
C 22
H 20
2 18
A 16
N 14
O 12
C 10
H 8
1 6
4
2

187 188 189 190 191 192 193
DAY
CH 2 BOLD CH 1 LIGHT
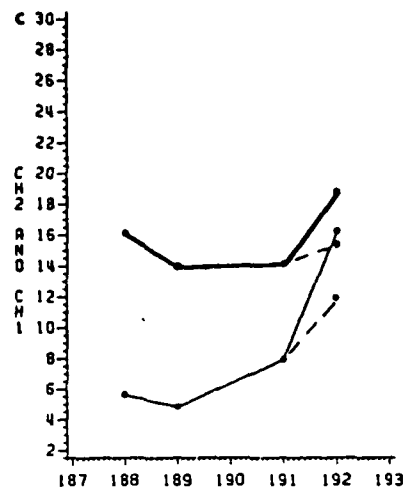ANGLE CORRECTION: NONE

LONGVIEW SKY/SURFACE CONDITIONS

DAY	TIME	SKY	VSBY	DP
188	20Z	CLR	35	55
	21Z	CLR	35	53
189	20Z	CLR	15	58
	21Z	CLR	15	56
191	20Z	40 BKN	6H	65
	21Z	30 OVC	2RW	68
192	20Z	35 SCT	7	68
	21Z	35 SCT	7	67

d

4.0
3.5
P
C 3.0
P
2.5
W
A 2.0
T
E 1.5
R
1.0
0.5
0.0

188 189 190 191 192 193
DAY

LONGVIEW
LAT=31.74   LON=94.78

b

20
18
16
14
C
H 12
D
I 10
F
8
6
4
2

187 188 189 190 191 192 193
DAY
CH 5-4 BOLD CH 2-1 LIGHT
ANGLE CORRECTION: 2-1 SUN

e

140
135
130
125
120
C 115
5 110
A 105
N 100
D
95
C
H 90
4 85
80
75
70
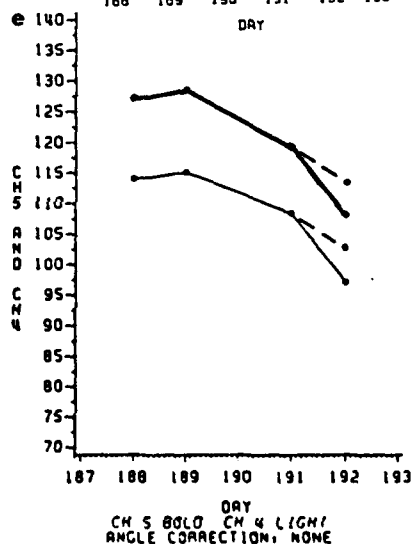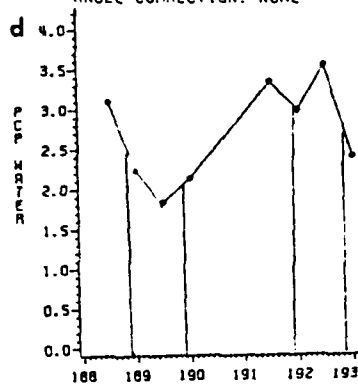
187 188 189 190 191 192 193
DAY
CH 5 BOLD CH 4 LIGHT
ANGLE CORRECTION: NONE

Figure 5.13   Longview, TX (Summer) Composite Chart, Location 3

189 were also recorded as clear but with visibility somewhat reduced from the previous day. These "clear" conditions were not representative of all sub-images, as will be discussed shortly.

Figure 5.13b shows, between days 188 and 189, an increase in CH 5-4 and a marked decrease in CH 2-1. The CH 5-4 trace rises as the precipitable water decreases but the CH 2-1 does not. The CH 2-1 trace is, apparently, more responsive to the decreasing view angle (day 189 was nadir) than to the absorption effects. The decrease in both the CH 2-1 and the CH 5-4 traces between days 191 and 192 are a combination of increased absorption, larger view angle and cloud contamination. Sky conditions on day 191 were much cloudier and visibility was reduced by haze. The atmospheric moisture content was much higher due to return flow around a stagnant high pressure system. Viewing conditions at satellite overpass on day 192 were slightly improved. Shortly before satellite overpass Longview recorded a wind shift, a drop in dewpoint and an increase in visibility. Scattered clouds were observed at 3500 ft. The CH 5-4 and CH 2-1 traces seem to adequately reflect the weather at Longview.

Figure 5.14b is a trace for a second Longview sub-image where the cloud screens indicated sub pixel clouds where a factor on day 189. Notice that the CH 5-4 trace decreases despite the fact that the precipitable water was decreasing. Although the cause is not understood, in general, slight
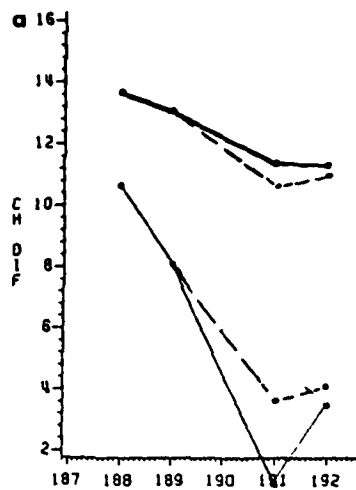
LONGVIEW
LAT=31.92 LON=93.98
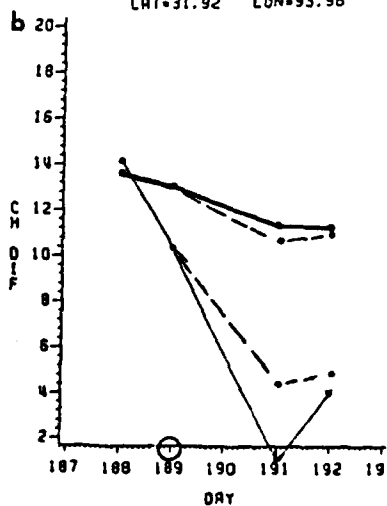
a

CH DIF

DAY
CH 5-4 BOLD   CH 2-1 LIGHT
ANGLE CORRECTION: NONE

c

CH 2 AND CH 1

DAY
CH 2 BOLD   CH 1 LIGHT
ANGLE CORRECTION: NONE

d

PCP WATER

DAY

b

CH DIF

DAY
CH 5-4 BOLD   CH 2-1 LIGHT
ANGLE CORRECTION: 2-1 SUN

e

CH 5 AND CH 4

DAY
CH 5 BOLD   CH 4 LIGHT
ANGLE CORRECTION: NONE

Figure 5.14   Longview, TX (Summer) Composite Chart, Location 4

cloud contamination tended to reduce the CH 5-4 difference.

The CH 2-1 trace for the second sub-image shows a steeper decline for day 189 than does the first sub-image. Again sub pixel clouds were probably the reason. The view angle change probably enhanced the effect.

Days 191 and 192, as previously mentioned, were much more cloud contaminated than the previous days. The atmosphere was also more moist. The combined cloud/moisture effects can be seen in the CH 5-4 trace in Figure 5.14b. Note that the near zero value of CH 2-1 indicates cloud saturation on day 191. Cloud screening reduces the problem, but residual cloudiness is still evident in the channel values and the cloud screen.

SPRINGFIELD, MO

Julian dates 188, 189, 191, and 192 (July 7, 8, 10 and 11, 1983)

Interpretation of the atmospheric conditions and their influence on the remotely sensed data presented quite a challenge for the Springfield sub-images. The upper air soundings for this case came from Monett, Mo (UMN), which is approximately 40 miles southwest of Springfield.

High pressure, both at the surface and aloft, dominated the central United States on day 188. The air was basically of continental origin, and hence relatively dry. The water

content was close to 50 percent of the seasonal normal. The atmosphere remained relatively dry through day 189.

The upper air data available from Monett, MO, for the day 188, 12Z sounding had missing data for many levels, therefore, a complete precipitable water analysis was not possible. However, inspection of the available data did show a moist layer from the surface to 877 mb. The data also showed a rather significant feature from 530 to 470 mb, a 7°C increase in dewpoint. Possible impacts of (is moist layer will be discussed later.

When the satellite overpass occurred the reported Springfield sky condition was a scattered layer of cirrus at 25000 ft and a visibility of 15 mi. One hour later a thin broken layer of cirrus was reported. A thin broken sky condition persisted for the remainder of the afternoon. The upper air sounding four hours after satellite overpass had a precipitable water content of 1.58 cm. The day 189 sky conditions were clear. On day 189 the morning and evening precipitable water amounts were 1.31 and 1.57 cm, respectively.
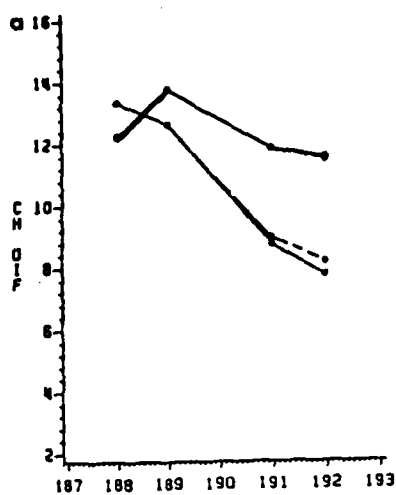
The atmospheric moisture increased steadily from day 189 through the remainder of the case study period. Skies remained clear on day 190 but a LAC scene was not available for study. The next available data was for day 191.

The 12Z sounding on day 191 indicated precipitable water of 3.30 cm. By the time of satellite overpass there were scattered clouds at 4500 feet. Dewpoints were in the

mid sixties. Day 192 was slightly more moist and more cloudy than day 191. Weather on both days was influenced by stagnant high pressure systems at the surface and aloft.

All of the sub-images for day 188 showed extremely high Channel 2 values. Most values were above twenty percent reflectance. These were the highest Channel 2 values observed in any of the case studies. Channel 1 values were also enhanced but not quite as much as Channel 2 (Figure 5.15b). The resulting CH 2-1 difference was also the highest observed in the case studies.

Day 189 Channel 2 values for Springfield were markedly lower as were the CH 2-1 values. For these two days the CH 2-1 and CH 5-4 traces were dissimilar. CH 2-1 dropped as CH 5-4 rose. The CH 5-4 trace appears well behaved with respect to the estimated and/or calculated water content of the atmosphere. The CH 2-1 behavior is most likely a combination of off nadir viewing and the influence of the thin broken cirrus layer. The layer may have been associated with the upper level dewpoint increase previously mentioned. Figure 5.16 compares Channel 2-1 scenes for the same locations for days 188 and 189. Day 188, as indicated by the symbols has generally larger values of CH 2-1. The sub-image has a very nonuniform appearance when compared to the same contour scene on day 189. A thin broken deck of cirrus may have caused the nonuniform nature of the scene with the small ice crystals preferentially reflecting the energy in Channel 2 to the satellite.

SPRINGFIELD SKY/SURFACE CONDITIONS

DAY	TIME	SKY	VSBY	DP
188	20Z	250 SCT	15	56
	21Z	.250 SCT	15	56
	22Z	250-BKN	15	58
189	20Z	CLR	15	57
	21Z	CLR	15	58
191	20Z	45 SCT	7	66
	21Z	45 SCT	7	66
192	20Z	MISSING		
	21Z	MISSING		

SPRINGFIELD MO
LAT=37.24   LON=93.31
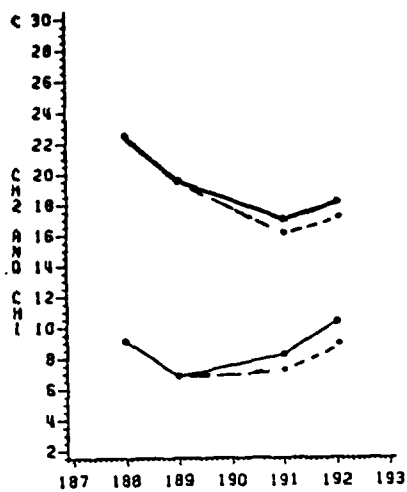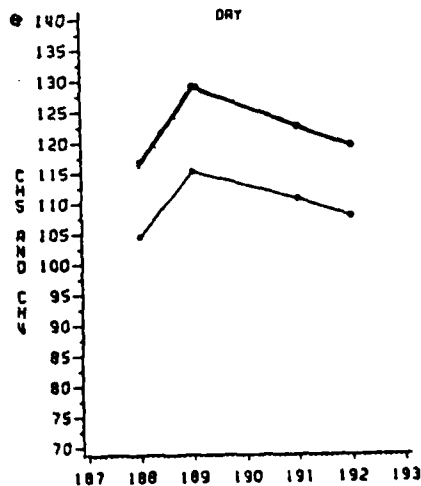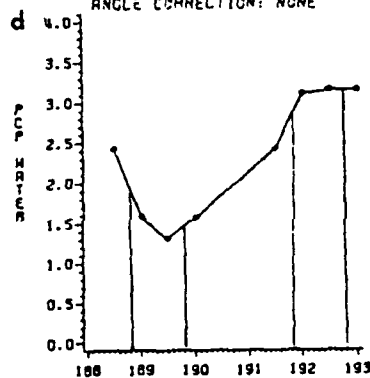
Figure 5.15   Springfield, MO (Summer) Composite chart
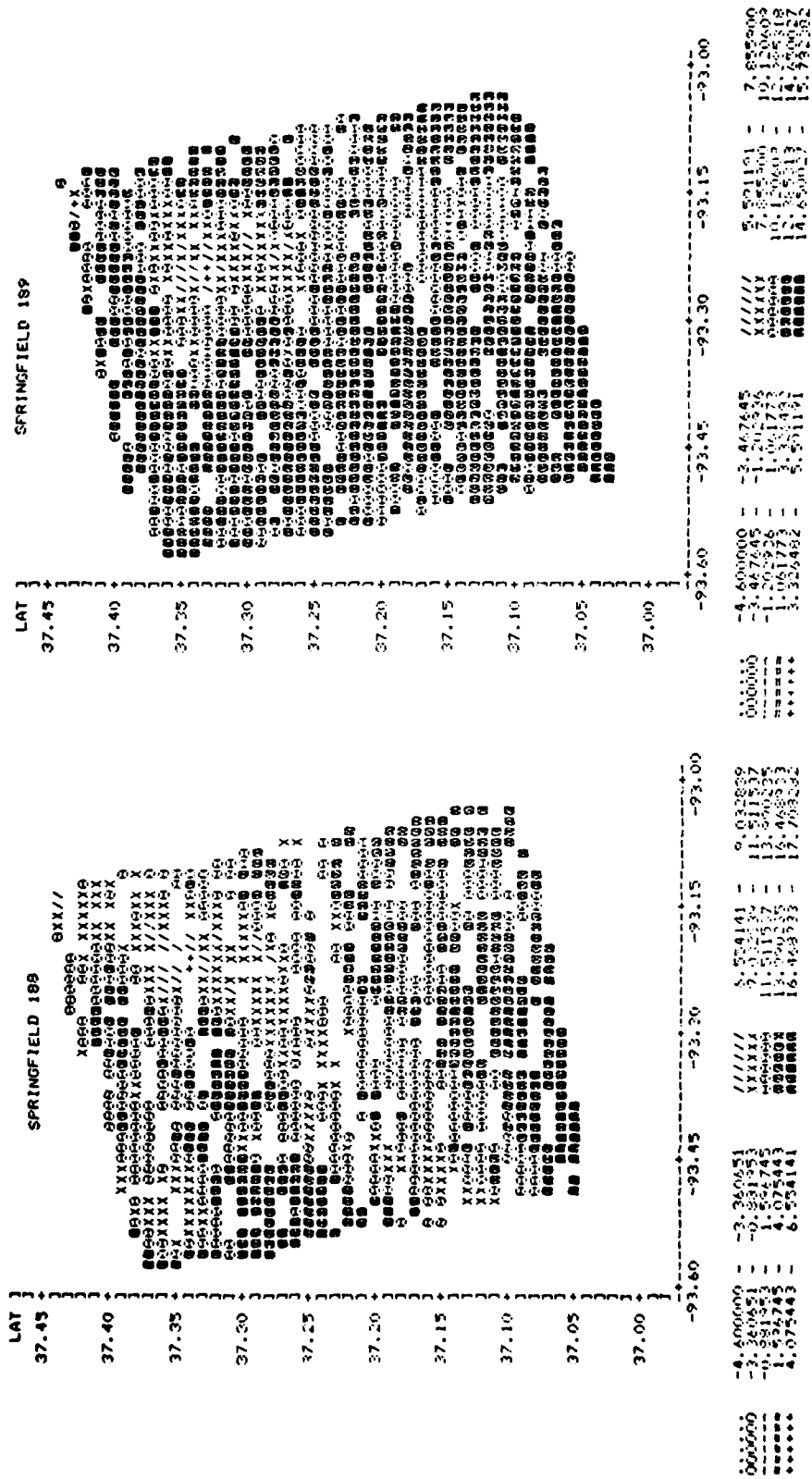
Figure 5.16 Springfield MO (Summer) CH 2-1 Contour Map

The CH 5-4 trace reflected the changing water content of the atmosphere and the trace behaved as expected. The Ch 2-1 trace again seemed to respond more to changing view angle than to water vapor absorption on days 188 and 189. The latter two days of the period had dramatic decreases in CH 5-4 and CH 2-1. The decreases were expected because of the increasing moisture and cloud content of each day's atmosphere.

LITTLE ROCK, AR

Julian dates 189, 191, and 192 (July 8, 10 and 11,1983)

The weather at Little Rock for this study was very similar to the weather at Longview for the same period. Day 189 was the driest day and least cloud-contaminated of the study. Moisture and clouds increased through day 192. Of the sub images analyzed, two had slight cloud contamination through the period. The remaining two images began with moderate cloud contamination on day 189. By day 191 both were heavily cloud contaminated.

The CH 5-4 trace is Figure 5.17b The CH 5-4 trace decreases as the atmospheric water content increases. The trace may also be responding to an increase in clouds over the period. CH 2-1 also decreases. The magnitude of the decrease is probably most influenced by the increasing cloudiness.

a (CH OIF)
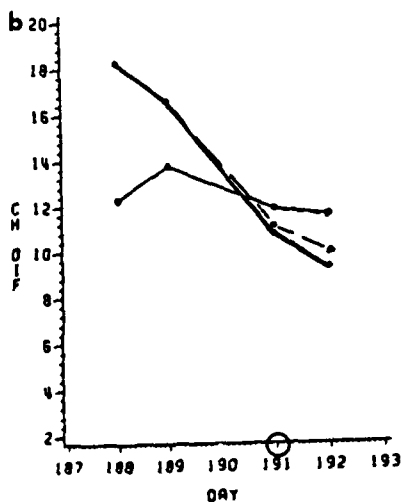CH 5-4 BOLD   CH 2-1 LIGHT
ANGLE CORRECTION: NONE

**c** (C AND CH I)
CH 2 BOLD   CH 1 LIGHT
ANGLE CORRECTION: NONE

LITTLE ROCK SKY/SURFACE CONDITIONS

DAY	TIME	SKY	VSBY	DP
189	20Z	50 SCT	12	64
	21Z	50 SCT	12	65
191	20Z	45 SCT	5H	63
	21Z	50 SCT	5H	64
192	20Z	-X 70 SCT	4H	63
	21Z	-X 60 SCT	4H	64

d (PCP WATER)

LITTLE ROCK
LAT=34.74   LON=92.6

b (CH OIF)
CH 5-4 BOLD   CH 2-1 LIGHT
ANGLE CORRECTION: 2-1 SUN

e (CH 5 AND CH 4)
CH 5 BOLD   CH 4 LIGHT
ANGLE CORRECTION: NONE
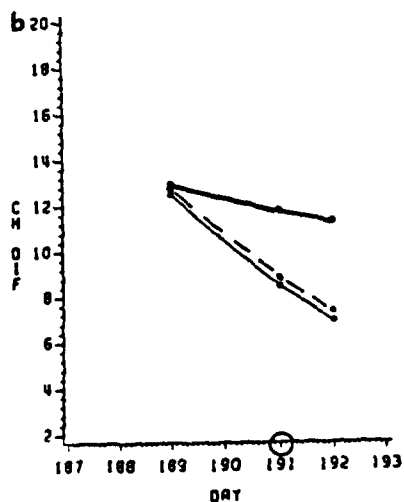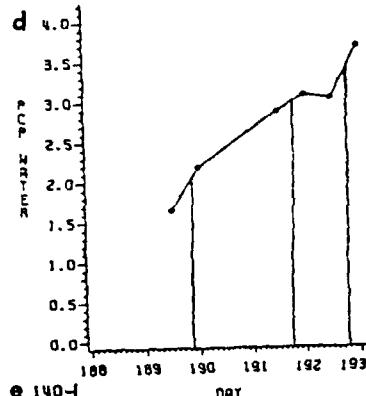
Figure 5.17   Little Rock, AR (Summer) Composite Chart

The second composite graph, Figure 5.18b, shows the CH 5-4 and CH 2-1 responses to more cloud-contaminated scenes from a second Little Rock sub-image on day 192. The clouds cause a sharp increase in CH 2-1.

BISMARCK, ND

Julian dates 222, 223, 224, and 225 (August 10, 11, 12 and 13, 1983)

A cold front passed through Bismarck just before the 00Z sounding on day 222. A dome of cool dry air lagged the front by several hours. The surface observation shows the surface, dry air intrusion at 12Z. Upper air drying probably began at 12 Z but the effect on the sounding (released about 1115Z) is not evident. The slope of the cool, dry air to the west, with height, is most likely responsible for the discrepancy in the observation.

Drying continued through the 00Z sounding for day 223. At the time of the satellite overpass a thin layer of scattered cirrus was reported. Moisture increased after 00Z on day 223 but sky conditions on that day remained clear. Southerly flow in advance of the next frontal system increased moisture on day 224. There was also a slight increase in clouds.

A second cold front passed Bismarck just before the day 225 00Z sounding. As before, the surface observation shows
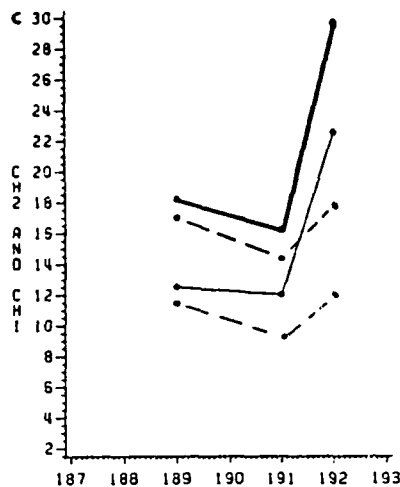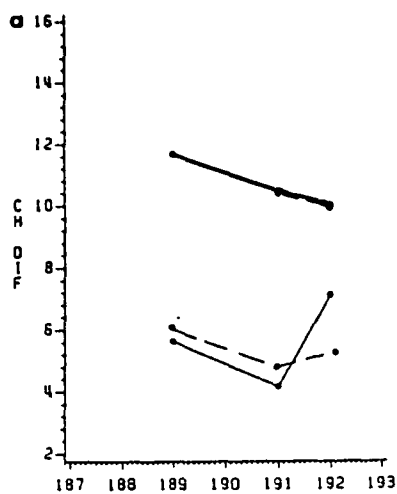
a

CH DIF

187 188 189 190 191 192 193
DAY
CH 5-4 BOLD   CH 2-1 LIGHT
ANGLE CORRECTION: NONE

c

CH2 AND CH1

187 188 189 190 191 192 193
DAY
CH 2 BOLD   CH 1 LIGHT
ANGLE CORRECTION: NONE

LITTLE ROCK SKY/SURFACE CONDITIONS

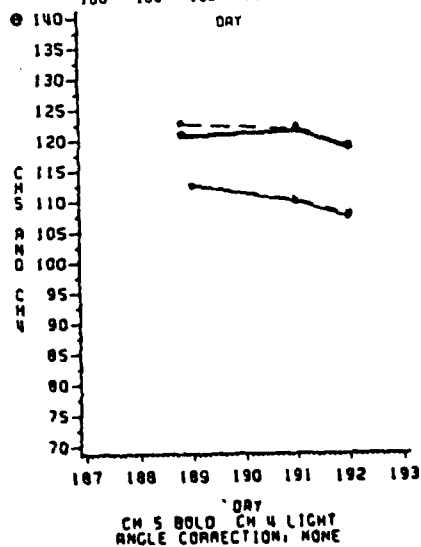| DAY	TIME	SKY	VSBY	DP
189	20Z	50 SCT	12	64
	21Z	50 SCT	12	65
191	20Z	45 SCT	5H	63
	21Z	50 SCT	5H	64
192	20Z	-X 70 SCT	4H	65
	21Z	-X 60 SCT	4H	64

LITTLE ROCK
LAT=34.91   LON=91.74

d

PCP WATER

188 189 190 191 192 193
DAY

b

CH DIF

187 188 189 190 191 192 193
DAY
CH 5-4 BOLD   CH 2-1 LIGHT
ANGLE CORRECTION: 2-1 SUN

e

CH5 AND CH4

187 188 189 190 191 192 193
DAY
CH 5 BOLD   CH 4 LIGHT
ANGLE CORRECTION: NONE
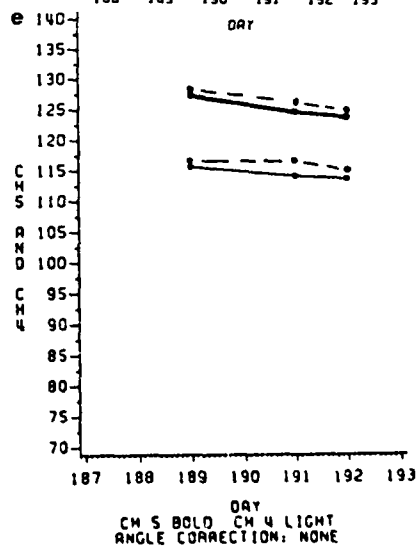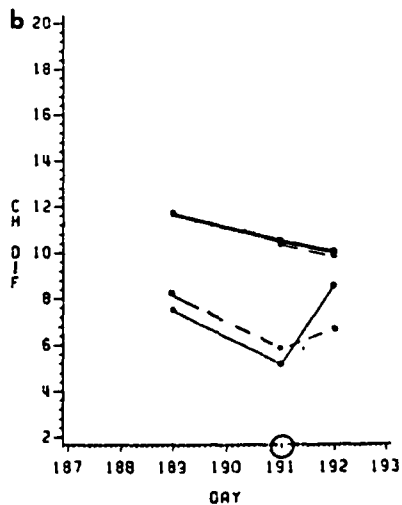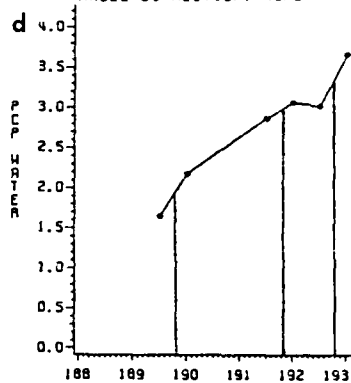
Figure 5.18   Little Rock, AR (Summer) Composite Chart

the effect of the front immediately. But the drying effect in the upper air data was not evident until the following morning. Day 225 is significantly drier and clearer than day 224.

The CH 5-4 and CH 2-1 traces (See Figure 5.19b) mirror the effects of the atmosphere. The CH 5-4 trace takes a significant plunge at the time of the largest atmospheric water loading. The CH 2-1 trace shows a similar trend.

In comparing the Bismarck CH 5-4 and CH 2-1 traces one should note that the dramatic changes in Ch 2-1 are absent compared to the July case studies for the Midwest. The vegetation around Bismarck was probably past peak greeness, thus, the CH 2-1 trace changes seem to be reduced compared to the July CH 2-1 trace changes for the Midwest. Holben and Fraser (1984) found larger variations in both the VIN and the NVI during off nadir viewing of heavy biomass scenes as compared to low biomass scenes. This research appears consistent with these findings.

CORRELATION ANALYSIS

To quantify the relationships discussed above, a SAS Ranked Correlation Procedure was run on the channel values, the channel difference values and the precipitable water data (The precipitable water data was linearly interpolated to the time of satellite overpass). The procedure was run on both unscreened and cloud screened data

a

CH DIF

CH 5-4 BOLD   CH 2-1 LIGHT
ANGLE CORRECTION: NONE

c

CH 2 AND CH 1

CH 2 BOLD   CH 1 LIGHT
ANGLE CORRECTION: NONE
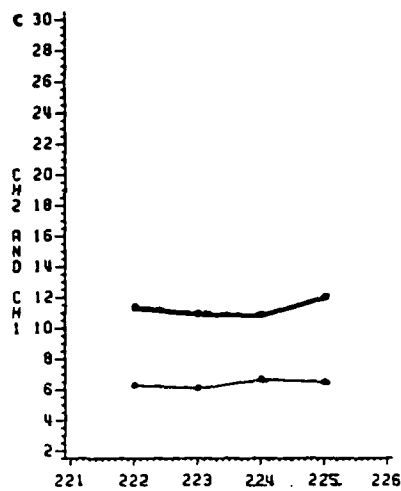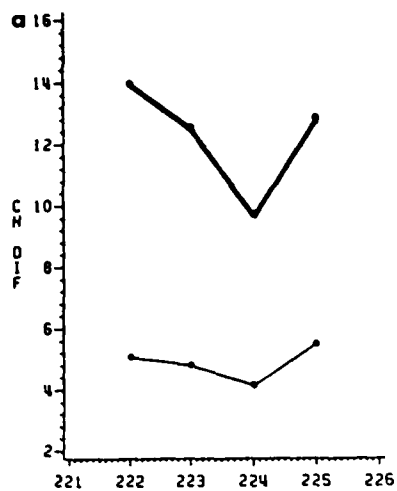
BISMARCK SKY/SURFACE CONDITIONS

DAY	TIME	SKY	VSBY	DP
222	20Z	250 SCT	12	49
	21Z	250 SCT	12	48
223	20Z	CLR	12	47
	21Z	CLR	12	49
224	20Z	70 SCT	12	59
		120 SCT		
	21Z	70 SCT	12	60
		120 SCT		
		250 SCT		
225	20Z	CLR	12	42
	21Z	CLR	12	39

BISMARK
LAT=46.24   LON=99.54

d

PCP WATER

DAY

b

CH DIF

CH 5-4 BOLD   CH 2-1 LIGHT
ANGLE CORRECTION: 2-1 SUN

e

CH 5 AND CH 4

DAY
CH 5 BOLD   CH 4 LIGHT
ANGLE CORRECTION: NONE
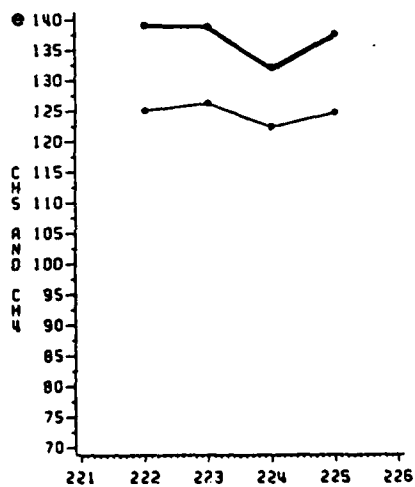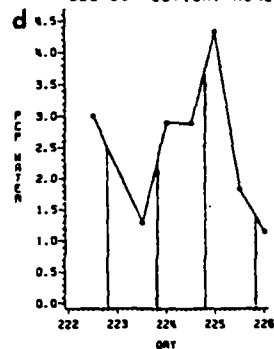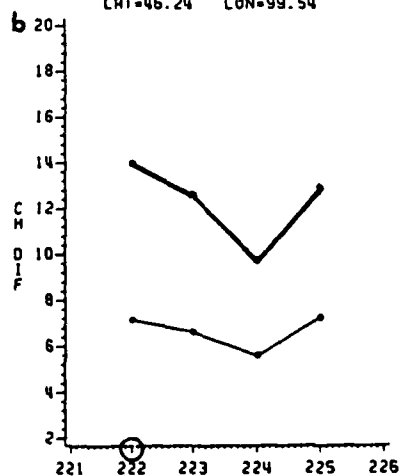
Figure 5.19 Bismarck, SD (Summer) Composite Chart

UNSCREENED DATA

As indicated throughout this report CH 5-4 difference was strongly correlated with precipitable water amounts. The correlation coefficient between the two variables was -.71. The correlation coefficent between CH 2-1 and precipitable water was only -.33.

The CH 5-4 difference and the various channel values used in this study had nearly equal strength in explaining the variability of the sun-corrected CH 2-1 difference. None of the variables appeared to play an dominating role in explaining the behavior of CH 2-1. When ranked, CH 5-4 was the most strongly correlated with CH 2-1 (r=.39). This correlation seems to indicated that differential absorption plays at least some role in both CH 2-1 and CH 5-4.

The CH 5-4 difference was most strongly correlated with Channel 1. This may be the result of the CH 5-4 difference being small (or absorption being large) when water vapor increases and produces clouds, thus increasing Channel 1. Channel 2 seems to have only a weak relationship with CH 5-4.

CLOUD SCREENED DATA

The correlation between CH 5-4 and precipitable water remained high at r =-.73 while the correlation coeeficent between CH 2-1 and precipitable water was -.31. Removing

the cloudiest pixels produced interesting results in from the analysis of correlation between the channel and the channel difference date. A strong correlation between the sun angle corrected CH 2-1 and Channel 2 emerged, r=.74. This indicates the Channel 2 energy is a driving mechanism in determining the CH 2-1 value when cloudiness is reduced or eliminated. This is an especially important piece of information, since Channel 2 is also subject to the most variation due to physical processes on the surface and in the atmosphere. Running a distant second in the correlation rankings with CH 2-1 was CH 5-4 (r=.36). Again this indicates the differential absorptive effects have at least some statistical importance for the behavior of CH 2-1.

While the statisical relationship between CH 2-1 and CH 5-4 is not what was originally hoped for, the correlation analysis provided some useful insight about which variables, and thus, indirectly which physical processes were most important in explaining the behavior of CH 2-1.

VIEW ANGLE

Throughout this report view angle has been noted as a factor which adds variability to the channel values and, perhaps more importantly, to the channel difference values. In practice, increasing view angle decreases the information content of the radiant signal. For this reason, nomalization to a view angle of zero is a desirable adjustment to

the radiance data. Singh (1984) states that division of the
radiance values by cosine α , where α is the view zenith
angle is necessary. A normalization of this type was tried
on the radiance data. The results were grossly overcor-
rected values of the channel data and the channel difference
values for large view angles.

Apparently, this calculation corrects for the reduction
of energy reaching the sensor due to off nadir view, but it
fails to account for the energy addition to the beam by path
radiance. The "corrected" CH 2-1 values from off nadir view
days were outside the realm of believability. Lacking an
appropriate view angle correction, no view angle corrections
were made.

DATA PROBLEMS

Garbled data was occasionally a problem in reading the
LAC tapes. Garbling of the earth location data makes a scan
line useless. More frequently short records or scan lines
were encountered. These scan lines were skipped. A series
of short records sometimes eliminated a location from study.
Additionally, some of the LAC tapes requested, for reasons
never determined, could not be read by the AMDAHL system.
Beyond the physical data problems the biggest problem with
data was the irregularity of LAC scene acquisition.

CONCLUSIONS AND RECOMMENDATIONS

The first objective of the research -- determining if differential absorption effects could be found over land by differencing the appropriate channel values, was successful. The CH 5-4 difference has been shown to be related to the amount of precipitable water in the atmospheric column. The CH 2-1 difference is, unfortunately, less related to the precipitable water content, presumably because of the over-powering scattering effect in Channel 2. Therefore, the second objective of relating the differential absorption effect to CH 2-1 variability was not nearly so successful.

Further research into the proper view angle correction (one that accounts for scattering) may improve the usefulness of CH 5-4 difference as a diagnostic tool for CH 2-1 variability. Further research may also prove useful in applying the differential absorption technique to GAC data. The GAC data is acquired often enough that small view angle images of most mid-latitude scenes are regularly available. If, as Duggin et al. (1982a) suggested, the scenes are limited to the central 25 percent of the AVHRR scan line, the view angle/scattering problem may be reduced enough to make the differential absorption calculation a useful diagnostic, or even, predictive tool.

LIST OF REFERENCES

Allison, L. J. and Schnapf, A., 1983. "Meteorological Satellites," in: Manual of Remote Sensing, 2nd Edition, edited by D. S. Simonett, Falls Church, VA: American Socie Photogrammetry, pp. 651-678.

Anding, D. and Kauth, R., 1970. "Estimation of Sea Surface Temperature from Space," Remote Sensing of Environment, 1:217-220.

Barnes, J. C. and Smallwood, M. D., 1982. TIROS-N Series Direct Readout Services Users Guide, U.S. Department of Commerce, NOAA, NESS, Washington, D.C.

Barnett, T. L., 1984. Department of Commerce, NOAA, NESDIS, Assesment Services Center, Columbia, MO, Personal Communications.

Barnett, T. L. and Thompson, D. R., 1982. "The Use of Large- Area Spectral Data in Wheat Yield Estimation," Remote Sensing of Environment, 12:509-518.

Barrett, E. C., 1974. Climatology From Satellites, New York: Methuen & Co., 418 pp.

Battan, L. J., 1984. Fundamentals of Meteorology, 2nd Edition, Englewood Cliffs, NJ: Prentice-Hall, Inc., 304 pp.

Biology Today 1972. Del Mar, CA: Communications Research Machines, Inc., 1020 pp.

Callison, R. D. and Cracknell, A. P., 1984. "Atmospheric Correction to AVHRR Brightness Temperatures for Waters Around Great Britain," Int J. Remote Sensing, 5(1): 185-198.

Chahine, M. T., 1983. "Interaction Mechanisms Within the Atmosphere," in Manual of Remote Sensing, 2nd Edition, Edited by D. S. Simonett, Falls Church, VA: American Societ Photogrammetry, pp. 165-230.

Charney, J. G. and Phillips, N. A., 1953. "Numerical Integration of the Quasi-Geostrophic Equations for Barotropic and Simple Baroclinic Flows," Journal of Meteorology, 10(2): 71-99.

Coulson, K. L., 1975. Solar and Terrestial Radiation, New York: Academic Press, Inc., 322 pp.

Dave, J. V. and Braslau, N., 1975. "Effects of cloudiness on the Transfer of Solar Energy Through Realistic Model Atmospheres," J. Appl. Met., 14:388

Dismachek, D. C.; Booth, A. L., and Leese, J. A., 1980. National Environmental Satellite Services Catalog of Products, 3rd Edition, NOAA Technical Memorandum, NESS 109, Washington, D.C. 120 pp.

Duggin, M. J.; Piwinski, D.; Whitehead, V. and Ryland, G., 1982. "Evaluation of NOAA-AVHRR Data for Crop Assesment," Applied Optics, 21(11): 1873-1875.

Duggin, M. J., Schoch, L. and Gray, T. I., 1982. "Effect of Subpixel-sized Cloud on Target Discrimination from Satellite Data," Applied Optics, 21: 2649-2650.

Fleagle, R. G. and Businger, J. A., 1980. An Introduction to Atmospheric Physics, New York: Academic Press, 432 pp.

Fraser, R. S. and Curran, R. J., 1976. "Effects of the Atmosphere on Remote Sensing," in: Remote Sensing of Environment, Edited by J. Lintz, Jr., and D. S. Simonett, Reading, MA: Addison-Wesley Publishing Company, pp. 34-84.

Gjessing, D. T., 1978. Remote Surveillance by Electromagnetic Waves, Ann Harbor, MI: Ann Arbor Science, 152 pp.

Goody, R. M. and Robinson, G. D., 1951. "REVIEWS OF MODERN METEOROLOGY-2: Radiation in the Troposphere and Lower Stratosphere," Quart. J. Roy. Meteorol. Soc., 77: 151-187.

Gray, T. I., Jr. and McCrary, D. G., 1981. Meteorological Satellite Data - A Tool to Describe the Health of the World's Agriculture AgRISTARS Report EW-NI-04042, JSC-17112, Lyndon B. Johnson Space Center, Houston, TX, 7 pp.

Gray, T. I., Jr. and McCrary, D. G., 1981. The Environmental Vegetation Index, A Tool Potentially Useful for Arid Land Management, AgRISTARS Report EW-N1-04076, JSC-17132, Lyndon B. Johnson Space Center, Houston, TX, 3pp.

Gray, T. I.; McCrary, D. G. and Armstrong, T. E., 1981. Characteristics of TIROS, GOES, DMSP and LANDSAT Systems, AgRISTARS Report EW-N1-04075, JSC-17131, LEMSO-16504, Lyndon B. Johnson Space Center, Houston, TX, 17 pp.

Gray, T. I., Jr and McCrary, D. G., 1982. An Application of Advanced Very High Resolution Radiometer Data to Monitor the World's Agriculture, AgRISTARS Report EW-N1-04000, JSC-12345, Lyndon B. Johnson Space Center, Houston, TX, 10 pp.

Gruber, A.; Ruff, Irwin, and Ernest C., 1983. Determination of the Planetary Radiation Budget From TIROS-N Satellites, U.S. Department of Commerce, NOAA Technical Report, NESDIS 3, Washington, D. C., 12 pp.

Hecht, E. and Zajac, A., 1979. Optics Reading MA: Addsion-Wesley Publishing Company. 565 pp.

Hoffer, R. M. and Johannsen, C. J., 1969. "Ecological Potential in Spectral Signature Analysis," in: Remote Sensing in Ecology, Athens, GA: University of Georgia Press, pp. 1-16.

Holben, B. and Fraser, R. S., 1984. "Red and Near-infrared Sensor Response to Off-nadir Viewing," *Int. J. Remote Sensing,* 1: 145-160.

Holben, B. N., Schutt, J. B. and McMurtrey, J. III, 1983. "Leaf Watter Stress Detection Utilizing Thematic Mapper Bands 3, 4 and 5 in Soybean Plants," *Int. J. Remote Sensing,* 4: 289-297

Horler, D. N. H.; Dockray, M., and Barber, J., 1983. "The Red Edge of Plant Leaf Reflectance," *Int. J. Remote Sensing,* 4(2): 273-288.

Horvath, N. C.; Gray, T. I., Jr., and McCrary, D. G., 1982. *Advanced Very High Resolution Radiometer (AVHRR) Data Evaluation For Use in Monitoring Vegetation, Volume 1 - Channels 1 and 2,* AgRISTARS Report EW-L2-04303, JSC-18243, LEMSCO-17383, Lyndon B. Johnson Space Center, Houston, TX, 94 pp.

Irbarne, J. W. and Cho, H. R., 1980. *Atmospheric Physics,* Dordrecht, Holland: D. Reidel Publishing Company, 212 pp.

Jackson, R. D.; Slater, P. N. and Printer, P. J., 1982. *Adjusting the Tassled Cap Brightness and Greeness Factors for Atmospheric Path Radiance and Absorption on a Pixel by Pixel Basis,* AgRISTARS Report, EW-U2-04334, JSC 18260, Lyndon B. Johnson Space Center, Houston, TX, 22 pp.

Justus, G. G., 1984. "Study of Cloud Screening and Analysis Methods for AgRISTARS Vegetation Index Products," Report prepared for NOAA, NESDIS, Georgia Institute of Technology Project G-35-670, Atlanta, GA.

Kauth, R. J. and Thomas, G. S., 1976. "A Graphic Description of the Spectral-Temporal Development of Agricultural Crops as Seen by Landsat," in: *Proceedings of the Symposium on Machine Processing of Remotely Sensed Data,* LARS, Purdue Univ., West Lafayette, IN, pp. 41-51.

Kellogg, W. W., 1982. "Early Satellite Program
        Developments," in: The Conception, Growth, Accom-
        plishments, and Future of Meteorological Satellites,
        NASA Conference Publication 2257, Marshall Space
        Flight Center, AL, pp. 1-4.

Kidwell, K. B., compiler, 1983. NOAA-Polar Orbiter Data
        (TIROS, NOAA-6, NOAA-7, and NOAA-8) Users Guide U.S.
        Department of Commerce, NOAA, NESDIS, NCDC, Washing-
        ton, D.C.

Kyle, T. G. and Goldman, A., 1975. Atlas of Computed Infra-
        red Atmospheric Absorption Spectra, National Center
        for Atmospheric Research Technical Note/STR-112,
        Boulder, CO.

Knipling, E. B., 1970. "Physical and Physiological Basis
        for the Reflectance of Visible and Near-Infrared
        Radiation from Vegetation," Remote Sensing of Envi-
        ronment 1:   155-159.

LaRocca, A. J. and Turner, R. E., 1975. Atmospheric Tran-
        smittance and Radiance: Methods of Calculation, IRIA
        Report, Environmental Research Institute of Michigan,
        Ann Arbor, MI.

Lauritson, L.; Nelson, G. T. and Porto, F. W., 1979. Data
        Extraction and Calibration of TIROS-N/NOAA Radiome-
        ters, U.S. Department of Commerce, Washington, D.C.,
        NOAA Technical Memorandum, NESS 107, 73 pp.

LeDuc, S. K., 1984. U.S. Department of Commerce, NOAA,
        NESDIS, Assesment Information Services Center, Colum-
        bia, MO, Personal Communication

Lillesand, T. M. and Kiefer, R. W., 1979. Remote Sensing
        and Image Interpretation, New York: John Wiley &
        Sons, 612 pp.

McClain, E. P., 1979. "Satellite Derived Earth Surface
        Temperatures," in: Quantitative Meterological Data
        From Satellites World Meteorological Organization
        Technical, Note 166, Geneva, Switzerland, pp. 60-86.

McClain, E. P.; Pichel, W. G.; Walton, C. C.; Ahmad, Z. and Sutton, J., 1983. "Multi-channel Improvements To Satellite-Derived Global Sea Surface Temperatures," Adv. Space Res. 2(6): 43-47.

McClatchey, R. A.; Benedict, W.S; Clough, S.A.; Burch, D.E.; Calfee, R. F.; Fox, K.; Ruthman, L.S. and Garing, J. S., 1973. Atmospheric Absorption Line Parameter Compilation, AFCRL-73-0096, Air Force Cambridge Research Lab, Bedford, MA.

McMillin, L. M., 1975. "Estimation of Sea Surface Temperatures From Two Infrared Window Measurements With Different Absorption," Journal of Geographical Research 80(36): 5113-5117. C.sp.goEEE:.EE

McMillin, L. M. and Sanyal, A., 1983. "The Use of Brightness Temperature Ratios to Retrieve Water Vapor," Preprinted From: Fifth Conference on Atmospheric Radiation. October 31-4 November 1983, Baltimore, Maryland.

Miller, A.; Thompson, J. C.; Peterson, R. E. and Haragan, D. R., 1983. Elements of Meteorology, 4th Edition, Columbus, OH: Charles E. Merrill Publishing Company, . 417 pp.

Myers, V. I., 1983. "Remote Sensing Application in Agriculture," in: Manual of Remote Sensing, 2nd Edition, Edited by D. S. Simonett, Falls Church, VA: American Society of Photogrammetry, pp. 2111-2228.

Nixon, P. R.; Wiegand, C. L.; Richardson, A. J. and Johnson, M. P., 1983. Methods of Editing Clouds and Atmopheric Layer Affected Pixels From Satellite Data, AgRIS-TARS Report EW-U3-00760, JSC-18596, Lyndon B. Johnson Space Center, Houston, TX, 46 pp.

NOAA Satellite Data Services Division, 1983. Vegetation Index User's Guide, U.S. Department of Commerce, NOAA, NESDIS, SDSD, Washington, D. C., 5pp.

Norwine, J. and Greegor, D. H., 1983. "Vegetation Classi-
fication Based on Advanced Very High Resolution
Radiometer (AVHRR) Satellite Imagery," Remote Sensing
of Environment, 13:69-87.

Otterman, J. and Robinove, C. J., 1981. "Effects of the
Atmosphere on the Detection of Surface Changes from
Landsat Multispectral Scanner Data," Int. J. Remote
Sensing, 2(4): 351-360.

Prabhakara, C.; Dalu, G. and Kunde, V. G., 1974. "Esti-
mation of Sea Surface Temperature From Remote Sensing
in the 11- to 13-μ Window Region," Journal of Geophy-
sical Research, 79(33): 5039-5043.

Purdom, J. F. W., Chairman, 1982. "Part III Satellite
Soundings and Their Uses," Preprint From: Workshop
on Satellite Meteorology, July 19-23, 1982, Fort
Collins, CO Colorado State University, Fort Collins,
CO, Cooperative Institute for Research in the Atmos-
phere.

Sabins, F. F., Jr., 3. Remote Sensing Principles and
Interpretation, San Francisco: W. H. Freeman and
Company, 426 pp.

Schneider; S. R., McGinnis, D. F., Jr. and Gatlin, J. A.,
1981. Use of NOAA/AVHRR Visible and Near-Infrared
Data for Land Remote Sensing. U.S. Department of
Commerce, NOAA Technical Report NESS 84, Washington
D.C., 48pp.

Sellers, W. D., 1965. Physical Climatology, University of
Chicago Press: Chicago, IL, Chapter 6.

Singh, S. M., 1984. "Removal of Atmospheric Effects on a
Pixel by Pixel Basis From the Thermal Infrared Data
From Instruments on Satellites. The Advanced Very
High Resolution Radiometer (AVHRR)," Int. J. Remote
Sensing, 5(1): 161-183.

Slater, P. N., 1980. Remote Sensing, Reading, MA:
Addison-Wesley Publishing Company, 575 pp.

Slater, P. N., 1983. "Photographic Systems for Remote Sensing," in: Manual of Remote Sensing, 2nd Edition, edited by D. S. Simonett, Falls Church, VA: American Society of Photogrammetry, pp. 231-289.

Smith, J. A., 1983. "Matter Energy Interaction in the Optical Region," in: Manual of Remote Sensing, 2nd Edition, edited by D. S. Simonett, Falls CHurch, VA: American Society of Photogrammetry, pp. 62-110.

Suits, G. H., 1983. "The Nature of Electromagnetic Radiation," in: Manual of Remote Sensing, 2nd Edition, edited by D. S. Simonett, Falls Church, VA: American Society of Photogrammetry, pp. 37-60.

Sutherland, R. A. and Bartholic, J. F., 1977. "Significance of Vegetation in Interpreting Thermal Radiation from a Terrestial Surface," Journal of Applied Meteorology, 16(8): 759-763.

Tappan, G., Horvath, N. C. and Doraiswamy, P. C., 1983. Use of NOAA-n Satellites for Land/Water Discrimination and Flood Monitoring, AgRISTARS Report EW-L3-04394 JSC-18594, Lyndon B. Johnson Space Center, Houston, TX, 33pp.

Thompson, D. R. and Wehmanen, D. A., 1979. "Using Landsat Digital Data to Detect Moisture Stress," Photogrammetric Engineering and Remote Sensing, 45(2): 201-207.

Tucker, C. J; Gatlin, J. A. and Schneider, S. R., 1984, "Monitoring Vegetation in the Nile Delta with NOAA-6 and NOAA-7 AVHRR Imagery," Photogrammetric Engineering and Remote Sensing, 50(1): 53-61

Tucker, C. J.; Holben, B. N.; Elgin, J. H. Jr. and McMurtrey, J. E., III, 1981. "Remote Sensing of Total Dry-Matter Accumulation in Winter Wheat," Remote Sensing of Environment, 11: 171-189.

U.S. Air Force, Air Research and Development Command, 1961. _Handbook of Geophysics,_ Revised Edition, New York: The MacMillan Company, Chapter 16.

Valley, S. L., ed., 1965. _Handbook of Geophysics and Space Environment,_ Air Force Cambridge Research Lab, Bedford, MA, New York, McGraw Hill.

Yates, H. W.; Tapley, J. D.; Schneider, S. R.; McGinnis, D. F. and Scofield, R. A., 1984. "The Role of Meteorological Satellites in Agricultural Remote Sensing," _Remote Sensing of Environment,_ 14: 219-233.

Wallace, J. M. and Hobbs, P. V., 1977. _Atmospheric Science An Introductory Survey,_ New York: Academic Press, Inc., 467 pp.

Wark, D. Q. and Fleming, H. E., 1966. "Indirect Measurements of Atmospheric Temperature Profiles From Satellites. 1 Introduction," _Mon. Weather Rev.,_ 94: p 351.

Wolfe, W. L. and Zissis, G. J., 1978. _The Infrared Handbook,_ Prepared by The Infrared Information and Analysis Center, Environmental Research Institute of Michigan for the Office of Naval Research, Department of the Navy, Washington, D.C.